

Structural and functional studies of the  
reovirus attachment protein  $\sigma 1$  and its  
interaction with the receptor JAM-A

Strukturelle und funktionelle Studien am Zelladsorptionsprotein  
 $\sigma 1$  des Reovirus und seiner Interaktion mit dem Rezeptor  
JAM-A

DISSERTATION

der Fakultät für Chemie und Pharmazie  
der Eberhard-Karls-Universität Tübingen

zur Erlangung des Grades eines Doktors  
der Naturwissenschaften

2009

vorgelegt von  
Eva Kirchner

Tag der mündlichen Prüfung: 26. Mai 2009

Dekan: Prof. Dr. L. Wesemann

1. Berichterstatter: Prof. Dr. T. Stehle

2. Berichterstatter: Prof. Dr. D. Rapaport

# Abstract

The attachment of viruses to host cells and subsequent viral entry are key steps in viral infection. Receptor recognition also serves an essential function in target cell selection. Mammalian orthoreoviruses (reoviruses) are highly tractable experimental models for studies of virus-receptor interactions and viral pathogenesis. Furthermore, they show promise as vectors for oncolytics and vaccines. Similarly to many other viruses, reoviruses use cell-surface carbohydrates and a cell adhesion molecule as receptors. How the usage of multiple receptors contributes to viral attachment is still unclear, and general rules for receptor recognition at an atomic level have not yet been established.

In this thesis, structural properties and receptor binding mechanisms of the reovirus attachment protein  $\sigma 1$  were analyzed.  $\sigma 1$  contains an unusual trimerization motif, the aspartic acid cluster, at its trimer interface. A  $\sigma 1$  protein, in which one of the aspartic acids of the cluster was mutated to asparagine (D345N), was analyzed regarding binding to the reovirus receptor JAM-A, and its crystal structure was solved to high resolution. The analysis of the D345N mutant provides information about the protonation state of the aspartic acids and the forces holding the  $\sigma 1$  trimer together. Moreover, interpretation of the D345N structure gives hints about conformational changes in  $\sigma 1$  occurring during viral entry, probably involving a partly or fully detrimerized  $\sigma 1$  molecule.

Furthermore, complexes formed between the attachment protein  $\sigma 1$  and the reovirus receptor, JAM-A, were examined. The crystal structures of the complexes formed between the  $\sigma 1$  proteins of two reovirus prototype strains and JAM-A were determined. The  $\sigma 1$  trimers engage three molecules of the JAM-A D1 domain at the homodimeric interface of JAM-A. The contact areas comprise a large number of polar and charged residues, suggesting that the interaction is dependent on pH. The dissociation constant of the JAM-A homodimer was determined using analytical ultracentrifugation and compared with the one of the  $\sigma 1$ -JAM-A complex. The thermodynamic forces occurring in the two interactions demonstrate how  $\sigma 1$  can disrupt JAM-A dimers in order to engage the JAM-A dimer interface. The structure of the  $\sigma 1$ -JAM-A complex was compared with the published structure of the adenovirus fiber-CAR complex. The similarities between both complexes

support the theory of an evolutionary link between the cell attachment mechanisms used by reovirus and adenovirus. Together, these studies add to the understanding of the mechanisms of reovirus cell attachment and reveal common strategies used by viruses to engage their cell-surface receptors.

# Contents

<b>Abstract</b>	<b>I</b>
<b>Abbreviations</b>	<b>VI</b>
<b>1 Introduction</b>	<b>1</b>
1.1 Viruses . . . . .	1
1.1.1 Definition and structure . . . . .	1
1.1.2 Icosahedral symmetry . . . . .	2
1.1.3 Viral life cycle . . . . .	3
1.2 Reoviruses . . . . .	4
1.2.1 Reovirus structure . . . . .	4
1.2.2 Infection of cells . . . . .	6
1.2.2.1 Attachment and entry . . . . .	6
1.2.2.2 Disassembly and transfer to the cytoplasm . . . . .	6
1.2.3 The attachment protein of reovirus . . . . .	8
1.2.3.1 The structure of $\sigma 1$ . . . . .	8
1.2.3.2 The aspartic acid cluster . . . . .	9
1.2.4 Reoviruses as therapeutic agents . . . . .	10
1.3 Junctional adhesion molecule-A . . . . .	11
1.3.1 Function of JAM-A . . . . .	11
1.3.2 JAM-A structure . . . . .	11
1.3.3 Predicted binding site for $\sigma 1$ . . . . .	13
1.4 Aims . . . . .	14
<b>2 Materials and Methods</b>	<b>15</b>
2.1 Materials . . . . .	15
2.1.1 Hardware . . . . .	15
2.1.1.1 General purpose equipment . . . . .	15
2.1.1.2 Cell lysis and chromatography . . . . .	16
2.1.1.3 X-ray crystallography . . . . .	16
2.1.2 Crystallographic software . . . . .	17
2.1.3 Kits and consumables . . . . .	17
2.1.3.1 Concentrators and filters . . . . .	17
2.1.3.2 Cloning and bacterial culture . . . . .	17
2.1.3.3 Protein purification and analysis . . . . .	18

2.1.3.4	Crystallization screens . . . . .	18
2.1.4	Plasmids and primers . . . . .	18
2.1.4.1	Plasmids . . . . .	18
2.1.4.2	Primers . . . . .	18
2.2	Methods . . . . .	19
2.2.1	Molecular biology . . . . .	19
2.2.1.1	Competent cells . . . . .	19
2.2.1.2	Glycerol stocks . . . . .	19
2.2.1.3	Purification of plasmid DNA . . . . .	19
2.2.1.4	PCR, agarose gel electrophoresis, and PCR purification . . . . .	20
2.2.1.5	Restriction, ligation and transformation . . . . .	21
2.2.1.6	Expression of recombinant proteins . . . . .	21
2.2.2	Protein purification and analysis . . . . .	22
2.2.2.1	General . . . . .	22
2.2.2.2	Assessment of protein concentration . . . . .	22
2.2.2.3	SDS-PAGE . . . . .	22
2.2.2.4	Purification of T3D $\sigma 1$ . . . . .	23
2.2.2.5	Purification of JAM-A . . . . .	25
2.2.2.6	Purification of the T3D $\sigma 1$ -JAM-A D1 complex . . . . .	27
2.2.2.7	Purification of the T1L $\sigma 1$ -JAM-A D1 complex . . . . .	27
2.2.2.8	Analytical scale size-exclusion chromatography . . . . .	28
2.2.3	X-ray crystallography . . . . .	29
2.2.3.1	Crystallization and crystal freezing . . . . .	29
2.2.3.2	X-rays and data collection . . . . .	31
2.2.3.3	Data processing . . . . .	33
2.2.3.4	Structure determination . . . . .	35
2.2.3.5	Structure refinement . . . . .	38
2.2.4	Analytical ultracentrifugation . . . . .	41
2.2.4.1	Sample preparation . . . . .	41
2.2.4.2	Sedimentation velocity experiments . . . . .	41
2.2.4.3	Sedimentation equilibrium experiments . . . . .	42
<b>3</b>	<b>Results</b> . . . . .	<b>45</b>
3.1	T3D $\sigma 1$ D345N . . . . .	45
3.1.1	Purification and crystallization of T3D $\sigma 1$ D345N . . . . .	45
3.1.2	Structural and functional analysis of T3D $\sigma 1$ D345N . . . . .	47
3.1.2.1	Structure of T3D $\sigma 1$ D345N . . . . .	47
3.1.2.2	Binding of T3D $\sigma 1$ D345N to JAM-A . . . . .	48
3.2	T3D $\sigma 1$ -JAM-A complex . . . . .	49
3.2.1	Purification of the T3D $\sigma 1$ -JAM-A complex . . . . .	49
3.2.1.1	Purification of T3D $\sigma 1$ and JAM-A D1 . . . . .	49
3.2.1.2	Generation of the T3D $\sigma 1$ -JAM-A complex . . . . .	51
3.2.2	Structure and stability of the T3D $\sigma 1$ -JAM-A complex . . . . .	51
3.2.2.1	Structure determination of the T3D $\sigma 1$ -JAM-A complex . . . . .	51
3.2.2.2	Overall structure of the T3D $\sigma 1$ -JAM-A complex . . . . .	52

3.2.2.3	Contacts in the T3D $\sigma$ 1-JAM-A interface . . . . .	54
3.2.2.4	Stability of the T3D $\sigma$ 1-JAM-A complex . . . . .	56
3.3	T1L $\sigma$ 1-JAM-A complex . . . . .	58
3.3.1	Purification of the T1L $\sigma$ 1 complex . . . . .	58
3.3.2	Structure determination of the T1L $\sigma$ 1-JAM-A complex . . . . .	59
3.3.3	Structure of the T1L $\sigma$ 1-JAM-A complex . . . . .	61
3.3.3.1	Structure of T1L $\sigma$ 1 . . . . .	61
3.3.3.2	The T1L $\sigma$ 1-JAM-A interface . . . . .	63
3.4	Stability of the JAM-A homodimer . . . . .	65
3.4.1	Mixing of JAM-A D1 and D1D2 . . . . .	65
3.4.2	Analytical ultracentrifugation . . . . .	66
<b>4</b>	<b>Discussion</b>	<b>67</b>
4.1	The aspartic acid cluster . . . . .	67
4.1.1	Mutations in the aspartic acid sandwich . . . . .	67
4.1.2	Comparison of T1L and T3D $\sigma$ 1 . . . . .	68
4.1.3	The aspartic acid cluster as a molecular switch . . . . .	68
4.2	The reovirus $\sigma$ 1-JAM-A complex . . . . .	71
4.2.1	Disruption of JAM-A homodimers . . . . .	71
4.2.2	Cell attachment by reovirus T3D $\sigma$ 1 . . . . .	73
4.2.3	Mutations in the $\sigma$ 1-JAM-A interface . . . . .	74
4.2.4	Related virus-receptor complexes . . . . .	75
4.2.4.1	Comparison to the adenovirus fiber-CAR complex . . . . .	75
4.2.4.2	JAM-A and CAR as receptors for other viruses . . . . .	77
4.2.5	Ig superfamily members as viral receptors . . . . .	77
<b>5</b>	<b>Outlook</b>	<b>79</b>
<b>6</b>	<b>Appendix</b>	<b>81</b>
6.1	Protein sequences and structures . . . . .	81
6.2	Crystallographic statistics and structure quality . . . . .	82
6.2.1	T3D $\sigma$ 1 D345N . . . . .	82
6.2.2	T3D $\sigma$ 1-JAM-A complex . . . . .	83
6.2.3	T1L $\sigma$ 1-JAM-A complex . . . . .	85
6.3	Analytical ultracentrifugation . . . . .	86
<b>7</b>	<b>References</b>	<b>87</b>
	<b>Publications</b>	<b>99</b>
	<b>Acknowledgments</b>	<b>100</b>
	<b>Academic teachers</b>	<b>101</b>
	<b>Curriculum vitae</b>	<b>102</b>

# Abbreviations

The commonly used abbreviations are used for chemical and physical units, the chemical elements, the essential amino acids as well as the bases occurring in DNA.

Ad	adenovirus
APS	ammonium persulfate
ASU	asymmetric unit
CAR	coxsackievirus and adenovirus receptor
CCD	charge-coupled device
CHES	N-cyclohexyl-2-aminoethanesulfonic acid
CNS	central nervous system
DNA	desoxyribonucleic acid
dNTP	desoxynucleotide triphosphates
ds	double-stranded
<i>E. coli</i>	Escherichia coli
EDTA	ethylenediaminetetraacetic acid
f	feline
FPLC	fast protein liquid chromatography
GSH	glutathione
GST	glutathione S-transferase
h	human
HEPES	4-(2-hydroxyethyl)-1-piperazineethanesulfonic acid
HIV	human immunodeficiency virus
Ig	immunoglobulin
IPTG	isopropyl $\beta$ -D-1-thiogalactopyranoside
ISVP	infectious/intermediate subvirion particle
JAM-A	junctional adhesion molecule-A
$K_D$	dissociation constant
LB	Luria Bertani
<i>LLG</i>	log likelihood gain
m	murine
MES	2-(N-morpholino) ethanesulfonic acid
MPD	2-methyl-2,4-pentanediol
Nco	<i>Nocardia corallina</i>

NCS	non-crystallographic symmetry
OD <sub>600</sub>	optical density at 600 nm
PCR	polymerase chain reaction
PEG	polyethylene glycol
Pfu	<i>Pyrococcus furiosus</i>
PMSF	phenylmethanesulphonyl fluoride
r. m. s. d.	root mean square deviation
RNA	ribonucleic acid
rpm	revolutions per minute
RT	room temperature
SA	sialic acid
SAP	shrimp alkaline phosphatase
SDS-PAGE	sodium dodecyl sulfate polyacrylamide gel electrophoresis
SE	sedimentation equilibrium
SLS	Swiss Light Source
SOB	super optimal broth
ss	single-stranded
SSM	secondary-structure matching
SV	sedimentation velocity
T1L	type 1 Lang
T2J	type 2 Jones
T3D	type 3 Dearing
T <sub>A</sub>	annealing temperature
TAE	Tris-acetate EDTA
Taq	<i>Thermus aquaticus</i>
TEMED	tetramethylethylenediamine
TfB	transforming buffer
Tris	tris(hydroxymethyl)aminomethane
UV	ultraviolet
VSV	vesicular stomatitis virus
wt	wild-type
Xho	<i>Xanthomonas holcicola</i>

# 1. Introduction

## 1.1. Viruses

The general information about viruses in this section is based on the book “Molekulare Virologie” by Susanne Modrow, Dietrich Falke, and Uwe Truyen (Modrow *et al.*, 2003).

### 1.1.1. Definition and structure

Viruses are infectious entities ranging from 16 to more than 300 nm in size. In contrast to cells, viruses do not divide in order to proliferate. Instead, they replicate inside the cells that they infect and can thus be termed intracellular parasites. They modify cellular processes and use them for their own replication. Therefore, it is not necessary for the viral genome to encode proteins for protein synthesis (e. g., ribosomes) or components of the energy generating metabolism. The viral gene products comprise the structural components of the virus, and may also contain regulatory proteins (e. g., transactivators) and enzymes (e. g., polymerases).

The shells of viral particles (capsids) are composed of proteins, with some virus types also containing a lipid bilayer membrane, the viral envelope. The membrane of these enveloped viruses is derived from the plasma membrane of infected cells, and contains viral and cellular proteins that are often glycosylated. The genetic material of viruses consists of single- or double-stranded (ss or ds) RNA or DNA and is organized as a linear, circular, or segmented genome.

Infection of a cell by a virus can have variable consequences: The cell can be destroyed and dies. It can also survive the infection, with or without releasing new viruses. As some viruses integrate their genes into the genome of the infected cell, the cells can also become immortal, dividing continuously. This transformation is a first step in the generation of virus-induced tumors.

### 1.1.2. Icosahedral symmetry

The protein shell, or capsid, that encloses the viral genome is in most cases either spherical or rod-shaped. While a rod-shaped capsid possesses helical symmetry, the more frequently occurring spherical capsids usually exhibit icosahedral symmetry which can be described by three rotation axes. A three-fold symmetry axis is located at each of the 20 triangles forming the icosahedron, a two-fold at the edges of the triangles, and a five-fold at the 12 icosahedral vertices.

If all 20 triangles forming an icosahedron are to make the same contacts to all their neighboring triangles, they have to be divided into three equivalent subunits. Therefore, 60 identical molecules are necessary to form the most simple form of an icosahedral virus. However, building a viral capsid with 60 subunits would require capsid proteins that are large and very complex. Therefore, most viruses use more than 60 non-identical subunits for capsid formation. As the subunits in these cases make similar, but not equivalent contacts, they are called quasi-equivalent. The principles of capsid composition of icosahedral viruses have been described by Caspar and Klug in 1962 (Caspar & Klug, 1962). They deduced the triangulation number  $T$  for description of capsid composition. For the most simple case of an icosahedron formed by 60 subunits,  $T = 1$ . The number  $n$  of subunits forming the viral icosahedron is  $n = 60 \times T$ . Allowed values for  $T$  are described by  $T = h^2 + hk + k^2$ , with  $h$  and  $k$  being integers, and  $h \geq k$ .  $h$  and  $k$  can be determined by counting the number of subunits when going from one five-fold to the next five-fold axis via six-fold symmetry axes generated by the subunits (figure 1.1). Thereby,  $h$  and  $k$  point in different directions. For values of  $T$  greater than 3, two possibilities exist for the  $h$  and  $k$  vectors, *dextro* and *laevo*, resulting in icosahedrons that are mirror images of each other.

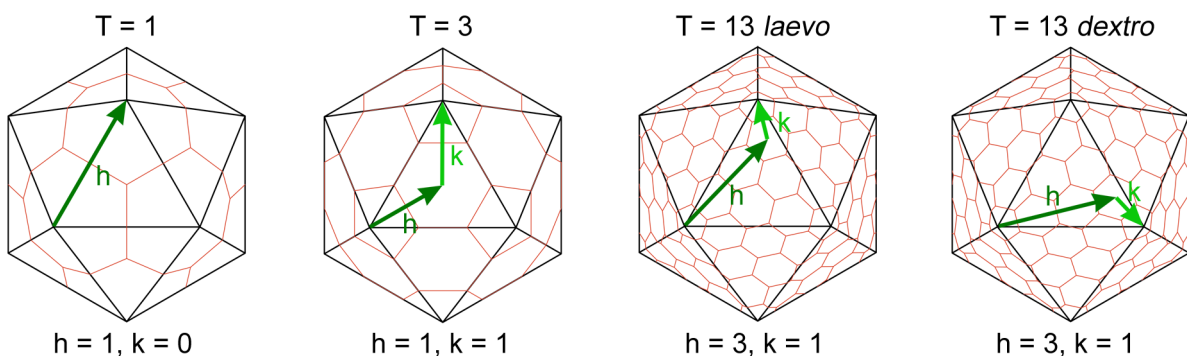


Figure 1.1: **Triangulation numbers of viral capsids.** Icosahedrons and capsid composition for different values of  $T$ . The icosahedral models were obtained from the icosahedral server ([http://viperdb.scripps.edu/icos\\_server.php](http://viperdb.scripps.edu/icos_server.php)).

### 1.1.3. Viral life cycle

The first step in viral infection of cells is the attachment to a receptor. Viruses use proteins or carbohydrates present on cellular surfaces as receptors. As the viral receptors are not always expressed on all cell types, receptor specificity often determines the tropism of viruses. For example, the receptor for human immunodeficiency virus (HIV), CD4, is nearly exclusively expressed on the surface of effector T cells and macrophages.

Uptake of non-enveloped viruses is usually mediated by endocytosis, often followed by sorting of the viruses into endosomes. In order to deliver the viral genome into the cytoplasm for replication, these viruses cleverly use the low pH environment of the endosome and endosomal proteases to trigger conformational changes and disassembly of the viral capsid. This leads to penetration of the endosomal membrane. Enveloped viruses follow two main strategies for entry, fusion of the viral envelope with either the plasma membrane or the endosomal membrane after receptor-mediated endocytosis. In both cases, the viral capsid is delivered into the cytoplasm. Receptor binding at the cell surface or the low pH environment of the endosome trigger conformational changes that lead to fusion of the viral envelope with the plasma membrane or the endosomal membrane, respectively.

Generally, viral DNA is transferred to the nucleus for replication, while viral RNA remains in the cytoplasm, but there are also many viruses not obeying this rule. The genome of positive-sense ssRNA viruses can be directly translated to proteins, producing among other proteins an RNA-dependent RNA polymerase that can subsequently replicate the viral genome. Negative-sense ssRNA viruses, however, have to bring their RNA-dependent RNA polymerase with them to produce positive-sense RNA from which the viral proteins can be translated. dsRNA viruses, such as reoviruses, also carry an RNA-dependent RNA polymerase in their capsids. The polymerase produces mRNA from the viral RNA that also serves as template for the synthesis of viral dsRNA. Thereby, these viruses use the unusual principle of conservative replication, i. e., the newly synthesized RNA does not contain a strand of the parental RNA. The RNA of retroviruses is transcribed to dsDNA by an RNA-dependent DNA polymerase and integrated in the genome of the host cell.

After expression of the structural proteins and replication of the viral genome, new viruses can be assembled. This process depends mostly on interactions among the different structural components and does not require the help of cellular enzymes. However, recent studies indicate that cellular chaperones might aid in the assembly process. Enveloped viruses are usually released from the cells by budding, where cellular membranes enclose the capsids. Non-enveloped viruses lyse the infected cells in order to be released.

## 1.2. Reoviruses

The *Reoviridae* are a family of non-enveloped viruses. Their name was deduced from “respiratory enteric orphan viruses,” because the first reoviruses were isolated from human respiratory and intestinal tracts, and no reovirus-associated disease was known (Sabin, 1959). Today, the *Reoviridae* also include viruses infecting insects, fish, and plants (Fields *et al.*, 1996). Orthoreoviruses, orbiviruses, and rotaviruses are among the most important family members. Within the orthoreovirus subfamily, viruses infecting mammals and birds can be distinguished. Mammalian orthoreoviruses, in the following referred to as reoviruses, are prototype members of the *Reoviridae* family.

Reoviruses infect respiratory and intestinal tracts but cause disease primarily in the very young (Mann *et al.*, 2002; Tardieu *et al.*, 1983; Tyler *et al.*, 2004). Three reovirus serotypes have been described, represented by the prototype strains type 1 Lang (T1L), type 2 Jones (T2J), and type 3 Dearing (T3D). Recently, another reovirus serotype was identified by protein sequence analysis. The Ndelle virus, originally assigned to the genus orbivirus, was reclassified as T4N (Attoui *et al.*, 2001).

The central nervous system (CNS) of newborn mice serves as a model system for studies of viral neuropathogenesis. Reovirus uptake occurs in the intestine. From there, the virus travels to the CNS and produces serotype-specific disease patterns (Morrison *et al.*, 1991; Tyler *et al.*, 1986; Weiner *et al.*, 1977, 1980): T1L travels to the CNS by hematogenous routes, infects ependymal cells, and causes nonlethal hydrocephalus. T3D uses primarily neural routes, infecting neurons, and leads to fatal encephalitis. As T2J is difficult to cultivate, little is known about the disease pattern of this serotype.

### 1.2.1. Reovirus structure

Reoviruses form non-enveloped, icosahedral particles, about 85 nm in diameter, that contain a segmented dsRNA genome. The ten dsRNA segments are named according to their length and consist of three large (L), three medium (M), and four small (S) segments (Shatkin *et al.*, 1968). They encode eleven proteins, named after their gene segments, *lambda* ( $\lambda$ ) for L, *mu* ( $\mu$ ) for M, and *sigma* ( $\sigma$ ) for S. Each gene segment encodes one protein, with the exception of S1, which encodes both  $\sigma$ 1 and  $\sigma$ 1s.

Only three of the encoded proteins are non-structural,  $\mu$ NS,  $\sigma$ NS, and  $\sigma$ 1s. The remaining proteins form two concentric shells, the outer capsid and the inner core (Dryden *et al.*, 1993). The inner core is an icosahedron with  $T = 1$ . It is formed by 60 asymmetric dimers of  $\lambda$ 1 with a high degree of non-equivalence in the inter-subunit contacts (Reinisch

*et al.*, 2000). 150 monomers of  $\sigma 2$  stabilize the capsid at three non-equivalent sites of the  $\lambda 1$  lattice (Reinisch *et al.*, 2000). The core is completed by ca. 24 copies of  $\mu 2$  and 12 copies of RNA-dependent RNA polymerase  $\lambda 3$  (Coombs, 1998; Dryden *et al.*, 1998). Pentamers of  $\lambda 2$  form turrets at the icosahedral vertices, spanning both the inner core and the outer capsid. The outer capsid (figure 1.2) exhibits fenestrated quasi  $T = 13$  *laevo* icosahedral symmetry, with the lattice being interrupted at the five-fold axes by the  $\lambda 2$  turrets. It is composed of 200 heterohexamers of  $\mu 1$  and  $\sigma 3$  ( $\mu 1_3\sigma 3_3$ ), (Dryden *et al.*, 1998; Liemann *et al.*, 2002; Metcalf, 1982).  $\mu 1$  is the membrane-penetration protein, and  $\sigma 3$  serves as a protective cap for  $\mu 1$ . At each icosahedral vertex, a trimer of reovirus attachment protein  $\sigma 1$  is anchored into a  $\lambda 2$  pentamer. The filamentous  $\sigma 1$  molecules protrude about 40 nm from the virion surface (Furlong *et al.*, 1988). With the exception of  $\sigma 1$ , the protein sequences of the viral proteins are 86-99 % identical among the reovirus serotypes (Dermody *et al.*, 1991; Seliger *et al.*, 1992; Wiener & Joklik, 1989). It is therefore not surprising that  $\sigma 1$  is the major determinant of the distinct tropism exhibited by the reovirus serotypes (Weiner *et al.*, 1980).

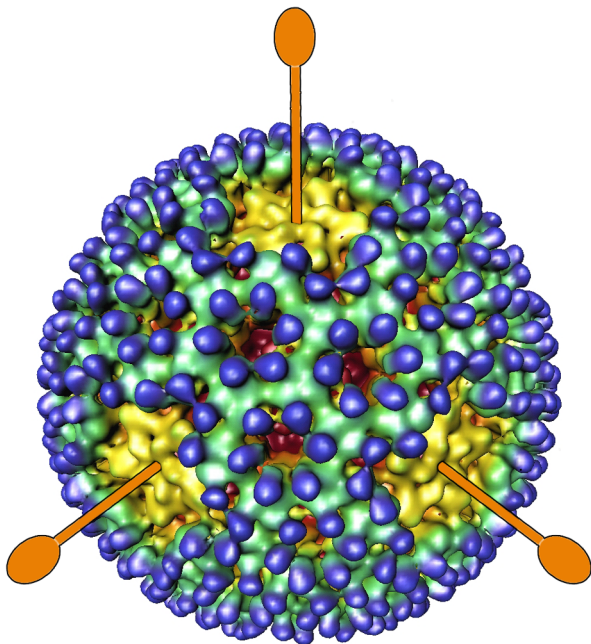


Figure 1.2: **T3D reovirus virion.** Cryo-electron microscopy reconstruction of a reovirus virion.  $\lambda 2$  pentamers are colored yellow,  $\sigma 3$  blue, and  $\mu 1$  green.  $\sigma 1$  (orange) is shown schematically. Figure modified from Nason *et al.* (2001).

## 1.2.2. Infection of cells

### 1.2.2.1 Attachment and entry

Reoviruses use both proteinaceous and carbohydrate receptors for attachment to cells. Receptor engagement is mediated by the attachment protein  $\sigma 1$ . The three prototype strains and all additionally tested field isolate strains use junctional adhesion molecule-A (JAM-A) as a receptor (Barton *et al.*, 2001b; Campbell *et al.*, 2005). In addition, T3D reovirus is known to bind  $\alpha 2,3$ - and  $\alpha 2,6$ -linked cell-surface sialic acid (SA) (Barton *et al.*, 2001a; Gentsch & Pacitti, 1987; Paul *et al.*, 1989). T1L is known to bind carbohydrates, but not SA (Chappell *et al.*, 2000). In contrast, it is still unclear if T2J uses carbohydrates as a receptor.

Reovirus cell attachment follows a multistep adhesion strengthening mechanism (Barton *et al.*, 2001a). Low-affinity binding to carbohydrate, adhering the virus to the cell surface, allows access and high-affinity binding to JAM-A (figure 1.3). Reovirus is internalized by receptor-mediated endocytosis, most likely utilizing a clathrin-dependent pathway (Borsa *et al.*, 1979, 1981; Ehrlich *et al.*, 2004; Sturzenbecker *et al.*, 1987). Uptake is mediated by  $\beta 1$  integrins (Maginnis *et al.*, 2006, 2008), which presumably bind reovirus  $\lambda 2$  via conserved integrin-binding motifs RGD and KGE (Breun *et al.*, 2001; Seliger *et al.*, 1987). The NPXY motifs in the cytoplasmic tail of the  $\beta 1$  integrins are necessary for targeting reovirions to the precise endocytic organelle that leads to functional disassembly (Maginnis *et al.*, 2008).

### 1.2.2.2 Disassembly and transfer to the cytoplasm

In the endosome, reovirus virions are disassembled in several steps (figure 1.3).  $\sigma 3$  is removed proteolytically,  $\sigma 1$  changes its conformation, and  $\mu 1$  is cleaved into N- and C-terminal fragments  $\mu 1N$  and  $\mu 1C$ , followed by cleavage of  $\mu 1C$  into  $\delta$  and  $\phi$  (Chang & Zweerink, 1971; Silverstein *et al.*, 1972; Sturzenbecker *et al.*, 1987). This results in the formation of the infectious subvirion particle (ISVP). ISVPs can also be generated in the intestinal lumen after peroral inoculation of mice. There, ISVPs form as a result of cleavage with the proteases chymotrypsin and trypsin (Bass *et al.*, 1990; Bodkin *et al.*, 1989). These ISVPs can penetrate the plasma membrane directly and do not require uptake by endocytosis, although infection using this pathway is not as efficient as endosomal uptake (Hooper & Fields, 1996; Lucia-Jandris *et al.*, 1993).

The endosomal ISVP is then converted to another intermediate, the ISVP\* (figure 1.3). Attachment protein  $\sigma 1$  is released, the  $\mu 1$   $\delta$  fragment changes its conformation, and

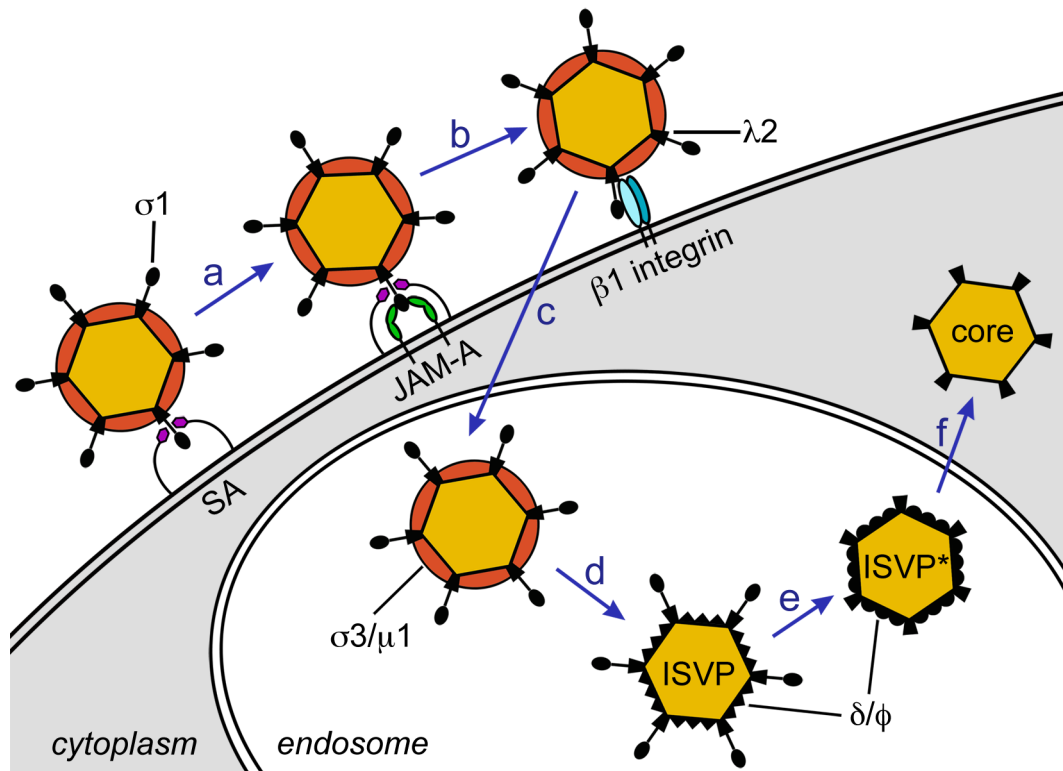


Figure 1.3: **The T3D reovirus entry pathway.** After low-affinity binding to sialic acid (SA), reovirus virions bind with high affinity to JAM-A (a). It is still unclear at which stage the receptors are released from the virion. Reovirus enters the cell by receptor-mediated endocytosis via a  $\beta 1$  integrin-dependent pathway. (b, c). In the low pH environment of the endosome, the outer capsid is cleaved by proteases. The loss of  $\sigma 3$  and cleavage of  $\mu 1$  into  $\mu 1N$  and  $\mu 1C$ , followed by cleavage of  $\mu 1C$  into  $\delta$  and  $\phi$ , yields the ISVP (d). The ISVP\* is formed by conformational rearrangements of the  $\mu 1$  cleavage fragments, exposing hydrophobic residues, and release of  $\mu 1N$  and  $\sigma 1$  (e). The  $\mu 1$  cleavage fragments mediate release of the core into the cytoplasm (f).

the overall hydrophobicity of the particle increases (Chandran *et al.*, 2002). Endosomal membrane penetration is mediated by fragments of the  $\mu 1$  protein. Autocatalytic cleavage of  $\mu 1$  into  $\mu 1N$  and  $\mu 1C$ , followed by release of  $\mu 1N$ , is required for membrane penetration (Odegard *et al.*, 2004).  $\mu 1N$  is a myristoylated hydrophobic peptide that is buried in the hydrophobic core of  $\mu 1$  prior to cleavage (Liemann *et al.*, 2002).  $\mu 1N$  forms pores in the membrane, facilitated by the presence of another  $\mu 1$  cleavage fragment,  $\phi$  (Ivanovic *et al.*, 2008). The pores are enlarged by an yet unknown mechanism, allowing the viral particles to escape into the cytosol. After removal of the remaining  $\mu 1$  cleavage fragments, the transcriptionally active core remains.

Activation of innate immune transcription factors NF- $\kappa$ B and IRF-3 induces apoptosis in cells infected by reovirus (Connolly *et al.*, 2000; Holm *et al.*, 2007). After penetration

of the endosomal membrane, the  $\mu 1$  cleavage fragment  $\phi$  activates NF- $\kappa$ B and initiates prodeath signaling (Danthi *et al.*, 2008). Activation of IRF-3 appears to be triggered by viral genomic dsRNA (Holm *et al.*, 2007).

### 1.2.3. The attachment protein of reovirus

#### 1.2.3.1 The structure of $\sigma 1$

The reovirus attachment protein  $\sigma 1$  forms a filamentous trimer, about 50 nm in length, with a globular C-terminal head and an elongated N-terminal tail (Fraser *et al.*, 1990). The structure of the C-terminal portion of T3D  $\sigma 1$  has been determined by X-ray crystallography (figure 1.4 A) (Chappell *et al.*, 2002). The head, consisting of residues 310-455, folds into two Greek-key motifs that assemble into an eight-stranded  $\beta$ -barrel. Apart from the loop between  $\beta$ -strands D and E (D-E loop), which contains a  $3_{10}$ -helix, the loops connecting the individual  $\beta$ -strands are short. Residues 246-309 of the tail form a triple  $\beta$ -spiral, where two antiparallel  $\beta$ -strands are connected by a short  $\beta$ -turn of four amino acids  $i$  to  $i + 3$ , with a conserved proline or glycine at position  $i + 2$ . Repeating units of this motif are connected by insertions of variable length. The triple  $\beta$ -spiral motif has been observed to date only in three other fibrous viral proteins: adenovirus fiber (van Raaij *et al.*, 1999), bacteriophage PRD1 (Merckel *et al.*, 2005), and avian reovirus  $\sigma C$  (Guardado Calvo *et al.*, 2005).

Sequence analysis suggests that  $\sigma 1$  residues N-terminal to the crystallized part (167-245) fold into five additional  $\beta$ -spiral repeats or a combination of  $\beta$ -spiral repeats and  $\alpha$ -helical coiled coil (Chappell *et al.*, 2002; Nibert *et al.*, 1990). The latter possibility is supported by a narrowing in this region observed in composite negative-stain electron micrographs (Fraser *et al.*, 1990) and recent structural data (Dirk Reiter, unpublished results). N-terminal to the  $\beta$ -spiral region, the sequence exhibits a repeating heptad sequence motif. This region is therefore predicted to form an amphipatic  $\alpha$ -helix, assembling into a trimeric  $\alpha$ -helical coiled coil (Nibert *et al.*, 1990). A short hydrophobic sequence at the N-terminus of  $\sigma 1$  presumably serves to anchor the protein into the  $\lambda 2$  pentamers on the virion surface (Dryden *et al.*, 1993; Furlong *et al.*, 1988).

Electron microscopy images and the crystal structure of  $\sigma 1$  display discrete regions of flexibility along the  $\sigma 1$  trimer that could aid in reovirus receptor engagement (Chappell *et al.*, 2002; Fraser *et al.*, 1990). One such region is located between the first and second  $\beta$ -spiral repeat below the head, another in the transition region between predicted  $\beta$ -spiral and  $\alpha$ -helical coiled coil, and one at the N-terminus of the molecule.

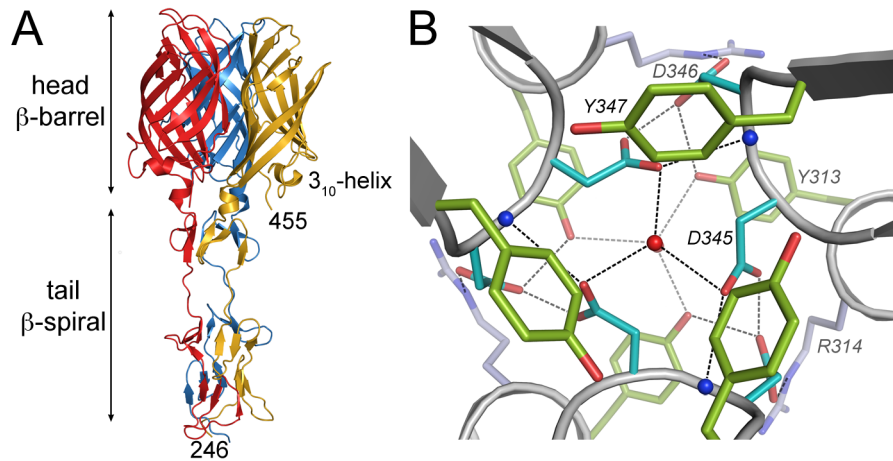


Figure 1.4: **Structure of T3D  $\sigma$ 1 and the aspartic acid cluster.** (A) Ribbon drawing of the T3D  $\sigma$ 1 trimer (Chappell *et al.*, 2002), with monomers shown in red, blue and yellow. (B) View of the aspartic acid cluster along the trimer axis from the top of the molecule (Schelling *et al.*, 2007). Oxygen atoms are colored red, nitrogen atoms blue. Water molecules are depicted as red, main chain nitrogen atoms of D346 as blue spheres. The water molecules are located on the trimer axis and thus only the upper one is clearly visible. Hydrogen bonds and salt bridges are shown as dotted lines.

The carbohydrate binding sites of  $\sigma$ 1 have been mapped to locations in the center of the molecule in the  $\beta$ -spiral region for T3D (residues 198, 202, and 204) and N-terminal to the head domain for T1L  $\sigma$ 1 (Chappell *et al.*, 1997, 2000). JAM-A binds to the  $\sigma$ 1 head (Barton *et al.*, 2001b; Schelling *et al.*, 2007). As all reovirus serotypes tested to date use JAM-A as a receptor (Barton *et al.*, 2001b; Campbell *et al.*, 2005), the JAM-A binding region was expected to be located at a conserved region of the protein. The largest region conserved between the reovirus serotypes is located around the  $\sigma$ 1  $3_{10}$ -helix in the D-E loop, which was therefore predicted to be part of the JAM-A binding site (Chappell *et al.*, 2002).

### 1.2.3.2 The aspartic acid cluster

The interface of the  $\sigma$ 1 trimer buries a surface area of about  $450 \text{ \AA}^2$  for each monomer and contains few conserved residues (Chappell *et al.*, 2002). The hydrophilic contact area is interrupted by a large water filled cavity along the trimer axis, about  $15 \text{ \AA}$  in height and  $10 \text{ \AA}$  in width (Schelling *et al.*, 2007). The cavity is sealed at the base of the head domain by an unusual arrangement of conserved aspartic acid residues, the aspartic acid cluster (figure 1.4B). Two aspartic acids, Asp345 and Asp346, are arranged in close proximity. The aspartic acids are located on the  $\beta$ -hairpin between  $\beta$ -strands B and C, with their

side chains pointing towards the center of the trimer. Two water molecules are located above and below the aspartic acid cluster. The six aspartic acids are sandwiched between two layers, each containing three tyrosines (Tyr313 and Tyr347), that shield the aspartic acid cluster from solvent. The Asp346 side chains form salt bridges with Arg314 from neighboring monomers. The Asp345 side chains contact the main chain nitrogens and carboxylate oxygens of the neighboring Asp346, but are not engaged in ionic interactions that would neutralize their negative charges. The location of these aspartic acids suggests therefore that they are protonated to avoid an accumulation of negative charge at the trimer interface. Molecular dynamics studies of T3D  $\sigma 1$  also indicate that Asp345 has to be protonated to allow trimerization of the  $\sigma 1$  head domain (Cavalli *et al.*, 2004).

Accumulating evidence suggests that conformational changes occur in  $\sigma 1$  during the entry process (Dryden *et al.*, 1993; Furlong *et al.*, 1988; Nibert *et al.*, 1995). The aspartic acid cluster could therefore conceivably act as a molecular switch between a trimerized and partly detrimerized  $\sigma 1$  (Schelling *et al.*, 2007). Neutral pH would not allow trimer formation, but low pH would favor trimerization. Once the trimer is formed, it is likely also stable at neutral pH, because the aspartic acid cluster is shielded from solvent. A similar pH dependent trimerization motif has been observed in the G protein of vesicular stomatitis virus (VSV G) (Roche *et al.*, 2006, 2007). The low pH form of VSV G also possesses an aspartic acid cluster at its trimer axis, although the three aspartic acids are located on  $\alpha$ -helices, not on  $\beta$ -hairpins. Trimerization of the VSV G aspartic acid cluster region is induced by low pH, leading to a substantial conformational change that triggers membrane fusion.

#### 1.2.4. Reoviruses as therapeutic agents

Determination of the molecular aspects of virus-receptor interactions enables the use of viruses in gene delivery for vaccines or therapeutic applications. Adenovirus-based vectors are today the viruses most widely tested in gene therapy approaches (Edelstein *et al.*, 2007). However, the targets for these vectors are limited to cells expressing adenovirus receptors. The structural analysis of reovirus  $\sigma 1$  and JAM-A revealed striking similarities to adenovirus attachment protein fiber and the coxsackievirus and adenovirus receptor, CAR, respectively (Stehle & Dermody, 2003, 2004). Given these similarities, generation of chimeric adenoviruses allows for the development of novel targets in gene therapy. Chimeric adenoviruses that express reovirus  $\sigma 1$  instead of fiber as their attachment protein could be retargeted from cells expression CAR to cells expressing JAM-A (Mercier *et al.*, 2004).

Furthermore, new approaches in cancer therapy make use of the oncolytic potential of viruses. Reovirus is one of the viruses capable of lysing tumor cells (Norman & Lee, 2000). Moreover, reovirus infects transformed cells more efficiently than non-transformed cells (Duncan *et al.*, 1978). In animal models, reovirus was successfully employed as a cancer therapeutic (Coffey *et al.*, 1998; Hirasawa *et al.*, 2002). It is now explored in Phase II clinical trials as a therapeutic virus against Ras-mediated human cancers (Stoeckel & Hay, 2006).

## 1.3. Junctional adhesion molecule-A

### 1.3.1. Function of JAM-A

JAM-A is used as a cellular receptor by all reovirus serotypes tested to date (Barton *et al.*, 2001b; Campbell *et al.*, 2005). In addition, feline calicivirus uses the feline homologue of JAM-A as a receptor (Makino *et al.*, 2006). JAM-A is a dimeric molecule located at tight junctions between endothelial and epithelial cells (Liu *et al.*, 2000; Martín-Padura *et al.*, 1998) and on the surface of platelets and leukocytes (Williams *et al.*, 1999). It regulates the migration of leukocytes across endothelial and epithelial barriers in response to inflammations (Del Maschio *et al.*, 1999; Woodfin *et al.*, 2007).

Tight junctions (reviewed in Tsukita *et al.* (2001)) are regions of cell-cell contact in vertebrates that serve three basic functions: holding cells together, blocking movement of integral membrane proteins to preserve specific functions of the basolateral and apical cell surfaces, and preventing the movement of molecules and ions through the space between cells. The most abundant proteins in tight junctions are claudins and occludin. They are integral membrane proteins and associate with intracellular membrane proteins (ZO proteins) that serve to anchor the junctions to the actin cytoskeleton. The JAM-A ectodomain interacts with leukocyte function-associated antigen-1 (LFA-1) (Ostermann *et al.*, 2002). The cytoplasmic tail of JAM-A contains a PDZ binding motif (Liu *et al.*, 2000; Martín-Padura *et al.*, 1998) and interacts with adaptor protein ZO-1 (Ebnet *et al.*, 2003).

### 1.3.2. JAM-A structure

JAM-A consists of two extracellular immunoglobulin (Ig)-like domains, a single transmembrane region, and a cytoplasmic tail (Martín-Padura *et al.*, 1998; Williams *et al.*, 1999). The crystal structures of the murine (m) and human (h) JAM-A extracellular

domains, D1 and D2, have been determined (figure 1.5 A) (Kostrewa *et al.*, 2001; Prota *et al.*, 2003). D1 belongs to the V-set, D2 to the I-set of Ig-like domains (section 4.2.5). JAM-A dimerizes via the membrane-distal D1 domains. The dimer interface is formed by the  $\beta$ -sheet composed of  $\beta$ -strands G, F, C, and C', and contains two hydrogen bonds and four salt bridges (figure 1.5B). The surprisingly large number of ionic contacts at the interface likely reflects the dynamic nature of the JAM-A dimer necessary for regulation of tight junction permeability. It is still unclear how this regulation is performed *in vivo*, but the influence of the charged residues can be demonstrated by subjecting JAM-A to non-physiologic conditions of low pH and moderately high ionic strength. These conditions lead to dissociation of the homodimers (Bazzoni *et al.*, 2000).

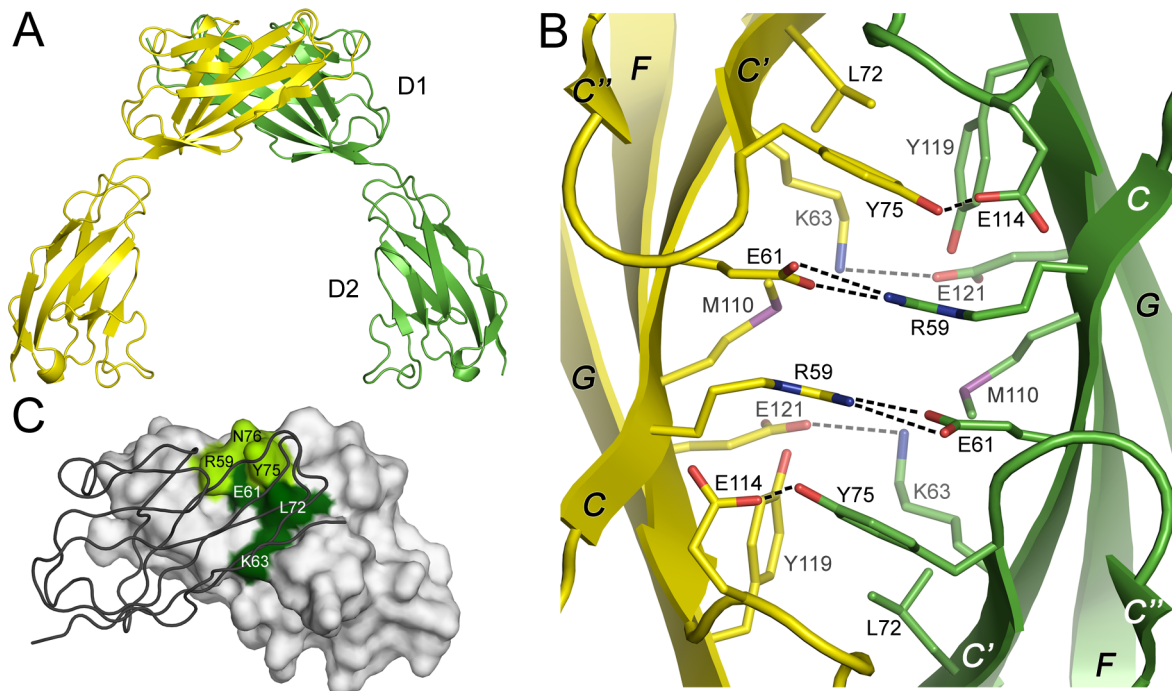


Figure 1.5: **JAM-A structure and predicted  $\sigma 1$  binding site.** (A) Ribbon drawing of the hJAM-A dimer. (B) Interface between two JAM-A monomers, viewed along the crystallographic dyad. Contact residues are located in the GFCC' faces of two D1 domains. Oxygen atoms are shown in red, nitrogen atoms in blue, and sulfur atoms in purple. Dashed lines represent hydrogen bonds and salt bridges. (C) View of the dimeric JAM-A D1 domain, oriented as in A. One monomer is shown as a space-filling representation. The opposing monomer is shown as a ribbon drawing. Residues required for efficient engagement of JAM-A by reovirus T3D are colored dark green; light green colored residues likely serve as additional contacts. Figure modified from Guglielmi *et al.* (2007), Prota *et al.* (2003).

### 1.3.3. Predicted binding site for $\sigma 1$

Crosslinking experiments of JAM-A dimers suggest that the binding site for reovirus attachment protein  $\sigma 1$  is located within the JAM-A homodimer interface (Forrest *et al.*, 2003). Crosslinking of JAM-A diminishes the capacity of reovirus to bind JAM-A both *in vitro* and on cells. Furthermore, it reduces the competitive effects of soluble JAM-A on reovirus attachment. Initial mutational studies of residues located on the JAM-A surface identified residues Ser57 and Tyr75 as important contributors for reovirus binding (Forrest *et al.*, 2003). Tyr75 is part of the JAM-A homodimer interface and Ser57 is located near the interface. Various JAM-A point mutants were analyzed using infectivity assays and surface plasmon resonance (Guglielmi *et al.*, 2007). This led to the identification of several additional residues in the JAM-A dimer interface that contribute to  $\sigma 1$  binding (figure 1.5 C). Glu61, Lys63, and Leu72 are required for efficient engagement of JAM-A by T3D reovirus, and Arg59, Tyr75, and Asn76 likely serve as additional contacts.

## 1.4. Aims

The major objective of this work was to understand how changes in the conformation of a viral attachment protein aid in viral entry and how a pathogenic virus engages its cell-surface receptor. Structural and functional analyses of reovirus attachment protein  $\sigma 1$  both alone and in complex with reovirus receptor JAM-A were conducted. The experiments summarized in this thesis sought to answer the following questions:

- How does a mutation in the aspartic acid cluster change the structure and the receptor binding properties of  $\sigma 1$ ?
- Does the mutation support the theory that the aspartic acids have to be protonated in order to form a stable  $\sigma 1$  trimer?
- Does the aspartic acid cluster serve a specific purpose during viral entry, e. g., causing trimerization or detrimerization of  $\sigma 1$ ?
- How does  $\sigma 1$  engage its receptor JAM-A at the atomic level?
- What are the residues necessary for complex formation in  $\sigma 1$  and JAM-A?
- As residues in the JAM-A dimer interface are necessary for binding to  $\sigma 1$ , how does  $\sigma 1$  gain access to the JAM-A dimer interface?
- Do the different reovirus serotypes engage JAM-A using the same binding sites?
- Does the interaction with JAM-A contribute to the distinct tropisms of the reovirus serotypes?

A precise understanding of reovirus attachment mechanisms is not yet available. However, studies of receptor binding by reovirus and other diverse virus groups are establishing a unifying mechanistic theme in which multiple interactions between viral attachment proteins and cell surface receptors occur during the attachment process. As reovirus provides an excellent model system for examination of general principles of viral attachment and entry, answering the above questions will help establish general mechanisms used by viruses to infect target cells. Cell selection, receptor recognition, and entry are the first steps in viral infection. Therefore, understanding these mechanisms is crucial for use of viruses as vectors for therapeutic purposes and development of antiviral drugs.

## 2. Materials and Methods

### 2.1. Materials

Product names mentioned in this document may be trademarks or registered trademarks of their respective owners.

#### 2.1.1. Hardware

##### 2.1.1.1 General purpose equipment

Autoclave VX-95	Systec, Wetztenberg, Germany
Centrifuge 5414 D	Eppendorf, Wesseling-Bertzdorf, Germany
Centrifuge Multifuge 1L-R	Kendro, Langenselbold, Germany
Centrifuge Sorvall RC-6	Kendro, Langenselbold, Germany
Gel Doc XR imaging system	Bio-Rad, Munich, Germany
Gel dryer Slab 2300	LKB, Bromma Sweden
Icemaker	Scotsman, Milan, Italy
Incubation Shaker Unitron	InforsHT, Bottmingen-Basel, Switzerland
Microwave NN-E203 WB	Panasonic, Hamburg, Germany
PCR cycler iCycler	Bio-Rad, Munich, Germany
pH meter PB-11	Sartorius, Göttingen, Germany
Photometer NanoDrop ND-1000	Thermo Scientific, Waltham, USA
Photometer SmartSpec Plus	Bio-Rad, Munich, Germany
Pipette Mettler (2.5 µl)	Mettler Toledo, Columbus, USA
Pipettes Pipetman	Gilson, Middleton, USA
Quartz cuvette (75 µl)	Helma, Jena, Germany
Scale 323S-OCE	Sartorius, Göttingen, Germany
Scale 4202S-OCE	Sartorius, Göttingen, Germany
Scale Genius	Sartorius, Göttingen, Germany
SDS-PAGE Mini Protean 3 Cell	Bio-Rad, Munich, Germany
SDS-PAGE Mini Sub-Cell GT	Bio-Rad, Munich, Germany
SDS-PAGE PowerPac Basic	Bio-Rad, Munich, Germany

Shaker DOS-10L	NeoLab, Heidelberg, Germany
Shaker Intelli-Mixer	NeoLab, Heidelberg, Germany
Sorvall Rotor SS34	Kendro, Langenselbold, Germany
Sorvall Rotor SLC4000	Kendro, Langenselbold, Germany
Sorvall Rotor 75002000	Kendro, Langenselbold, Germany
SpeedVac Heto Vacuum Centrifuge	Heto, Allerød, Denmark
Transilluminator Universal Hood II	Bio-Rad, Munich, Germany

### 2.1.1.2 Cell lysis and chromatography

High pressure homogenizer EmulsiFlex	Avestin, Ottawa, Canada
Sonicator Digital Sonifier 250	Branson, Danbury, USA
Analytical FPLC Smart	GE Healthcare, Uppsala, Sweden
FPLC BioLogic Duo Flow	Bio-Rad, Munich, Germany
Peristaltic EconoPump	Bio-Rad, Munich, Germany
Pharmacia LKB Controller LCC-501 Plus	GE Healthcare, Uppsala, Sweden
Pharmacia LKB Pump P-500	GE Healthcare, Uppsala, Sweden
Pharmacia LKB REC 102	GE Healthcare, Uppsala, Sweden
Affinity column GSTrap FF 5 mL	GE Healthcare, Uppsala, Sweden
Anion exchanger MonoQ 5/50 GL	GE Healthcare, Uppsala, Sweden
Desalting column PD-10	GE Healthcare, Uppsala, Sweden
Column Superdex 75 16/60	GE Healthcare, Uppsala, Sweden
Column Superdex 75 PC 3.2/30	GE Healthcare, Uppsala, Sweden

### 2.1.1.3 X-ray crystallography

24 well crystallization plates	Hampton research, Aliso Viejo, USA
22 mm siliconized cover slides	Hampton research, Aliso Viejo, USA
96 well Intelli-Plates	Art Robbins, Sunnyvale, USA
Sealing for 96 well plates	HJ-Bioanalytik, Mönchengladbach, Germany
Capillaries	Hampton Research, Aliso Viejo, USA
Crystallization Robot Freedom Evo	Tecan, Männedorf, Switzerland
Depression wells	Hampton research, Aliso Viejo, USA
Fiber loops and magnetic bases	Hampton research, Aliso Viejo, USA
Microscope MZ16	Leica, Wetzlar, Germany
Microscope S6E	Leica, Wetzlar, Germany
Cryosystem X-Stream	Rigaku/MSC, The Woodlands, USA
Detector Mar345 dtb	Mar research, Hamburg, Germany
Detector MarCCD 225 at SLS	Mar research, Hamburg, Germany
Optics Varimax HF	Rigaku/MSC, The Woodlands, USA
Rotating Anode Micromax 007 HF	Rigaku/MSC, The Woodlands, USA
Vacuum grease Baysilone	GE Bayer Silicones, Leverkusen, Germany

### 2.1.2. Crystallographic software

All structural figures were prepared using PYMOL (DeLano, 2002). Contact areas were calculated using AREAIMOL (CCP4, 1994).

CCP4	CCP4 (1994)
CNSSOLVE	Brünger <i>et al.</i> (1998)
COOT	Emsley & Cowtan (2004)
HKL	HKL research, Inc., Charlottesville, USA
MAR345DTB	Marresearch GmbH, Hamburg, Germany
PHENIX	Adams <i>et al.</i> (2002)
VOIDOO	Kleywegt & Jones (1994)
XDS	Kabsch (1993)

### 2.1.3. Kits and consumables

Unless stated otherwise, chemicals were ordered from Merck (Darmstadt, Germany), Roth (Karlsruhe, Germany) or Sigma Aldrich (Munich, Germany).

#### 2.1.3.1 Concentrators and filters

Centrifugal filters (0.22 $\mu\text{m}$ )	Corning, Corning, USA
Concentrators Microcon YM3	Millipore, Schwabach, Germany
Concentrators Ultra 4 and Ultra 15	Millipore, Schwabach, Germany
Membrane filters (0.45 and 5 $\mu\text{m}$ )	Millipore, Schwabach, Germany
Syringe top filters (0.2 $\mu\text{m}$ )	VWR International, Vienna, Austria

#### 2.1.3.2 Cloning and bacterial culture

6x loading dye for agarose gels	Fermentas, St. Leon-Rot, Germany
BL21 (DE3)	Merck (Novagen), Darmstadt, Germany
BL21 (DE3) pLysS	Merck (Novagen), Darmstadt, Germany
DH5 $\alpha$	personal stock from Thilo Stehle
dNTPs	Promega, Mannheim, Germany
LB medium	Sigma Aldrich, Munich, Germany
Miniprep kit	Promega, Mannheim, Germany
Nova Blue	Merck (Novagen), Darmstadt, Germany
PfuUltra High-Fidelity DNA polymerase	Stratagene, La Jolla, USA
Restriction enzymes (NcoI, XhoI)	Fermentas, St. Leon-Rot, Germany
SOB medium	Fluka, Munich, Germany
T4 DNA ligase	Fermentas, St. Leon-Rot, Germany
Tag polymerase LC	Fermentas, St. Leon-Rot, Germany
Wizard Plus SV Minipreps	Promega, Mannheim, Germany

## 2.1.3.3 Protein purification and analysis

Acrylamide-Bisacrylamide Rotiphorese Gel 30	Roth, Karlsruhe, Germany
Bradford Protein Assay	Bio-Rad, Munich, Germany
Coomassie Brilliant Blue R-250	Bio-Rad, Munich, Germany
Page Ruler protein ladder	Fermentas, St. Leon-Rot, Germany
SDS-PAGE 10x buffer Rotiphorese	Roth, Karlsruhe, Germany
Thrombin	GE Healthcare, Uppsala, Sweden
Trypsin from bovine pancreas	Sigma-Aldrich, Munich, Germany
Trypsin inhibitor from soy bean type I-S	Sigma-Aldrich, Munich, Germany

## 2.1.3.4 Crystallization screens

Crystal Screen 1 and 2	Hampton research, Aliso Viejo, USA
Additive Screen	Hampton research, Aliso Viejo, USA
Wizard I, II and III	Emerald BioSystems, Bainbridge Island, USA

## 2.1.4. Plasmids and primers

## 2.1.4.1 Plasmids

pET-15b	Merck (Novagen), Darmstadt, Germany
pGEX-4T-3	GE Healthcare, Uppsala, Sweden

## 2.1.4.2 Primers

Primers were ordered from biomers.net, Ulm, Germany. T1L primers were designed by Cezar Böttinger. Sequences for T7 and pGEX primers were taken from vector manuals of Novagen and GE Healthcare, respectively.

Table 2.1: **Primer sequences.**

PRIMER	SEQUENCE	$T_A$ [°C]
<i>Cloning primers</i>		
T1L_F308+Glu NcoI (forward)	ACTCCATGGAGCTTCCGACATACAGGTACCCT	63
T1L_R470Xho1 (reverse)	ACTGCTCGAGTCACCTCACATTGCATGGATACATGAT	63
<i>Sequencing primers</i>		
pGEX forward	GGGCTGGCAAGCCACGTTTGGTG	62
pGEX reverse	CCGGGAGCTGCATGTGTCAGAGG	62
T7 forward	TAATACGACTCACTATAG	56
T7 reverse	CCGCTGAGCAATAACTAG	56

## 2.2. Methods

### 2.2.1. Molecular biology

#### 2.2.1.1 Competent cells

Chemically competent bacteria were produced for heat shock transformation of *E. coli* strains Nova Blue, DH5 $\alpha$ , and BL21 DE3.

100 mL sterile SOB medium were induced with 1 mL overnight bacterial culture and grown at 37 °C to an OD<sub>600</sub> of 0.5. Bacteria were cooled for 10 min on ice, and centrifuged for 10 min at 4 °C and 1700 *g*. The bacterial pellet was resuspended in 20 mL cold Tfb 1. After 10 min on ice, bacteria were centrifuged as above. The pellet was resuspended in 4 mL cold Tfb 2. 100  $\mu$ L aliquots were frozen at -80 °C.

Competent cells were produced by different members of the lab, most frequently by Alexandra Thor.

<i>Tfb 1</i>	100 mM RbCl	<i>Tfb 2</i>	10 mM MOPS
	50 mM MnCl <sub>2</sub>		10 mM RbCl
	30 mM potassium acetate		75 mM CaCl <sub>2</sub>
	10 mM CaCl <sub>2</sub>		15 % (v/v) glycerol
	15 % (v/v) glycerol		pH 6.8 (at RT with KOH)
	pH 5.8 (at RT with KOH)		

#### 2.2.1.2 Glycerol stocks

900  $\mu$ L of an overnight bacterial culture were mixed with 300  $\mu$ L of a sterile 50 % glycerol solution and frozen at -80 °C.

#### 2.2.1.3 Purification of plasmid DNA

Isolation of plasmids from bacteria was carried out using a miniprep kit according to the manufacturers' instructions. DNA concentration was determined using a spectrophotometer. For double stranded DNA, an absorption of 1.0 at 260 nm corresponds to a concentration of 50  $\mu$ g/mL.

#### 2.2.1.4 PCR, agarose gel electrophoresis, and PCR purification

DNA for insertion into plasmids was amplified by polymerase chain reaction (PCR) with PfuUltra High Fidelity DNA polymerase because of its low error rate. For verification of clones, the less expensive Taq polymerase was used. The templates for these control PCRs were taken directly out of bacterial colonies from agar plates (colony PCRs). The composition of the PCR reactions was calculated according to the manufacturers' instructions. The reaction volume was 50  $\mu$ L for amplification PCRs and 20  $\mu$ L for control PCRs.

*PCR program:*

1x	1.	95 °C	2 min (4 min for colony PCR)
30x	2.	95 °C	30 s
		T <sub>A</sub>	30 s
		72 °C	1 min
1x	3.	72 °C	10 min
1x	4.	4 °C	$\infty$

Agarose gel electrophoresis was used to verify PCR reactions. 0.54 g agarose were melted in 30 mL TAE buffer in a microwave. After casting the gel, 1.5  $\mu$ L ethidiumbromide solution (10 mg/mL) were added. PCR samples were mixed with 6x loading dye. Gels were run for 1 h at 120 V and analyzed using UV light.

50x TAE, 250 mL	60.5 g Tris
	14.3 mL glacial acetic acid
	25 mL EDTA 0.5 M pH 8.0

The DNA amplified by PCR was purified using isopropanol precipitation. Two PCR reactions (100  $\mu$ L) were mixed with 110  $\mu$ L isopropanol (-20 °C) and 10  $\mu$ L sodium acetate (3 M pH 5.2, 4 °C) and precipitated at -20 °C for 30 min. The sample was centrifuged for 10 min at 4 °C and 14,000 *g*, the supernatant was discarded and the pellet was washed with 75  $\mu$ L 70 % ethanol (-20 °C). The DNA was centrifuged again for 5 min at 4 °C and 14,000 *g*, the supernatant was discarded and the pellet was dried for 5 min in a vacuum centrifuge. The DNA was resuspended in 20  $\mu$ L H<sub>2</sub>O and the concentration was determined.

### 2.2.1.5 Restriction, ligation and transformation

Plasmids and inserts were subjected to double digest with the respective restriction enzymes. The composition of the reaction mixture (20  $\mu$ L) was calculated according to the manufacturers' instructions. The DNA was digested at 37 °C for 4 h. After 3.5 h, 3  $\mu$ L SAP were added to the plasmid digestion sample to prevent self-ligation. The enzymes were heat-inactivated at 65 °C for 20 min.

The digested DNA was purified using ethanol precipitation. 60  $\mu$ L 100 % ethanol (-20 °C) and 3  $\mu$ L sodium acetate (3 M pH 5.2, 4 °C) were added to the restriction samples. The DNA was precipitated at -80 °C overnight, recovered as described for isopropanol precipitation, and resuspended in 10  $\mu$ L H<sub>2</sub>O.

The DNA was ligated with a ratio of insert to plasmid of 3:1. The amount of insert was calculated according to equation 2.1 (*kbp* = kilobasepairs):

$$ng(\text{insert}) = \frac{3}{1} \cdot \frac{ng(\text{plasmid}) \cdot kbp(\text{insert})}{kbp(\text{plasmid})} \quad (2.1)$$

The ligation reaction (10  $\mu$ L) was mixed according to the manufacturers' instructions and incubated at 20 °C overnight. Heat-inactivation of the ligase was performed at 65 °C for 10 min.

Competent bacteria (section 2.2.1.1) were transformed with ligated plasmids or plasmids from minipreps. 100  $\mu$ L competent cells were thawed on ice. 3  $\mu$ L of the ligation mixture or 1  $\mu$ L purified plasmid were added, followed by incubation on ice for 5 min. The cells were exposed to a heat-shock at 42 °C for 30 s and cooled down on ice for 2 min. 500  $\mu$ L of LB medium were added, bacteria were incubated at 37 °C for 30 min and 50-200  $\mu$ L were plated on agar plates (7 g agar in 500 mL LB medium) with 50  $\mu$ g/mL ampicillin.

DNA sequencing was carried out at MWG (Ebersberg, Germany) with the appropriate control primers (T7 forward and reverse for the pET-15b vector, pGEX forward and reverse for the pGEX-4T-3 vector).

### 2.2.1.6 Expression of recombinant proteins

1 L of LB medium with 50  $\mu$ g/mL ampicillin was induced with 1 mL overnight bacterial culture. For T3D  $\sigma$ 1 and JAM-A expression, the bacteria were allowed to grow at 37 °C to an OD<sub>600</sub> of 0.6-0.9 and induced with 0.4 or 0.2 mM IPTG, respectively. The proteins were expressed overnight at 20 or 25 °C. For T1L  $\sigma$ 1 expression, bacteria were induced at an OD<sub>600</sub> of 1.2 with 1 mM IPTG and the protein was expressed overnight at 30 °C.

## 2.2.2. Protein purification and analysis

### 2.2.2.1 General

All buffers used for protein purification were filtered through 0.45  $\mu\text{m}$  filters. For usage on FPLC systems, buffers were degassed using sonication in a water bath or a water-jet vacuum pump. Unless stated otherwise, all purification steps were carried out at 4  $^{\circ}\text{C}$ .

### 2.2.2.2 Assessment of protein concentration

The protein concentration was assessed using either Bradford assay or absorption at 280 and 260 nm. For the Bradford assay (Bradford, 1976), Bradford solution and sample were mixed according to the manufacturers' instructions and absorption was measured at 595 nm ( $A_{595}$ ). The protein concentration was calculated according to equation 2.2, based on a calibration curve by Pierre Schelling ( $V$ : sample volume).

$$c[\text{mg/mL}] = \frac{A_{595} - 0.004}{0.051 \cdot V[\mu\text{L}]} \quad (2.2)$$

The protein concentration according to absorption at 280 and 260 nm ( $A_{280}$  and  $A_{260}$ ) was calculated as shown in equation 2.3 (Layne, 1957).

$$c[\text{mg/mL}] = 1.55 \cdot A_{280} - 0.76 \cdot A_{260} \quad (2.3)$$

### 2.2.2.3 SDS-PAGE

SDS-PAGE (Laemmli, 1970) was used to separate proteins analytically according to their molecular weights. Samples were mixed with 4x protein sample buffer and run on the gel for 1 h at 180 V.

<i>4 SDS gels:</i>	<i>4 % stacking gel</i>	<i>15 % separation gel</i>
H <sub>2</sub> O	6.10 mL	3.50 mL
Tris 1.5 M pH 6.8	2.50 mL	
Tris 1.5 M pH 8.8		3.75 mL
SDS 10 % (w/v)	100 $\mu\text{L}$	150 $\mu\text{L}$
acrylamide-bisacrylamide	1.30 mL	7.50 mL
TEMED	10 $\mu\text{L}$	7.50 $\mu\text{L}$
APS 10 % (w/v)	100 $\mu\text{L}$	150 $\mu\text{L}$

---

<i>4x protein sample buffer</i>	20 mL glycerol
	20 mL Tris 1 M pH 6.8
	10 mL 10 % SDS
	1.63 mL EDTA 0.5 M pH 8.0
	4 mL $\beta$ -mercaptoethanol
	20 mg bromophenol blue

Gels were placed in coomassie staining solution, heated for 30 s in the microwave and stained for 15 min on an orbital shaker. Gels were then destained in coomassie destaining solution. When protein crystals were used as a sample for SDS-PAGE, gels were stained with silver staining after the protocol by Nesterenko *et al.* (1994) to allow detection of nanogram quantities of protein.

<i>Coomassie staining solution, 500 mL</i>	0.5 g coomassie brilliant blue
	250 mL methanol
	30 ml glacial acetic acid

<i>Coomassie destaining solution, 500 mL</i>	25 mL methanol
	37.5 mL glacial acetic acid

#### 2.2.2.4 Purification of T3D $\sigma$ 1

Constructs of wt and D345N T3D  $\sigma$ 1 comprising residues 293-455 were obtained from Pierre Schelling and Kristen Guglielmi (Vanderbilt University), respectively. Both proteins had been cloned with an N-terminal GST tag into pGEX-4T-3 and were expressed in BL21 (DE3) pLysS (wt) or BL21 (DE3) (D345N) cells. The initial purification protocol was developed by Pierre Schelling. The proteins were cloned with a thrombin cleavage site between GST and  $\sigma$ 1, but cleavage with thrombin led to precipitation of  $\sigma$ 1. As the cleavage site can also be recognized by trypsin, trypsin instead of thrombin was used to cleave the fusion protein.

Proteins were expressed as described in section 2.2.1.6. The bacterial cultures were centrifuged at 4,000 *g* for 10 min to form a cell pellet and resuspended in 40 mL  $\sigma$ 1 lysis buffer. Cells were lysed using either three passes through a high-pressure homogenizer (wt) or 1-2 min 50 % duty-cycle sonification with a sonicator (D345N). Lysed cells were cen-

trifuged at 15,000  $g$  for 30 min, and the supernatant was filtered through 5 and 0.45  $\mu\text{m}$  filters.

The GST- $\sigma 1$  fusion proteins were purified using a 5 mL GSTrap column. The column was equilibrated with 10 mL  $\sigma 1$  buffer with a flow rate of 1 mL/min using a peristaltic pump. The clarified supernatant was loaded onto the column with a flow rate of 0.5 mL/min. The column was transferred to the FPLC system and washed with 100 mL  $\sigma 1$  buffer, 25 mL  $\sigma 1$  ATP-Mg<sup>2+</sup> buffer, and 30 mL  $\sigma 1$  buffer with a flow rate of 1 mL/min. The column was eluted with 30 mL GSH elution buffer. 1 mL fractions were collected. The column was re-equilibrated with 30 mL  $\sigma 1$  buffer.

<i><math>\sigma 1</math> buffer</i>	50 mM Tris (from 1 M stock pH 7.8) 3 mM EDTA (from 0.5 M stock pH 8.0)
<i><math>\sigma 1</math> lysis buffer</i>	50 mL $\sigma 1$ buffer with 1% Triton X-100 (from 20% stock) 2 mM $\beta$ -mercaptoethanol 1 mM PMSF 100 $\mu\text{g}/\text{mL}$ lysozyme
<i><math>\sigma 1</math> ATP-Mg<sup>2+</sup> buffer</i>	33 mL $\sigma 1$ buffer with 20 mM MgSO <sub>4</sub> 10 mM ATP adjusted to pH 7.8 with NaOH
<i>GSH elution buffer</i>	40 mL $\sigma 1$ buffer with 30 mM GSH adjusted to pH 8.05 with NaOH

The protein concentration in the fractions was determined using the Bradford assay (section 2.2.2.2). Fractions were pooled so that the final concentration approached 1 mg/mL. A 1 mg/mL trypsin solution was prepared freshly, and 1  $\mu\text{g}$  trypsin was added per 1 mg protein. The protein sample was incubated at 20 °C for 4-6 h. The cleavage reaction was stopped with a 1:1 amount of trypsin inhibitor (from a 1 mg/mL stock solution). In order to remove GSH and to equilibrate the sample in anion-exchange buffer A, 3x 2.5 mL of the protein solution were passed over three PD-10 desalting columns in par-

allel, according to the manufacturers' instructions. The rest of the protein solution was frozen at  $-80^{\circ}\text{C}$  and pooled with leftovers from following purifications.

A MonoQ anion-exchange column was washed at 0.5 mL/min with 5 mL  $\text{H}_2\text{O}$ , 4 mL 1 M NaCl, and 5 mL  $\text{H}_2\text{O}$ , and then equilibrated using 6 mL anion-exchange buffer A, 6 mL anion-exchange buffer B, and 12 mL anion-exchange buffer A. The protein solution was loaded onto the column, and the column was washed with 5 mL anion-exchange buffer A. The protein was eluted at 0.7 mL/min in a linear gradient consisting of the following steps for the T3D  $\sigma 1$  wt protein: 0-10 % anion-exchange buffer B in 7 mL, 10-20 % buffer B in 14 mL, 20-40 % buffer B in 14 mL, and 7.5 mL 100 % buffer B. The gradient for T3D  $\sigma 1$  D345N ranged from 0-40 % buffer B in 25 mL at 0.5 mL/min. Fractions of 0.5 mL were collected. The column was washed with 10 mL anion-exchange buffer A and 10 mL  $\text{H}_2\text{O}$ . Samples of the fractions of the elution peaks were subjected to SDS-PAGE (section 2.2.2.3), and those that contained pure T3D  $\sigma 1$  without GST impurities were pooled and frozen at  $-80^{\circ}\text{C}$ .

The proteins contained two extra amino acids at the N-terminus due to cloning: Gly291 and Ser292.

*anion-exchange buffer A* 20 mM HEPES pH 7.1

*anion-exchange buffer B* 20 mM HEPES pH 7.1  
400 mM NaCl (from 5 M stock)

### 2.2.2.5 Purification of JAM-A

The construct of human JAM-A D1 (residues 28-129) was obtained from Pierre Schelling. It had been cloned with an N-terminal GST tag into pGEX-4T-3. The initial purification protocol was developed by Pierre Schelling. The protein was expressed in BL21 (DE3) cells as described in section 2.2.1.6 and the cleared supernatant was prepared as described for T3D  $\sigma 1$  D345N (section 2.2.2.4) with JAM-A lysis buffer.

The GST-JAM-A fusion protein was purified on a 5 mL GStrap column. The column was equilibrated using 10 mL JAM-A buffer with a flow rate of 1 mL/min on a peristaltic pump. The clarified supernatant was loaded onto the column with a flow rate of 0.5 mL/min. The column was transferred to the FPLC system and washed with 60 mL JAM-A wash buffer, 25 mL JAM-A ATP- $\text{Mg}^{2+}$  buffer, 20 mL JAM-A buffer, 20 mL JAM-A high salt buffer, 50 mL JAM-A buffer, and 15 mL thrombin cleavage buffer at a flow rate of 1 mL/min.

---

<i>JAM-A buffer</i>	as $\sigma$ 1 buffer (section 2.2.2.4) using a 1 M Tris stock pH 7.5
<i>JAM-A lysis buffer</i>	as $\sigma$ 1 lysis buffer (section 2.2.2.4) with 50 mM NaCl (from 5 M stock) using a 1 M Tris stock pH 7.5
<i>JAM-A wash buffer</i>	JAM-A buffer with 150 mM NaCl (from 5 M stock) 0.1 % Triton X-100 (from 20 % stock)
<i>JAM-A ATP-Mg<sup>2+</sup> buffer</i>	as $\sigma$ 1 ATP-Mg <sup>2+</sup> buffer (section 2.2.2.4) adjusted to pH 7.5 with NaOH
<i>JAM-A high salt buffer</i>	JAM-A buffer with 1 M NaCl (from 5 M stock)
<i>thrombin cleavage buffer</i>	20 mM Tris pH 7.8 (from 1 M stock) 150 mM NaCl (from 5 M stock) 2.5 mM CaCl <sub>2</sub> (from 1 M stock)

The column was removed from the FPLC system in order to perform the cleavage. 150 units of thrombin (from 1 unit/ $\mu$ L stock) were added to 4.6 mL thrombin cleavage buffer and applied to the column using a syringe. The GST-JAM-A fusion protein was incubated with thrombin at 20 °C overnight. Cleaved JAM-A was eluted at a peristaltic pump with 7 mL JAM-A buffer. GST was removed from the column with GSH elution buffer (section 2.2.2.4), and the column was re-equilibrated with 30 mL JAM-A buffer. To verify purity and cleavage efficiency, samples of elution and GST removal were subjected to SDS-PAGE (section 2.2.2.3). JAM-A was frozen at -80 °C.

The protein contained two extra amino acids at the N-terminus due to cloning: Gly26 and Ser27. The construct for expression of the JAM-A D1 E121A mutant was obtained from Kristen Guglielmi (Vanderbilt University) and purified in the same way as the wt protein. For analytical scale size-exclusion chromatography (section 2.2.2.8), the JAM-A D1D2 construct, used for structure determination of human JAM-A (Prota *et al.*, 2003),

was purified as described above for JAM-A D1. The construct contained residues 27-233 and three additional amino acids at the N-terminus due to cloning: Gly24, Ser25, and Met26.

#### 2.2.2.6 Purification of the T3D $\sigma$ 1-JAM-A D1 complex

Two consecutively connected 60 cm Superdex 75 columns were equilibrated with 240 mL size-exclusion buffer at a flow rate of 0.25 mL/min overnight. Purified T3D  $\sigma$ 1 wt and JAM-A D1 were concentrated to 1-1.5 mg/mL and mixed at a monomeric molar ratio of 1:1.2 to ensure saturation of  $\sigma$ 1 with JAM-A. After incubation on ice for 30 min, up to 4 mL of the protein mix were loaded onto the size-exclusion columns with a flow rate of 0.7 mL/min to separate the complex from excess JAM-A D1. The proteins were eluted with 240 mL size-exclusion buffer. Fractions of 4 min (2.8 mL) were collected between 65 and 240 mL of the elution. The purity of the T3D  $\sigma$ 1-JAM-A D1 complex was verified by SDS-PAGE (section 2.2.2.3). Fractions that contained complex were pooled and frozen at -80 °C.

*size-exclusion buffer* 20 mM Tris pH 7.5 (from 1 M stock)  
100 mM NaCl (from 5 M stock)

#### 2.2.2.7 Purification of the T1L $\sigma$ 1-JAM-A D1 complex

A construct corresponding to residues 308-470 of T1L  $\sigma$ 1 was amplified by PCR and cloned into pET-15b as described in sections 2.2.1.4 to 2.2.1.5 using NcoI and XhoI restriction sites. The wt JAM-A D1 construct was the same as described in section 2.2.2.5. T1L  $\sigma$ 1 was purified without an affinity tag as a complex with JAM-A D1 using JAM-A-affinity chromatography.

The proteins were expressed in BL21 (DE3) cells as described in section 2.2.1.6. The clarified supernatant of JAM-A D1 was prepared as described in section 2.2.2.5. JAM-A expression produces more than the tenfold amount of soluble protein compared to  $\sigma$ 1 expression. Therefore, 4/5 of the clarified supernatant of JAM-A were frozen for later use, and only 1/5 was loaded onto a 5 mL GSTrap column using a peristaltic pump and a flow rate of 0.5 mL/min. The column was washed with 30 mL  $\sigma$ 1 buffer (section 2.2.2.4) at 1-2 mL/min. The clarified supernatant of T1L  $\sigma$ 1 was prepared as described in section 2.2.2.4 for T3D  $\sigma$ 1 D345N. It was loaded onto the column with 0.5 mL/min. As JAM-A and GST both form dimers, high molecular weight complexes of GST-JAM-A bind to the GSTrap column. Binding of  $\sigma$ 1 disrupts those complexes and washes GST-JAM-A- $\sigma$ 1

complexes off the column. For this reason, the flowthrough of the first T1L  $\sigma$ 1 application was passed over the column a second time to allow the GST-tagged complexes to bind to the column again. The column was washed with 50 mL  $\sigma$ 1 buffer at 1-3 mL/min.

Cleavage of the GST-JAM-A fusion protein was carried out as described in section 2.2.2.5. The T1L  $\sigma$ 1-JAM-A complex was eluted from the column with 20 mL of  $\sigma$ 1 buffer, and fractions of 2 mL were collected. GST was removed from the column with GSH elution buffer (section 2.2.2.4), and the column was re-equilibrated with 30 mL  $\sigma$ 1 buffer. Samples of the elution fractions were subjected to SDS-PAGE (section 2.2.2.3). The samples containing the T1L  $\sigma$ 1-JAM-A complex were pooled and frozen at  $-80^{\circ}\text{C}$ .

A 60 cm Superdex 75 column was equilibrated with 130 mL size-exclusion buffer (section 2.2.2.6) at 1 mL/min. Samples from several affinity purifications were pooled and concentrated to 3-4 mg/mL. Up to 2 mL of sample were loaded onto the size-exclusion column with a flow rate of 0.8 mL/min to separate the complex from excess JAM-A D1. The proteins were eluted with 130 mL size-exclusion buffer. Fractions of 2 min (1.6 mL) were collected between 34 and 110 mL of the elution. The purity of the T1L  $\sigma$ 1-JAM-A D1 complex was verified by SDS-PAGE (section 2.2.2.3). Fractions that contained the complex were pooled and frozen at  $-80^{\circ}\text{C}$ . Due to cloning, T1L  $\sigma$ 1 contained two extra amino acids at the N-terminus: Met306 and Glu307.

### 2.2.2.8 Analytical scale size-exclusion chromatography

Analytical scale size-exclusion chromatography was performed using a SMART system with a Superdex 75 PC 3.2/30 column. The column was equilibrated with 3 mL size-exclusion buffer (section 2.2.2.6) at 50  $\mu\text{L}/\text{min}$ . 20  $\mu\text{L}$  sample were loaded onto the column. The proteins were eluted with 2.25 mL size-exclusion buffer. 50  $\mu\text{L}$  fractions were collected between 0.85 and 2.25 mL of the elution.

The effect of pH on complex stability was investigated by concentrating purified T3D  $\sigma$ 1-JAM-A D1 complex, T3D  $\sigma$ 1, JAM-A D1, or JAM-A D1 E121A to 10 % of the original volume using spin concentrators. The samples were diluted in 20 mM citrate buffers pH 4.0, 4.5, or 5.0, or 20 mM Hepes pH 7.4 and re-concentrated. This procedure was repeated five times. Size-exclusion chromatography was performed using the respective buffer for each sample with 100 mM NaCl added.

## 2.2.3. X-ray crystallography

### 2.2.3.1 Crystallization and crystal freezing

**Theory** X-rays with a wavelength of about 0.5 to 2.0 Å (0.05-0.2 nm) are ideal to obtain atomic resolution for macromolecules, as a carbon-carbon bond has a length of 1.5 Å. Structure determination with X-rays depends on X-ray diffraction at a crystal lattice. One single molecule would not generate enough measurable diffraction, and moreover, it would be quickly destroyed by the X-rays. Therefore, X-ray crystallography depends on the growth of crystals in which the molecules are arranged regularly. The crystals used are typically 50-800 μm in size. Smaller crystals diffract only weakly, and larger crystals absorb too much of the incident X-rays. Most proteins keep their native conformation in the crystal, because the crystals have high solvent contents between 50 and 70 %.

Crystals are grown by precipitating a protein from its solution. Pure protein in a buffer, usually at 2-20 mg/mL, is mixed with a crystallization solution containing different combinations of buffers at various pH values, salts, additives and precipitants such as polyethylene glycols (PEGs), ammonium sulfate, or 2-methyl-2,4-pentanediol (MPD). The solution is brought to supersaturation. Small aggregates form, which serve as the nuclei for crystal growth. Crystals grow by attachment of new molecules to the nuclei and microcrystals. After initial crystallization conditions have been found, they can often be improved by changing the concentrations of the components, the temperature, the pH, and other variables.

Vapor diffusion is the method most commonly used to crystallize proteins. In the hanging drop method, about 1 μL of protein solution is mixed with the same amount of crystallization solution on a siliconized microscope glass cover slip. The slip is placed upside down over a well in a crystallization plate containing about 500 μL crystallization solution and sealed with grease. The concentration of the crystallization solution in the drop is lower compared to the well, resulting in vapor diffusion from the drop to the well. The protein concentration in the drop increases until supersaturation is reached and crystal growth can begin. If a robot is used to set up the protein drops, sitting drop crystallization is commonly used. Instead of on an upside-down cover slip, the crystallization drop is placed on a small plateau above the well solution, and the crystallization plate is sealed with an adhesive film.

Protein crystals are highly ordered assemblies of macromolecules. The smallest repeating unit of a crystal is the unit cell, with the vertices of the unit cells defining the crystal lattice. The unit cell is described by its edges (a, b, and c) and the angles between them

( $\alpha$ ,  $\beta$ , and  $\gamma$ ). Depending on the properties of these lattice constants, seven crystal systems can be distinguished (triclinic, monoclinic, orthorhombic, tetragonal, tri-/hexagonal, rhombohedral, and cubic). Most unit cells contain symmetry elements (rotation and screw axes), dividing the cell into smaller partitions, the asymmetric units (ASU). If the symmetry operations are applied to the ASU, the content of the whole unit cell can be generated. In order to solve a structure, it is therefore sufficient to determine the structure of the molecules contained in one ASU.

Protein crystals are very sensitive to radiation damage caused by X-rays during data collection. X-rays hitting the crystal lead to the formation of radicals that destroy the macromolecules. To avoid radiation damage, crystals are cryocooled prior to and during data collection. The crystal is transferred with the help of a capillary into crystallization solution containing a cryoprotectant (e.g. glycerol, glucose, or MPD), fished with an appropriately sized fiber cryoloop, and flash-frozen in liquid nitrogen or in the cryostream of the X-ray system (100 K). Cryoprotectant and flash freezing prevent the formation of crystalline ice that would damage the protein crystal structure. If a crystal is frozen, the forming of radicals still takes place, but their movement in the crystal is limited. A major disadvantage of cryocooling is the fact that the imperfectness of the crystal usually increases. As a real, non-ideal crystal is composed of small mosaic blocks, this imperfectness is called the mosaicity of the crystal.

**Experiments** Crystallization drops of T3D  $\sigma$ 1 D345N and the T3D  $\sigma$ 1-JAM-A complex were set up manually with the hanging drop method using 24 well plates. 0.7-1  $\mu$ L protein solution were mixed with the same amount of crystallization solution, while the well contained 500  $\mu$ L crystallization solution. The T1L  $\sigma$ 1-JAM-A complex crystals were grown using sitting drop crystallization with a Tecan crystallization robot in 96 well plates. The sitting drops contained 300-450  $\mu$ L protein solution mixed with the same amount of crystallization solution. The well volume was 100  $\mu$ L. The initial search for crystallization conditions was carried out using the Hampton and Wizard crystal screens. Crystal plates were incubated at 20, 16, 12, or 4  $^{\circ}$ C and evaluated first after 3-4 days. The detailed crystallization conditions are described in the results section.

Crystallization of the T3D  $\sigma$ 1-JAM-A complex yielded thin crystal plates growing in clusters. In order to grow larger and single crystals, streak seeding was carried out. Well solutions and crystallization drops on cover slides were prepared freshly. A part of a cat whisker (collected after natural loss) glued to a pipette tip was used to touch a crystal cluster in a drop where crystals had already formed. The cat whisker was drawn through

the new drop and the well was sealed. With this procedure, microcrystals are transferred into the new drop, acting as nuclei for crystal growth.

For data collection, the crystals were taken out of the drop with a capillary (0.3-1.0 mm, depending on crystal size) and transferred to a depression well with 25  $\mu$ L crystallization solution. A single crystal was selected and transferred to depression wells containing 25  $\mu$ L crystallization solution with half and, after that, final concentration of cryoprotectant, e.g., 15 and 30 % glycerol. The crystal was fished with a cryoloop (0.05-1.0 mm, depending on crystal size) and flash-frozen in liquid nitrogen.

### 2.2.3.2 X-rays and data collection

**Theory** The monochromatic X-rays needed for crystallography are usually generated using K-shell emission from a rotating copper anode in vacuum. High voltage application (40 kV) produces highly accelerated electrons from the cathode hitting the anode. As most of the electron energy is converted to heat, the anode is rotated and cooled with water. Some electrons, however, knock other electrons out of the copper atom's lowest energy orbital, the K-shell. Then, an electron of higher energy can fall into the K-shell. The energy lost by the falling electron shows up in an emitted X-ray photon. Two characteristic wavelengths can be observed,  $K\alpha$  and  $K\beta$ , depending on the origin of the falling electron, the L- or the M-shell, respectively. The  $K\beta$  radiation is filtered using e.g. nickel, and the remaining  $K\alpha$  radiation with the characteristic wavelength of 1.54178  $\text{\AA}$  is used for data collection.

Synchrotrons, designed to study particle collisions, are devices for circulating electrons or positrons at a velocity close to that of light. The circulating electrons emit intense X-rays in the tangential direction that can be used for crystallography. The main advantages of synchrotron radiation are the high intensity leading to higher resolution datasets and faster data collection, and the tunability of the wavelength. The latter can be useful to solve the phase problem (section 2.2.3.4).

When X-rays hit a crystal, the X-rays interact with the macromolecules' electrons, so that the crystal lattice planes act as semipermeable mirrors on which a portion of the X-rays is diffracted. The diffracted X-rays have the same wavelength as the incident beam, but their phase and amplitude depend on the distribution of scattering matter, i. e., electrons, in the unit cell. The amplitudes and phases are related to the content of the unit cell by a mathematical relationship, the Fourier transform. The lattice that is observed upon diffraction of X-rays is related to the crystal lattice by an inverse relationship, and

is therefore called the reciprocal lattice. The positions of lattice points in the reciprocal lattice are described with the indices  $h$ ,  $k$ , and  $l$ .

In 1912, Sir William Lawrence Bragg described the conditions under which diffraction leads to constructive interference, causing a reflection  $(h,k,l)$  that can be observed on photographic film, or, today, on a detector. Bragg's law states that a reflection can be observed if the path difference between two beams hitting crystal lattice planes with a distance  $d$  under an angle  $\theta$  is a multiple of the utilized wavelength  $\lambda$  (equation 2.4 and figure 2.1 A).

$$n\lambda = 2d \sin \theta \quad (2.4)$$

A graphical representation of Bragg's law is the Ewald sphere, conceived by Paul Peter Ewald. If a sphere is drawn around a crystal with a radius of  $1/\lambda$ , only those reciprocal lattice points  $(h,k,l)$  can be observed as reflections that lie on the surface of the sphere (figure 2.1 B, C). The beam passing directly through the crystal is called the direct beam. The lattice point with the indices  $(0,0,0)$  is the origin of the reciprocal lattice. It is defined as the position where the direct beam hits the surface of the Ewald sphere.

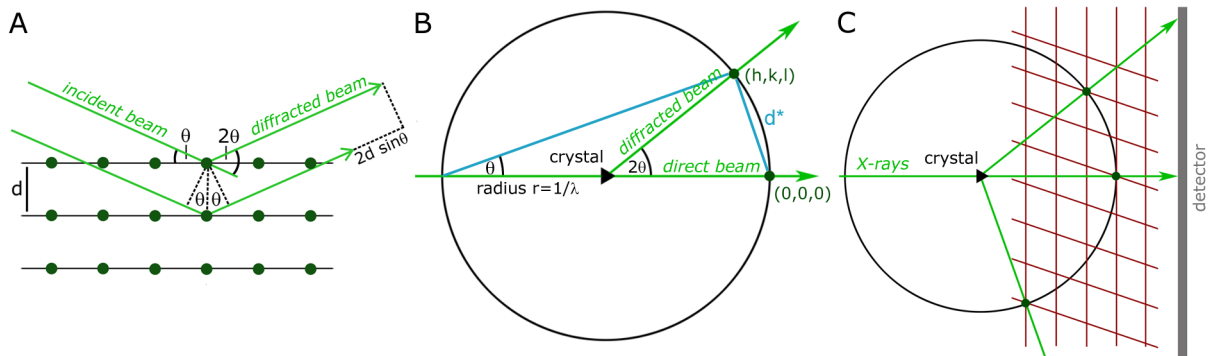


Figure 2.1: **Bragg's law and Ewald sphere.** (A) Bragg's law;  $d$ : distance of lattice planes,  $\theta$ : angle of incidence. (B) Ewald sphere in two-dimensional representation;  $r$ : radius of the sphere,  $\lambda$ : X-ray wavelength,  $(h,k,l)$ : coordinates of a reflection,  $d^* = 1/d$ . (C) Ewald sphere with a two-dimensional reciprocal lattice shown in red.

The diffracted X-rays fulfilling Bragg's law lead to reflections, also called spots, that are collected on a detector, usually an image plate or a CCD area detector. On an image plate, electrons are excited by X-ray photons, and some of the energy is retained in the detector material. When scanned with a red laser, the energy is emitted as blue light that can be measured with a photomultiplier. The emitted light is proportional to the number of photons to which the detector area was exposed, and thus the intensity of the spots can be determined. A charge-coupled device (CCD) detector uses a semiconductive material

with a photoactive (silicon) and a transmission region. The photoactive region, a capacitor array, accumulates an electric charge potential proportional to the light intensity at a particular spot. After exposure, the capacitors transfer their contents to their neighbors, until they end up at a corner of the plate. There, their charge is converted to a voltage in a charge amplifier and recorded. The advantage of CCD over image plate detectors is their fast readout and low noise. They are often used at synchrotrons.

In order to collect all the reflections from a crystal on the detector, i. e., to obtain a complete dataset, the crystal must be rotated during data collection. Usually, one image is recorded while the crystal is rotated  $0.25\text{-}2^\circ$  about an axis perpendicular to the X-ray beam, to measure a continuous data range. Then, the next image can be recorded. Depending on the symmetry of the crystal, the range of degrees needed for a complete dataset ranges from a few degrees (high symmetry) to  $360^\circ$  (no symmetry).

**Experiments** Only the crystals of T3D  $\sigma$ 1 D345N diffracted well enough to collect a dataset at the X-ray system in the lab. Higher resolution data and datasets for the T3D  $\sigma$ 1-JAM-A and T1L  $\sigma$ 1-JAM-A complexes were collected at the Swiss Light Source (SLS) at beamlines PX I and PX III with a MarCCD detector. The T3D  $\sigma$ 1 D345N dataset was collected from a single crystal at a wavelength of  $1\text{ \AA}$ , an oscillation angle of  $1.5^\circ$  and a beam intensity of 10 %. In the case of the T3D  $\sigma$ 1-JAM-A complex, the crystals were very thin and had to be exposed for a relatively long time (10 s to an unattenuated beam; oscillation range  $1\text{-}1.5^\circ$ , wavelength  $0.919880\text{ \AA}$ ) to yield diffraction better than  $4\text{ \AA}$ . The T1L  $\sigma$ 1-JAM-A complex dataset was collected from a single crystal at a wavelength of  $1\text{ \AA}$ , an oscillation angle of  $1^\circ$ , and 7 s exposure at 100 % beam intensity.

### 2.2.3.3 Data processing

**Theory** In order to obtain a list of reflections with the corresponding intensities from the recorded images, the data must be indexed, integrated and scaled. During indexing, computer programs search for spots on the images. Together with the distance to the detector and the wavelength used, the distances and angles between the spots are used to calculate the parameters of the unit cell. The programs also suggest a possible crystal system, depending on the unit cell parameters. During the integration step, the intensity of each reflection on the images is determined, and the unit cell and data collection parameters are refined. Scaling is used to bring each image to the same level, using the fact that the symmetry in the crystal requires the intensity of some reflections to be identical. Scaling is necessary because the X-rays damage the crystals, meaning that

the reflections generally become weaker during data collection, and to compensate for changes in the intensity of the X-ray beam. Thus, the scaling factors used also give a hint about data quality and crystal damage. Moreover, reflections that were not fully recorded on one single image (so-called partials) are added, and symmetry related reflections are merged during scaling. The result of scaling is a file containing all unique reflections (h,k,l) and their intensities, and statistics for assessing data quality. This allows choosing a reasonable resolution cutoff based on the following parameters.

The data processing  $R$ -factors (reliability factors) are a measure of the overall quality of the intensity data.  $R_{\text{sym}}$  measures how identical symmetry-related reflections are,  $R_{\text{merge}}$  also includes reflections that were measured more than once (equation 2.5). The  $R$ -factors measure the ratio between the mean difference between values which should be the same and the mean magnitude of measured values.

$$R_{\text{merge}} = \frac{\sum_{hkl} \sum_i^n |I_{hkl,i} - \bar{I}_{hkl}|}{\sum_{hkl} \sum_i^n I_{hkl,i}} \quad (2.5)$$

where  $I$  is the intensity of a reflection  $hkl$ ,  $\bar{I}$  the average intensity of symmetry-related observations of a reflection,  $i$  the symmetry-related reflection to  $hkl$ , and  $n$  the multiplicity. As  $R_{\text{merge}}$  increases with the redundancy of the data, a redundancy-independent merging  $R$ -factor,  $R_{\text{meas}}$ , was introduced (equation 2.6 (Diederichs & Karplus, 1997)). The  $R$ -values increase with higher resolution.

$$R_{\text{meas}} = \frac{\sum_{hkl} \sqrt{\frac{n}{n-1}} \sum_i^n |I_{hkl,i} - \bar{I}_{hkl}|}{\sum_{hkl} \sum_i^n I_{hkl,i}} \quad (2.6)$$

As the intensity of the reflections generally decreases at higher resolutions, the signal-to-noise ratio  $I/\sigma I$ , meaning the ratio between the mean intensity  $I$  and the standard deviation of the measurements  $\sigma I$ , is another important value to assess data quality. Plotting the mean intensity against  $(\sin^2\theta)/\lambda^2$  (another way to express the resolution) yields a characteristic curve, the Wilson temperature factor plot (Wilson, 1949). The intensity is high at low resolution, and falls as the resolution increases. Solvent effects cause a dip at about 5 Å. From about 4 Å on, the intensity falls linearly, because the solvent contribution becomes very small. The slope of this linear region is called the Wilson  $B$ -factor and represents the decrease of intensity in diffraction due to static crystal disorder and thermal vibration.

The completeness of the dataset is the ratio between the number of unique reflections measured and the total number of unique reflections. The accuracy of the intensity measurement can also be estimated with the redundancy, or multiplicity, of the dataset, which is the ratio between the total number of intensity measurements and the total number of unique reflections measured.

**Experiments** Data for T3D  $\sigma 1$  D345N and the T3D  $\sigma 1$ -JAM-A complex were processed using programs in the HKL package. The crystals of the T3D  $\sigma 1$ -JAM-A complex were damaged severely in the X-ray beam. Therefore, data from several different crystals had to be merged to obtain a complete dataset. Data were collected from several dozen crystals, and datasets that scaled together best were selected for further processing. The final dataset was assembled from three crystals. Radiation damage caused a dramatic decrease in high-resolution intensities. Therefore, all processed data files were analyzed between the integration and scaling step with a FORTRAN program written by Thilo Stehle called IOSIG. The program lists the  $I/\sigma I$  values for a chosen number of resolution ranges (so-called bins). For every image, a resolution cutoff was determined when  $I/\sigma I$  reached 1.5. Another FORTRAN program written by Thilo Stehle (CUTOFF) was used to filter the reflections that fell beyond the resolution cutoff for each image. The quality of the dataset was greatly improved by this procedure. The T1L  $\sigma 1$ -JAM-A complex dataset was processed with the XDS package (Kabsch, 1993). In this case, no filtering of the data was necessary. The space group was determined using the program POINTLESS (CCP4, 1994).

Data collection and refinement statistics, together with the data processing  $R$ -factors used in the different datasets, can be found in the appendix.

#### 2.2.3.4 Structure determination

**Theory** As described in section 2.2.3.2, the X-rays diffracted on a crystal have the same wavelength as the incident beam, but a phase and amplitude depending on the contents of the unit cell. By determining phases and amplitudes of the diffracted waves and applying a Fourier transform, the content of the unit cell, i. e., the structure of the protein, can be determined. Both phase and amplitude are contained in the structure factor  $F$  that is related to the indices (h,k,l) as shown in equation 2.7.

$$F_{hkl} = \sum_{j=1}^N f_j \exp [2\pi i(hx_j + ky_j + lz_j)] \quad (2.7)$$

where the summation is over all atoms  $j$ ;  $f_j$  is the scattering factor, a diffraction contribution from atom  $j$  in position  $xyz$ .  $F$  is a complex number, expressed as a vector in the Gaussian plane, whose length  $|F|$  and angle  $\phi$  correspond to amplitude and phase, respectively. The amplitude  $|F_{hkl}|$  can be determined easily via the intensity  $I_{hkl}$  of a measured reflection (equation 2.8). However, the phase  $\phi$  can not be measured. This is called the phase problem.

$$I_{hkl} \sim F_{hkl}^2 = |F_{hkl}|^2 \quad (2.8)$$

The first step in determining a structure is to convert the intensities obtained after scaling to structure factor amplitudes. Furthermore, the Matthews coefficient  $V_M$ , introduced by Brian W. Matthews (Matthews, 1968), gives an estimation about how many copies of the protein  $n_{mol}$  are contained in one ASU of the crystal. As the protein molecules have a relatively constant density, they have a characteristic volume of  $1.3 \text{ \AA}^3/\text{Da}$ . The coefficient is thus usually in the range of  $1.9\text{-}4.2 \text{ \AA}^3/\text{Da}$  and is calculated using the volume of the unit cell  $V$ , the molecular weight of the protein  $M$ , and the number of ASUs in the unit cell  $n_{ASU}$  (equation 2.9).

$$V_M = \frac{V}{M \cdot n_{ASU} \cdot n_{mol}} \quad (2.9)$$

If the structure of a closely related protein is known (a homologue with the same overall fold, a mutant, or individual components of a protein complex), the structure can then be solved with the method of molecular replacement. The model structure is rotated and translated in space to fit the structure to be determined. To reduce the parameters to be computed simultaneously, the rotation and translation functions are determined independently in so-called Patterson space. As the square of the amplitudes are represented by the intensities (equation 2.8), the intensities can be understood as the product of scattering with itself. Using a Fourier transform on the intensities leads to the Patterson function, deduced by Lyndo Patterson. It is the so-called convolution of the scattering structure with itself and describes all the  $N^2$  vectors between the different atoms  $N$  of a structure, including self-vectors. These vectors are independent from the phase of the scattered X-rays and very similar in closely related structures. By transforming the coordinates from the model to theoretical intensities and calculating the Patterson function, and then trying to superpose it on the Patterson function of the intensities measured, a model with initial phases can be determined, and then refined in the following steps.

Two different programs were used for molecular replacement, AMoRE (Navaza, 1994) and PHASER (McCoy *et al.*, 2005, 2007), both in the CCP4 package (CCP4, 1994). AMoRE defines the orientation with the rotation function and determines the displacement with the translation function via the correlation of the observed and calculated intensities. It calculates the correlation coefficient  $cc_F$  and the  $R$ -factor  $R_{AMoRe}$  between the observed and calculated amplitudes to judge the quality of the molecular replacement. PHASER uses maximum likelihood methods instead of correlation functions for molecular replacement. It estimates the quality of the solutions from rotation and translation search using the log likelihood gain ( $LLG$ ) and the  $Z$ -score. The  $LLG$  measures how much better the measured data can be predicted with the model than with a random distribution of the same atoms. The  $Z$ -score is the  $LLG$  minus the mean  $LLG$  for a random sample of orientations, divided by the root mean square deviation (r. m. s. d) of a random sample of  $LLG$  values from the mean. A translation function  $Z$ -score for a correct solution usually has a value greater than 5. A solution is definitely correct if it has a  $Z$ -score greater than 8, if there is no translational non-crystallographic symmetry (NCS).

After an initial model of the structure has been determined, phases are available, and a first electron density map can be calculated using equation 2.10. The electron density  $\rho$  at a position in the unit cell  $xyz$  is determined using the volume of the unit cell  $V$  and the structure factors  $F_{hkl}$ .

$$\rho_{xyz} = \frac{1}{V} \cdot \sum_h \sum_k \sum_l F_{hkl} \exp[-2\pi i(hx + ky + lz)] \quad (2.10)$$

Usually, an electron density map contains two times the observed structure factors  $F_{obs}$  minus the structure factors calculated from the model  $F_{calc}$  ( $2F_{obs} - F_{calc}$  map). Furthermore, a difference map with  $F_{obs} - F_{calc}$  shows errors in the model more clearly by displaying regions where atoms are missing or wrongly oriented.

**Experiments** The program SCALEPACK2MTZ (CCP4, 1994) was used to calculate structure factor amplitudes from the intensities of the T3D  $\sigma 1$  D345N and T3D  $\sigma 1$ -JAM-A datasets. This program was also used to mark 10% of the reflections in each dataset for the calculation of the  $R$ -factor  $R_{free}$  (section 2.2.3.5) (Brünger, 1992). The structure of T3D  $\sigma 1$  D345N was solved using AMoRE with the structure of wt T3D  $\sigma 1$  (Schelling *et al.*, 2007) as search model. As the unit cell dimensions and space group of both protein crystals were identical, both trimers contained in the ASU of the wt T3D  $\sigma 1$  structure were included in the search model. Molecular replacement was carried out including data between 15 and 3 Å resolution and yielded a  $cc_F$  of 83.6 and an  $R_{AMoRe}$  of 27.9%.

The structure of the T3D  $\sigma$ 1-JAM-A complex was solved using one trimer from the wt T3D  $\sigma$ 1 structure (Schelling *et al.*, 2007) as search model in PHASER including data between 12 and 3.4 Å resolution. The Matthews coefficient  $V_M$  was 4.96 Å<sup>3</sup>/Da for one, 2.48 Å<sup>3</sup>/Da for two complexed  $\sigma$ 1 trimers in the ASU, with 75 and 50 % solvent content, respectively. For a protein complex of 87kDa, 50 % solvent content is relatively low, but two  $\sigma$ 1 trimers were found in the asymmetric unit with a refined  $LLG$  of 2649 and translation function  $Z$ -scores of 26.1 and 33.9 for the two trimers. However, no result was obtained during the search for the JAM-A D1 domains with the hJAM-A structure (Prota *et al.*, 2003) as a search model. In an electron density map calculated using only the phases obtained with the two  $\sigma$ 1 trimers, the position and orientation of the six JAM-A D1 molecules could be identified clearly. One JAM-A D1 molecule from each trimeric complex was placed into the electron density manually, and the four others were rotated into their positions by secondary-structure matching (SSM) superposition (Krissinel & Henrick, 2004) of the first two monomeric  $\sigma$ 1-JAM-A complexes onto the other  $\sigma$ 1 monomers in COOT (Emsley & Cowtan, 2004), followed by rigid body refinement (section 2.2.3.5). Adding the six copies of JAM-A D1 reduced the overall  $R$ -factor  $R_{work}$  (section 2.2.3.5, equation 2.11) from 40.1 % to 34.7 %.

For solving the structure of the T1L  $\sigma$ 1-JAM-A complex, the structure of one trimeric T3D  $\sigma$ 1-JAM-A complex was truncated to the last common atom with the CCP4 program CHAINSAW, using a T1L-T3D  $\sigma$ 1 sequence alignment performed with LALIGN (Huang & Miller, 1991). This coordinate file was used for molecular replacement in PHASER. The Matthews coefficient  $V_M$  was 3.94 Å<sup>3</sup>/Da for one trimeric complex in the ASU, with 69 % solvent content, so the molecular replacement search was carried out searching for one complex including data between 8 and 3.2 Å resolution. Only one unique solution was found, with a  $LLG$  of -1230 and a translation function  $Z$ -score of 8.5. A negative  $LLG$  means that the model might be much worse or less complete than expected, but a  $Z$ -score greater than 8 indicates a definite solution.

### 2.2.3.5 Structure refinement

**Theory** After solving a structure, the atom coordinates and temperature factors ( $B$ -factors, a measure of how much an atom oscillates or vibrates around its specified position) need to be refined. The methods used were rigid body refinement, simulated annealing, restrained coordinate refinement, and individual  $B$ -factor refinement. They were applied using non-crystallographic symmetry (NCS) restraints, and combined with manual model building and data sharpening. The refinement procedures try to minimize energies and

to find the model that produces the best agreement between calculated and observed structure factor amplitudes  $F_{calc}$  and  $F_{obs}$ . The refinement progress is monitored by observing the refinement  $R$ -factors. They measure how well the refined structure predicts the observed data and are calculated according to equation 2.11.

$$R = \frac{\sum ||F_{obs}| - |F_{calc}||}{\sum |F_{obs}|} \quad (2.11)$$

It was found that a model can be easily overfitted by the refinement programs, leading to a low  $R$ -factor despite of an incorrect model. Therefore, Axel T. Brünger introduced the unbiased  $R$ -factor  $R_{free}$  to assess model and refinement quality (Brünger, 1992). In analogy to cross-validation methods, a portion of the reflections (5-10 %) is flagged as “free” and not included in the refinement. The  $R_{free}$  calculated from this test set of reflections is an unbiased estimate of the improvement of the model. It is usually higher than the  $R$ -factor  $R_{work}$  calculated from the other 90-95 % of reflections used in refinement.

After solving a structure, the individual components of the protein, e. g., the monomers or subdomains, can be refined as rigid bodies. Afterwards, simulated annealing (Brünger & Rice, 1997) may be carried out. Simulated annealing is a mathematical procedure that helps to find the global energy minimum. A control parameter  $T$  allows changing of a position  $x$ . The higher  $T$ , the more changes to the position are allowed. This is equivalent to giving a molecule kinetic energy by increasing the temperature  $T$  so that the atoms are allowed to change their position  $x$ . Sidechains or entire loops that are trapped in local energy minima in the wrong conformation can thereby adapt the correct one. Finally, restrained coordinate refinement refines the positions of all atoms whilst constraining parameters like bond lengths and angles (Engh & Huber, 1991).

If NCS is present in the protein, e. g., between the individual components of a multimer, restraints between similar parts of the structures can be defined. This is especially helpful when refining a structure at a relatively low resolution worse than 3 Å. Data sharpening (Gamblin *et al.*, 1996) is a procedure that adds a sharpening  $B$ -factor to the structure factor amplitudes. Adding the  $B$ -factor obtained from the Wilson plot (section 2.2.3.3), results in a new Wilson plot with a slope close to zero for the linear part, thus giving the reflections at higher resolutions a greater weight. The corresponding electron density becomes sharper, and more noise is observed, but data sharpening can help to position sidechains at relatively low resolutions. Manual model building was carried out in COOT (Emsley & Cowtan, 2004). The coordinate file and the electron density maps ( $2F_{obs} - F_{calc}$  map and  $F_{obs} - F_{calc}$  difference map, section 2.2.3.4) are loaded into the program and parts

of the structures that are different than the model or omitted in molecular replacement can be built using the refinement options in COOT.

**Experiments** The two trimers of the T3D  $\sigma 1$  D345N structure were refined in REFMAC5 (Murshudov *et al.*, 1997) in the CCP4 package (CCP4, 1994). Following rigid body refinement and changing amino acid 345 from Asp to Asn in COOT, coordinates and  $B$ -factors were refined while using 6-fold NCS restraints between the  $\sigma 1$  monomers. As the structure was basically identical to wt T3D  $\sigma 1$  (Schelling *et al.*, 2007), refinement was straightforward and not much model building had to be carried out. Water molecules were placed into the electron density by an automatic function implemented in Coot.

After solving the T3D  $\sigma 1$ -JAM-A complex structure, rigid body refinement with all 12 rigid bodies (2x  $\sigma 1$  trimer, each subunit with one JAM-A D1 bound) in REFMAC5 did not work properly. The refinement was therefore carried out in CNS SOLVE (Brünger *et al.*, 1998). Rigid body refinement was followed by simulated annealing, restrained individual  $B$ -factor refinement and restrained coordinate refinement (CNS conjugate gradient minimization). Despite the relatively low resolution of 3.4 Å,  $B$ -factors were refined individually because unrestrained group  $B$ -factor refinement (i. e., refining one overall  $B$ -factor for all atoms) was unstable. Data sharpening was used to improve the electron density maps. As the  $B$ -factor obtained from the Wilson plot was 64.5 Å<sup>2</sup>, a sharpening  $B$ -factor of 70 Å<sup>2</sup> was added to the structure factor amplitudes in the CCP4 program CAD. Two groups of NCS restraints were defined during refinement. One group contained the six copies of  $\sigma 1$ , the other the six copies of JAM-A. Loops that participated in crystal contacts and did not have the same structures in all copies were omitted from the restraining procedure.

The structure of the T1L  $\sigma 1$ -JAM-A complex was refined in PHENIX (Adams *et al.*, 2002). The search model used for molecular replacement had been generated by aligning T3D and T1L  $\sigma 1$  and truncating all amino acid side chains in the T3D  $\sigma 1$  structure to the last common atom. After rigid body refinement, several of the truncated sidechains were visible in the electron density maps and could be completed in COOT. Following another round of rigid body refinement, simulated annealing was carried out. This led to a tremendous decrease in  $R$ -factors from an  $R_{work}$  of 46.9 to 30.8% and an  $R_{free}$  of 45.9 to 35.6%. The remaining truncated amino acids were completed in COOT. The structure was then refined using restrained individual coordinate and  $B$ -factor refinement with NCS restraints between the three  $\sigma 1$  and the three JAM-A D1 molecules.

## 2.2.4. Analytical ultracentrifugation

### 2.2.4.1 Sample preparation

To determine the dissociation constant ( $K_D$ ) of the JAM-A D1 homodimer, analytical ultracentrifugation and analysis of the data was performed by Holger Strauss (Nanolytics Gesellschaft für Kolloidanalytik mbH, Potsdam, Germany). After GST affinity chromatography (section 2.2.2.5) out of 800 mL bacterial culture, JAM-A D1 was subjected to size-exclusion chromatography using a 60 cm Superdex 75 column equilibrated with 130 mL size-exclusion buffer (section 2.2.2.6). Analytical ultracentrifugation requires a protein concentration of 1-5 mg/mL, and buffer that is in dialysis equilibrium with the protein solution for dilutions and as an optical reference. Therefore, the protein must not be concentrated after size-exclusion chromatography, and fractions eluting before the protein peak can be used as reference buffer. JAM-A D1 was concentrated to 18 mg/mL, loaded onto the column and eluted with 130 mL size-exclusion buffer at a flow rate of 0.8 mL/min. Fractions of 2 min (1.6 mL) were collected between 34 and 110 mL. The purity of the fractions containing JAM-A D1 was assessed using SDS-PAGE. Pure fractions were pooled (10 mg, 1.6 mg/mL) and sent to Potsdam on ice, because freezing can lead to aggregates that bias ultracentrifugation results.

Two types of ultracentrifugation runs were performed by Holger Strauss, sedimentation velocity (SV) and sedimentation equilibrium (SE) experiments (reviewed in Lebowitz *et al.* (2002)). The experiments were carried out at 25 °C using a BeckmanCoulter (Krefeld, Germany) XI-I analytical ultracentrifuge equipped with interference optics and two-sector titanium centerpieces of 12 or 20 mm optical pathlengths (Nanolytics, Germany).

### 2.2.4.2 Sedimentation velocity experiments

**Theory** SV experiments are performed to characterize proteins. The method allows to determine the hydrodynamic shape and the oligomeric state and stoichiometry of heterogeneous interactions. A centrifugal force applied to a sample causes the depletion of macromolecules at the meniscus. Thereby, a concentration boundary is formed that moves towards the bottom of the centrifuge cell as a function of time. The Svedberg equation defines the sedimentation coefficient of a macromolecule  $s$  and the parameters that determine it (equation 2.12). The  $s$ -value is measured in units of Svedberg (S), where  $1S = 10^{-13}s$ .

$$s = \frac{u}{\omega^2 r} = \frac{M(1 - \bar{v}\rho)}{N_A f} = \frac{MD(1 - \bar{v}\rho)}{RT} \quad (2.12)$$

where  $u$  is the observed radial velocity of the macromolecule,  $\omega$  the angular velocity of the rotor,  $r$  the radial position,  $\omega^2 r$  the centrifugal field,  $M$  the molar mass,  $\bar{v}$  the partial specific volume,  $\rho$  the density of the solvent,  $N_A$  Avogadro's number,  $f$  the frictional coefficient,  $D$  the diffusion coefficient,  $R$  the gas constant, and  $T$  the temperature.

The frictional coefficient  $f_0$  for a smooth, compact spherical protein can be determined using the Stokes equation (equation 2.13).

$$f_0 = 6\pi\eta R_0 \quad (2.13)$$

with  $\eta$  as the viscosity of the solution, and  $R_0$  the radius of the sphere. Combining the Svedberg and Stokes equations and substituting the values for the constants at a 20 °C leads to  $s_{sphere}$ , the maximum  $s$ -value that can be obtained for a protein of a given mass (equation 2.14), because a compact sphere has the minimum surface area.

$$s_{sphere} = 0.012 \frac{M^{2/3}(1 - \bar{v}\rho)}{\bar{v}^{1/3}} \quad (2.14)$$

The runs are performed at a fixed speed with several different concentrations until all material has sedimented. During the runs, the optical system of the ultracentrifuge measures the interference (or absorption) of the sample. To evaluate the quaternary state of the protein, it is investigated if the determined  $s$ -value is consistent with the molar mass (calculated from the sequence) of a protein monomer. The ratio of the experimental frictional coefficient to the minimum frictional coefficient  $f/f_0$  measures the maximum shape asymmetry from a sphere. Thus, the approximate shape of the molecule can be determined.

**Experiments** 400  $\mu$ L protein solution at five concentrations between 0.06 and 1.31 mg/mL were centrifuged at 50 krpm until all material had sedimented. Every two minutes, the concentration profiles were scanned. The data were evaluated using the  $c(s)$ -function in the program SEDFIT 9.4 (Schuck, 2000).

### 2.2.4.3 Sedimentation equilibrium experiments

**Theory** SE is the method of choice for molar mass determinations and the study of self-association and heterogeneous interactions. The dissociation constant  $K_D$  of an interaction can be determined with high accuracy for affinities up to the micromolar range.

The centrifugal fields used are lower than the ones used for SV runs. Different protein concentrations are centrifuged at several velocities until the sedimentation equilibrium is reached. At sedimentation equilibrium, the net transport vanishes throughout the solution, that is, the sedimentation equals the diffusion. At this point, the concentration distribution in the sample from the top to the bottom of the centrifuge tube approaches an exponential function. For a mixture of noninteracting ideally sedimenting solutes, the measured signal as a function of radial position  $a(r)$  takes the form of equation 2.15.

$$a(r) = \sum_n c_{n,0} \varepsilon_n d \exp \left[ \frac{M_n(1 - \bar{v}_n \rho) \omega^2}{2RT} \cdot (r^2 - r_0^2) \right] + \delta \quad (2.15)$$

where the summation is over all species  $n$ ;  $c_{n,0}$  is the molar concentration of species  $n$  at a reference position  $r_0$ ;  $M_n$  is the molar mass,  $\bar{v}_n$  the partial specific volume, and  $\varepsilon_n$  the molar extinction coefficient;  $d$  is the optical path length and  $\delta$  is a baseline offset. Equation 2.15 shows that the exponential distribution at SE is the sum of the exponentials of the macromolecular species present in solution. The concentration of each component varies exponentially with  $r^2$  as a function of  $M_n(1 - \bar{v}_n \rho) \omega^2 / 2RT$ . The term  $M_n(1 - \bar{v}_n \rho)$  is called the buoyant or reduced molar mass, that is, the mass of a macromolecule acted on in solution by the centrifugal field is reduced by the mass of the displaced solvent. Using exponential fitting functions, the molar mass can be determined from this exponential model.

Equation 2.15 can be modified to describe the SE of reversibly formed protein complexes. Equilibrium constants and mass action law must be introduced to obtain equation 2.16. The molar concentration at the reference point of all oligomeric species is  $K_n(c_{1,0})^n$ , with the subscript 1 denoting the monomer.  $M_n$  is substituted with  $nM_1$  in each exponential term.  $\bar{v}$  is considered constant.

$$a(r) = \sum_n n \varepsilon_1 d K_n (c_{1,0})^n \exp \left[ \frac{nM_1(1 - \bar{v} \rho) \omega^2}{2RT} \cdot (r^2 - r_0^2) \right] + \delta \text{ with } K_1 = 1 \quad (2.16)$$

The association constants  $K_n$  are defined from the monomer to the n-mer. As the oligomeric state of the protein has been determined using SV, exponential fits can be used to calculate the association constant.

**Experiments** Four initial protein concentrations between 1.6 and 0.16 mg/mL were prepared. 150  $\mu$ L of these solutions were centrifuged at three different velocities (17.5, 25.0, 35.0 krpm). The program MATCH was used to assess if the apparent sedimentation

and chemical equilibrium had been attained. The equilibrium gradients were globally analyzed using NONLIN. Both programs can be obtained at <http://www.biotech.uconn.edu/auf/?i=aufftp>. Suitable models to describe the experimental data were selected based on minimized variance and visual inspection of the residuals run pattern. Different initial starting values for the floated parameters were used to confirm that the parameters were well defined by the data.

## 3. Results

### 3.1. T3D $\sigma$ 1 D345N

The T3D  $\sigma$ 1 construct, comprising residues 293-455, contains the head domain plus one  $\beta$ -spiral repeat. This construct was designed to omit the flexible region between the two C-terminal  $\beta$ -spiral repeats, while still binding JAM-A, in order to yield better diffracting crystals than the ones used for the initial structure determination of T3D  $\sigma$ 1 (Chappell *et al.*, 2002; Schelling *et al.*, 2007). After the high resolution structure of the wt protein was solved by Pierre Schelling, several mutants centered at the aspartic acid cluster (section 1.2.3.2) were generated by site-directed mutagenesis by Kristen Guglielmi (Vanderbilt University). At the aspartic acid cluster, two aspartates from each  $\sigma$ 1 molecule (Asp345 and 346) approach each other closely at the trimer interface. As molecular dynamics studies suggested that Asp345 must be protonated to allow  $\sigma$ 1 trimer formation (Cavalli *et al.*, 2004), Asp345 was mutated to asparagine to resemble a protonated aspartate. The D345N mutant was purified, crystallized, and its structure was solved to high resolution.

#### 3.1.1. Purification and crystallization of T3D $\sigma$ 1 D345N

T3D  $\sigma$ 1 was purified using GST-affinity and anion-exchange chromatography (section 2.2.2.4). Figure 3.1 shows a representative purification. The protein was induced in *E. coli*. The cells were lysed, and the cleared supernatant was loaded onto a GSTrap column. After elution from the GSTrap column, fractions 5-10 were pooled (figure 3.1 A). The GST- $\sigma$ 1 fusion protein was cleaved with trypsin, desalted, and loaded onto a MonoQ anion exchange column. Elution from the anion-exchange column always yielded several peaks (figure 3.1 B). The first peak contained T3D  $\sigma$ 1 D345N, and the other peaks contained GST (figure 3.1 C). Fractions 18-24 were pooled. A single purification from 1 L bacterial culture yielded 1.5 mg pure T3D  $\sigma$ 1 D345N.

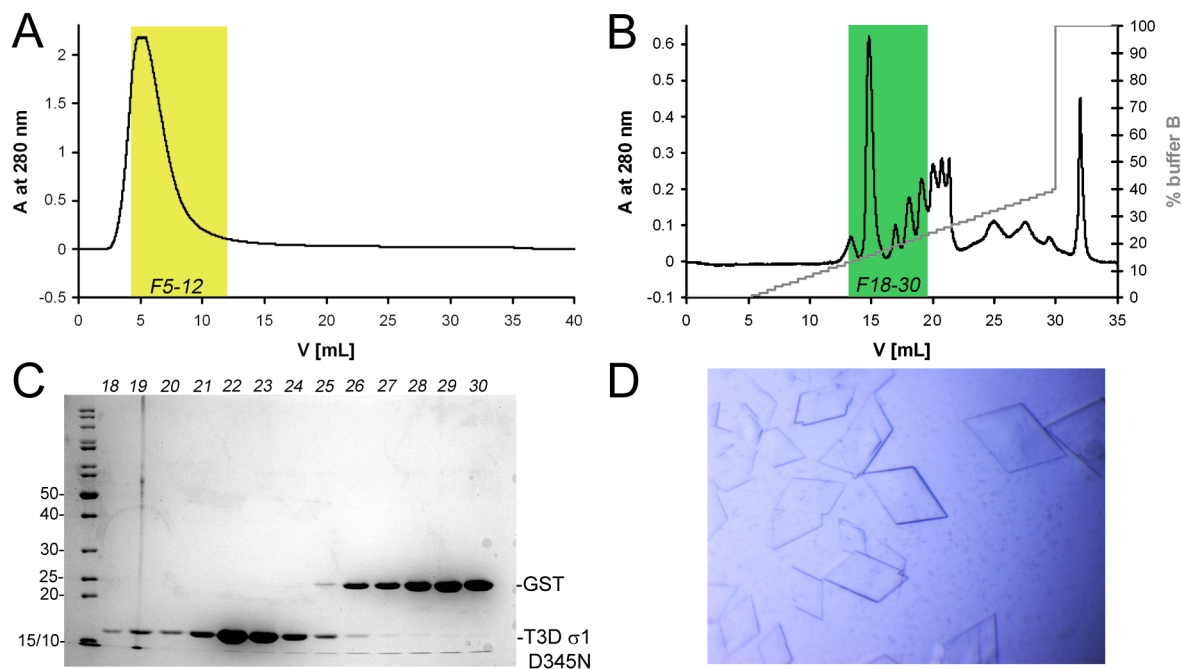


Figure 3.1: **Purification and crystals of T3D  $\sigma 1$  D345N.** (A) Elution profile of the GST-affinity chromatography. Highlighted in yellow are fractions 5-12 which were pooled and subjected to trypsin cleavage. (B) Elution profile of the anion-exchange chromatography. Fractions 18-30 (highlighted in green) were loaded onto the SDS gel shown in panel C. (C) SDS-PAGE of samples from anion exchange. Positions of GST (25 kDa) and T3D  $\sigma 1$  D345N (18 kDa) are indicated. Molecular weight standards are marked on the left in units of kDa. (D) Crystals of T3D  $\sigma 1$  D345N, about 200  $\mu\text{m}$  in diameter.

For crystallization, the protein was concentrated to 8 mg/mL. Screening for crystals using the hanging drop method (section 2.2.3.1) was carried out with 0.7  $\mu\text{L}$  protein mixed with 0.7  $\mu\text{L}$  crystallization solution in the Wizard I&II screens at 20  $^{\circ}\text{C}$ . In parallel, screening was also done using conditions similar to those used to crystallize T3D  $\sigma 1$  wt (10-12 % PEG 8000, 0.2 M magnesium sulfate, 0.1 M sodium cacodylate pH 6.9, 20  $^{\circ}\text{C}$ ) (Schelling *et al.*, 2007). This latter approach yielded the most promising crystals. Crystals obtained around this condition were largest and diffracted best. For the final crystallization condition, the temperature was lowered to 16  $^{\circ}\text{C}$ . This prevented the formation of crystal clusters and permitted the growth of single crystals. The PEG concentration was increased to 20 %, and the pH of the cacodylate buffer was 6.7. The content of the ASU of the wt T3D  $\sigma 1$  crystals revealed one glycerol molecule that participated in crystal packing. Therefore, 1 % glycerol was added to the T3D  $\sigma 1$  D345N crystallization solution. The protein was concentrated to 8.6 mg/mL, and 1.5  $\mu\text{L}$  protein were mixed with 1.5  $\mu\text{L}$  crystallization solution. Single crystals appeared after three days (figure 3.1 D). They had

the same rhombical shape and size as the crystals of wt T3D  $\sigma 1$ . The crystals were frozen with 20 % glycerol as cryoprotectant added to the crystallization solution.

### 3.1.2. Structural and functional analysis of T3D $\sigma 1$ D345N

#### 3.1.2.1 Structure of T3D $\sigma 1$ D345N

One T3D  $\sigma 1$  D345N crystal was used to collect a dataset to 1.85 Å at the SLS beamline PX I (Villigen, Switzerland). Data processing revealed that both wt and D345N mutant crystallized in the same monoclinic spacegroup ( $P2_1$ ) with nearly identical unit cell parameters. The structure was solved by molecular replacement with the wt T3D  $\sigma 1$  structure as the search model. The wt structure had been refined to 1.75 Å resolution (Schelling *et al.*, 2007). As in the wt structure, two  $\sigma 1$  trimers are present in one ASU of the crystal. Detailed data collection and refinement statistics can be found in the appendix (table 6.2 on page 82).

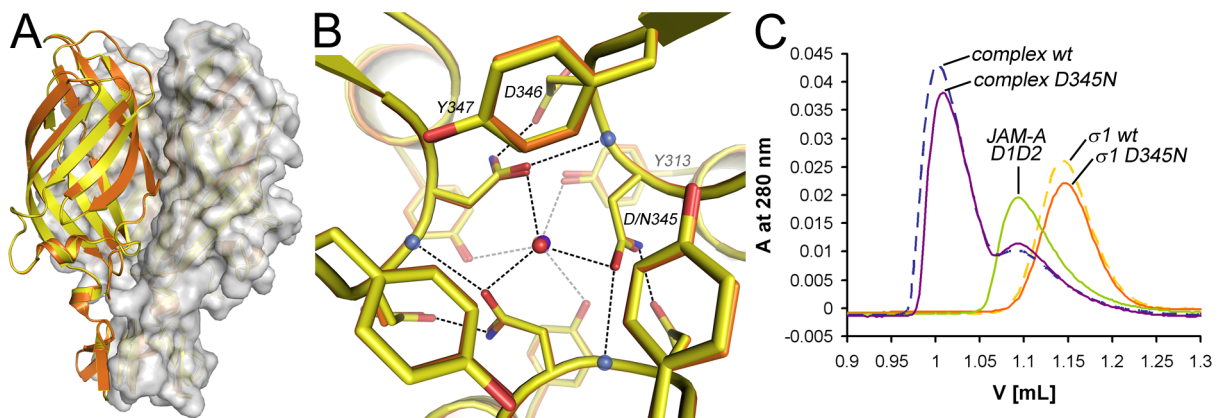


Figure 3.2: **Structure of T3D  $\sigma 1$  D345N and binding to JAM-A.** (A) Superposition of the T3D  $\sigma 1$  wt (yellow) and D345N (orange) trimers. Two subunits are shown in surface representation. (B) Superposition of the T3D  $\sigma 1$  wt (yellow) and D345N (orange) aspartic acid cluster regions viewed along the trimer axis from the top of the molecule. Oxygen atoms are colored red, nitrogen atoms blue. Water molecules are depicted as red (wt) and purple (D345N), main chain nitrogen atoms of D346 as blue spheres. The water molecules are located on the trimer axis and thus only the uppermost one is clearly visible. Hydrogen bonds are shown as dotted lines. (C) Elution profiles of size-exclusion chromatography runs of wt and D345N T3D  $\sigma 1$ , JAM-A D1D2, and complexes of wt and D345N  $\sigma 1$  with JAM-A D1D2.

The structure of T3D  $\sigma 1$  D345N is nearly identical to the structure of the wt molecule (figure 3.2 A; section 1.2.3.1). As in the wt structure, two residues from each  $\sigma 1$  molecule are located in the generously allowed regions of the Ramachandran plot: His388 and Asn345. His388 is fixed in its position by a salt bridge to Glu348, and Asn345 is located

on the  $\beta$ -hairpin between  $\beta$ -strands B and C in the aspartic acid cluster. The region of the aspartic acid cluster (section 1.2.3.2) is identical in the wt and the D345N structures (figure 3.2B). Even the two water molecules above and below residue 345 are located at the same positions. The structure of the D345N mutant was determined in order to test the hypothesis that Asp345 has to be protonated in the wt to allow  $\sigma 1$  trimer formation. No structural changes could be observed upon replacement of Asp345 with asparagine. The amino groups of the mutated Asn345 form the same hydrogen bonds to the carboxyl group of Asp346 as a protonated Asp345 in the wt. The  $\sigma 1$  D345N structure provides thus further evidence that Asp345 in the wt must be protonated in order to allow formation of a functional  $\sigma 1$  trimer.

### 3.1.2.2 Binding of T3D $\sigma 1$ D345N to JAM-A

T3D  $\sigma 1$  D345N was analyzed for receptor binding properties and the capacity to form trimers by analytical scale size-exclusion chromatography (section 2.2.2.8). Uncomplexed JAM-A D1D2 dimers (section 2.2.2.5) and the wt and D345N  $\sigma 1$  trimers elute at volumes corresponding to 68 and 52kDa, respectively (figure 3.2C). These values were calculated based on a column calibration by Pierre Schelling. Wt or D345N  $\sigma 1$  were mixed with JAM-A D1D2 at a monomeric molar ratio of 1:1.2 to ensure saturation of  $\sigma 1$  with JAM-A. After incubation on ice for 30 min, the samples were submitted to size-exclusion chromatography. Both wt and D345N  $\sigma 1$  showed binding to JAM-A D1D2 by a shift in the elution volume corresponding to a higher molecular weight, compared to the elution volumes of the uncomplexed proteins (figure 3.2C). Thus, wt and D345N  $\sigma 1$  are indistinguishable by size-exclusion chromatography both alone and in complex with JAM-A. This result is in agreement with surface plasmon resonance experiments conducted by Kristen Guglielmi (Vanderbilt University): GST-tagged JAM-A D1D2 was immobilized on a biosensor surface with a GST-specific antibody. Purified wt or D345N  $\sigma 1$  were injected across the biosensor surface, and both showed saturable and reversible binding to JAM-A with a similar affinity (Schelling *et al.*, 2007).

## 3.2. T3D $\sigma$ 1-JAM-A complex

In order to define the structural basis of the interaction between  $\sigma$ 1 and JAM-A, a complex of T3D  $\sigma$ 1 and JAM-A was purified and crystallized. The wt T3D  $\sigma$ 1 construct, used previously to determine the high resolution structure of  $\sigma$ 1 (Schelling *et al.*, 2007), contained the head domain plus one  $\beta$ -spiral repeat (residues 293-455). The JAM-A construct comprised only the D1 domain (residues 28-129), which was shown to be both necessary and sufficient for binding to  $\sigma$ 1 (Forrest *et al.*, 2003). These domain boundaries allow for the two proteins to form a stable interaction, but exclude potential regions of flexibility that could hinder crystal formation.

### 3.2.1. Purification of the T3D $\sigma$ 1-JAM-A complex

T3D  $\sigma$ 1 and JAM-A D1 were purified individually, and the proteins were mixed to form the T3D  $\sigma$ 1-JAM-A complex. The complex was further purified using size-exclusion chromatography.

#### 3.2.1.1 Purification of T3D $\sigma$ 1 and JAM-A D1

GST-affinity and anion-exchange chromatography were used to purify T3D  $\sigma$ 1 (section 2.2.2.4). Chromatograms and an SDS gel of a representative purification are shown in figure 3.3. After elution from the GSTrap column, fractions 4-12 were pooled (figure 3.3 A).

The GST- $\sigma$ 1 fusion protein was cleaved with trypsin. As in the case of T3D  $\sigma$ 1 D345N (section 3.1.1), elution from the anion-exchange column yielded several peaks. The first peak contained  $\sigma$ 1, while the others contained GST (figure 3.3 B, C). Fractions 12-16 were pooled. A single purification from 1 L bacterial culture yielded 1.5 mg pure T3D  $\sigma$ 1.

JAM-A D1 was purified using GST-affinity chromatography with on-column thrombin cleavage (section 2.2.2.5). Figure 3.3 shows samples of the elution after cleavage of the GST-JAM-A fusion protein. A single purification from 1 L bacterial culture yielded 10 mg pure JAM-A D1.

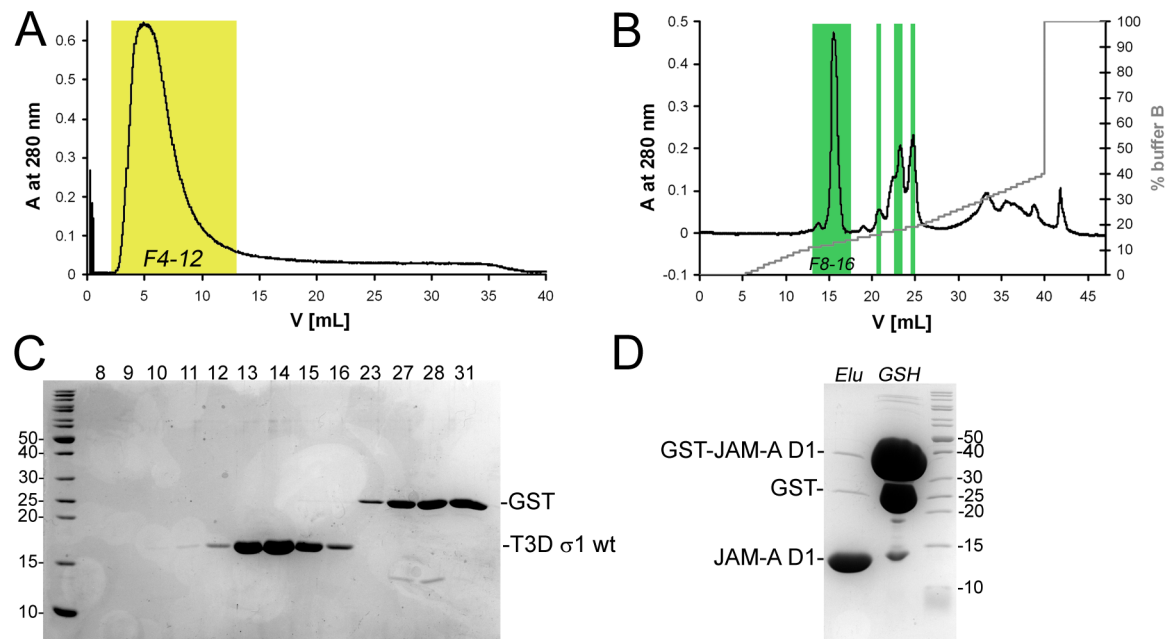


Figure 3.3: **Purification of T3D  $\sigma$ 1 wt and JAM-A D1.** (A) Elution profile of the GST-affinity chromatography. Fractions 4-12 (highlighted in yellow) were pooled and the fusion protein was cleaved with trypsin. (B) Chromatogram of the anion-exchange chromatography. Highlighted in green are the fractions that were loaded onto the SDS gel shown in panel C (8-16, 23, 27-28, and 31). (C) SDS-PAGE of the samples from anion exchange. Positions of GST (25 kDa) and T3D  $\sigma$ 1 wt (18 kDa) are indicated. Molecular weight standards are marked on the left in units of kDa. (D) SDS-PAGE of the elution (Elu) and GSH wash (GSH) of the JAM-A D1 purification. Positions of the GST-JAM-A D1 fusion protein (36 kDa), GST (25 kDa), and JAM-A D1 (11 kDa) are indicated. Molecular weight standards are marked on the right in units of kDa.

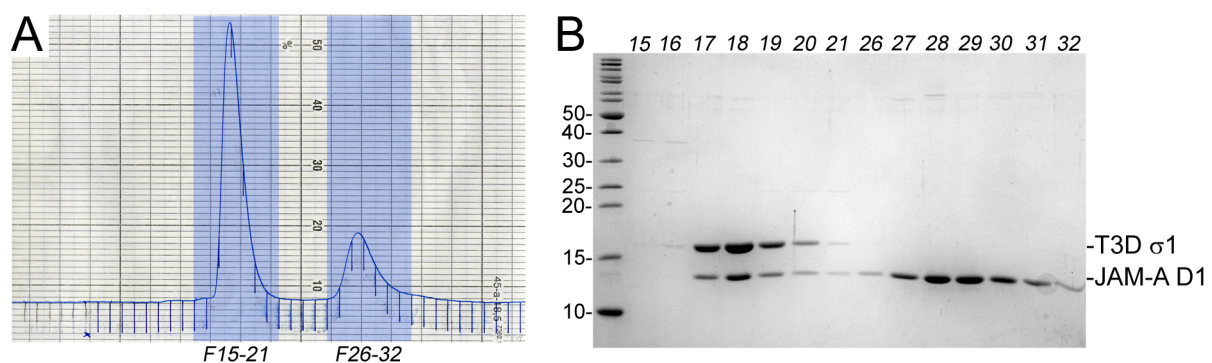


Figure 3.4: **Generation of the T3D  $\sigma$ 1-JAM-A complex.** (A) Size-exclusion chromatogram of the T3D  $\sigma$ 1-JAM-A complex purification. Fractions highlighted in blue (15-21 and 26-32) were loaded onto the SDS gel shown in B. (B) SDS-PAGE of the fractions of the size-exclusion chromatography. Positions of T3D  $\sigma$ 1 (18 kDa) and JAM-A D1 (11 kDa) are indicated. Molecular weight standards are marked on the left in units of kDa.

### 3.2.1.2 Generation of the T3D $\sigma$ 1-JAM-A complex

To form the complex, T3D  $\sigma$ 1 was mixed with an excess of JAM-A D1 at a monomeric molar ratio of 1:1.2 to ensure saturation of  $\sigma$ 1 with JAM-A (section 2.2.2.6). Figure 3.4 shows a representative purification of the T3D  $\sigma$ 1-JAM-A complex. The complex (87 kDa) elutes from the size-exclusion column earlier than the excess of JAM-A D1 dimer (22 kDa) (figure 3.4). Fractions 17-21, containing both  $\sigma$ 1 and JAM-A, were pooled.

## 3.2.2. Structure and stability of the T3D $\sigma$ 1-JAM-A complex

### 3.2.2.1 Structure determination of the T3D $\sigma$ 1-JAM-A complex

The T3D  $\sigma$ 1-JAM-A complex was concentrated to 4 mg/mL and crystallized using the hanging drop method (section 2.2.3.1). The best crystallization condition was obtained in the Wizard I screen (0.1 M CHES pH 9.5, 30 % PEG 3000) at 20 °C. The crystals were thin, elongated plates growing in clusters. When the crystals were transferred to depression wells, single crystals could be obtained from the clusters. Upon replacement of PEG 3000 with PEG 3350 and the use of streak seeding (section 2.2.3.1), the size of the crystals could be increased from a length of 200 to 600  $\mu$ m (figure 3.5 A, B).

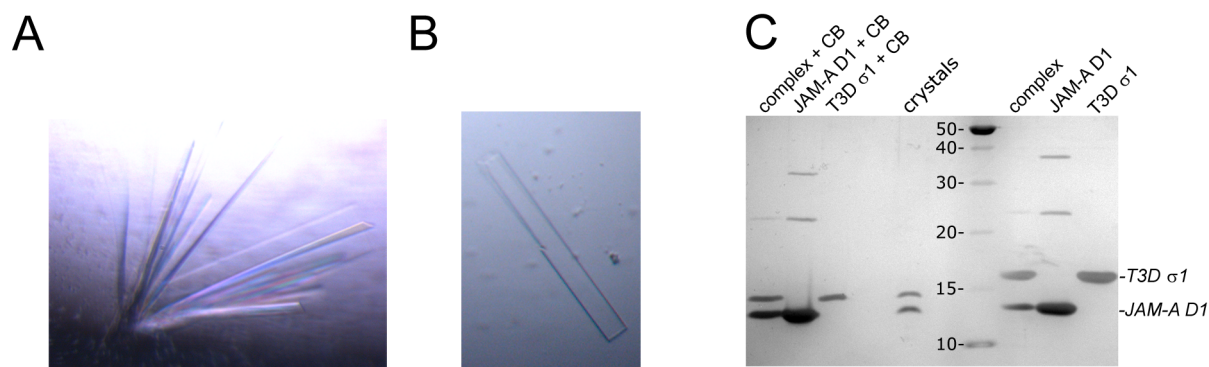


Figure 3.5: **Crystals of the T3D  $\sigma$ 1-JAM-A complex.** (A, B) Crystal cluster (A) and single crystal after transferring to a depression well (B) of the T3D  $\sigma$ 1-JAM-A complex, about 600  $\mu$ m in length. (C) SDS gel of complex crystals. T3D  $\sigma$ 1, JAM-A D1, and complex of both were used as controls, with and without crystallization solution (CB) added. Positions of T3D  $\sigma$ 1 (18 kDa) and JAM-A D1 (11 kDa) are indicated. The higher molecular weight bands in the JAM-A D1 lanes are GST (25 kDa) and GST-JAM-A D1 (36 kDa) impurities. Molecular weight standards are marked in the middle in units of kDa.

As the crystals did not diffract at the X-ray source in the lab, SDS-PAGE (section 2.2.2.3) was performed in order to investigate if the crystals contained the T3D  $\sigma$ 1-JAM-A complex. To remove the protein solution and precipitated protein, the crystals were

transferred into depression wells containing crystallization buffer. The crystals were mixed with SDS sample buffer, the sample was vortexed, and loaded onto an SDS gel (figure 3.5 C). Protein samples of T3D  $\sigma$ 1, JAM-A D1, and the complex were used as controls, both in their original buffer and mixed with crystallization solution. Adding crystallization solution to the control proteins altered their electrophoretic mobility considerably. SDS-PAGE confirmed that the crystals indeed contained T3D  $\sigma$ 1 and JAM-A D1. Crystals were flash-frozen with 20 % glycerol as cryoprotectant added to the crystallization solution.

Diffraction data were collected at the PX I beamline of the SLS (Villigen, Switzerland). The final dataset was assembled from three individual crystals (section 2.2.3.3). The structure was solved using molecular replacement (section 2.2.3.4) and refined to 3.4 Å resolution (table 6.3 on page 83 in the appendix). The crystals belong to the orthorhombic space group  $P2_12_12$  and contain two  $\sigma$ 1 trimers, each complexed with three JAM-A D1 monomers, in the ASU. The presence of six individual complexes allowed us to impose sixfold NCS restraints during refinement (section 2.2.3.5), helping to obtain a reliable model at the relatively low resolution of 3.4 Å. Electron density is visible for most of the side chains, including those located at the interface between  $\sigma$ 1 and JAM-A (figure 6.1 on page 84 in the appendix), allowing for assignment of contacts. Real-space correlation plots, depicting the correlation between model and data against the protein sequence, show good agreement between the refined coordinates and the measured dataset (figure 6.2 on page 84 in the appendix).

### 3.2.2.2 Overall structure of the T3D $\sigma$ 1-JAM-A complex

The crystallized T3D  $\sigma$ 1-JAM-A complex consists of a  $\sigma$ 1 trimer ligated by three JAM-A D1 monomers. Each D1 monomer interacts with one  $\sigma$ 1 subunit (figure 3.6 A). Numerous contacts are formed between the  $\sigma$ 1 and JAM-A molecules, shielding a combined contact area (the sum of contact areas on both proteins) of 1622 Å<sup>2</sup> from solvent. Crystal packing results in additional contacts between the molecules. However, the interactions described here are common between all  $\sigma$ 1-JAM-A pairs and thus represent interactions that would also occur in solution. In comparison to structures of isolated  $\sigma$ 1 and JAM-A (Chappell *et al.*, 2002; Protá *et al.*, 2003; Schelling *et al.*, 2007), the architecture of both  $\sigma$ 1 and JAM-A are largely preserved. Differences are observed primarily in side chain orientations at the  $\sigma$ 1-JAM-A interface.

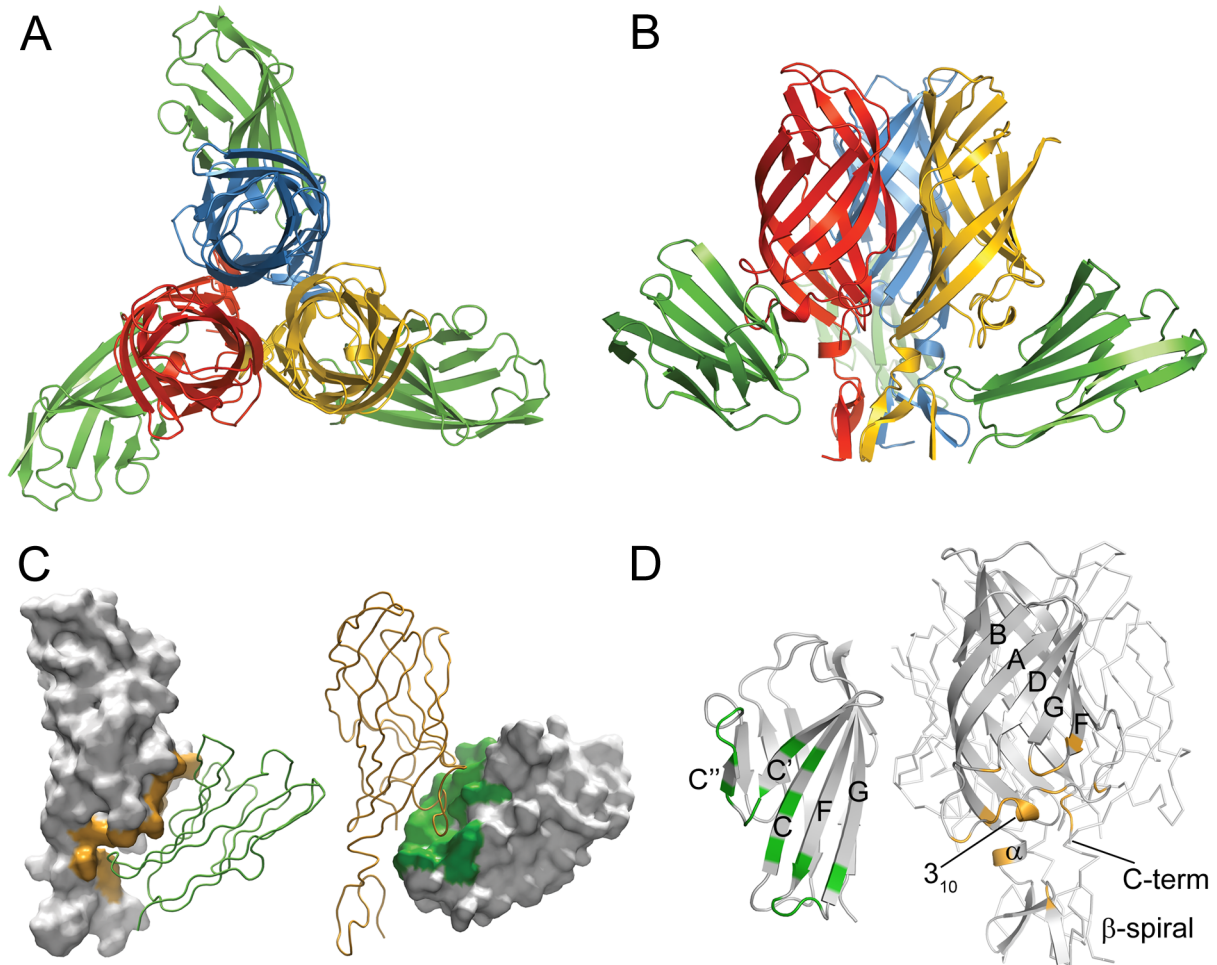


Figure 3.6: **Structure of the T3D  $\sigma$ 1-JAM-A complex.** (A, B) Ribbon drawings of the T3D  $\sigma$ 1-JAM-A complex viewed along the trimer axis (A) and from the side (B).  $\sigma$ 1 subunits are shown in blue, yellow, and red; JAM-A D1 is shown in green. (C) Surface representation of the contact area of reovirus  $\sigma$ 1 (orange, left) and JAM-A D1 (green, right). Interacting partners are shown as ribbon traces. (D) Ribbon drawings of JAM-A D1 (left) and  $\sigma$ 1 (right). All contacting residues within a distance cutoff of 4 Å are colored green (JAM-A) or orange ( $\sigma$ 1). Secondary structure elements are labeled. Figure modified from Kirchner *et al.* (2008).

JAM-A residues involved in contact formation are located at the most membrane-distal part (top) of the D1 domain and on the face that mediates homodimer formation. These regions in JAM-A pack tightly into a recessed region of  $\sigma$ 1 just below the  $\beta$ -barrel (figure 3.6 B-D). Residues at the JAM-A dimer interface form extensive contacts with the D-E loop and the  $3_{10}$ -helix of  $\sigma$ 1 at the upper boundary of the recessed region, whereas the top of JAM-A D1 contacts residues in the  $\beta$ -spiral of the  $\sigma$ 1 tail at its lower boundary.

Four of the six  $\sigma$ 1-JAM-A pairs present in the ASU have similar structures and feature the same interactions. The analysis of the complex presented here is based on these pairs. The remaining two  $\sigma$ 1-JAM-A pairs exhibit larger intermolecular distances of up to 1.2 Å,

resulting in fewer contacts and higher crystallographic temperature factors. The total buried surface area for these two interacting pairs is about 60 Å<sup>2</sup> less. Crystal packing is very tight for a protein complex this size, with only 50 % solvent content (Matthews, 1968). However, the two JAM-A D1 molecules that exhibit larger intermolecular distances to  $\sigma$ 1 are located at positions in the crystal lattice where they can not form crystal contacts. Flash-cooling of the crystals prior to data collection may have partially dislodged JAM-A D1 from its binding site at these locations (Rodgers, 1994).

### 3.2.2.3 Contacts in the T3D $\sigma$ 1-JAM-A interface

Two main contact areas can be distinguished on T3D  $\sigma$ 1 in the complex with JAM-A: a larger contact region located around the  $\sigma$ 1 D-E loop and its  $3_{10}$ -helix, directly below the  $\beta$ -barrel, and a smaller region composed of the top of the most C-terminal  $\beta$ -spiral of the  $\sigma$ 1 tail and the  $\alpha$ -helix between the  $\sigma$ 1 head and tail domains (figure 3.7A).

Residues in the upper, larger contact area interact with residues located on the JAM-A homodimer interface. The contact area is dominated by polar interactions, which include several hydrogen bonds and two salt bridges. The  $\sigma$ 1  $3_{10}$ -helix forms the center of the contact area. Here, mainly main chain interactions of residues Thr380, Gly381, and Asp382 are formed with the side chain atoms of JAM-A residues Glu61, Asn76, and Arg59, respectively (figure 3.7B). Furthermore, residues Val371 and Glu384 in the  $\sigma$ 1 D-E loop, and Asp423 in the  $\sigma$ 1 F-G loop contact JAM-A residues Asn76, Lys78, Lys63, and Ala81 (figure 3.7C). Hydrophobic interactions are also present in this contact area: Trp421, located on the terminal part of  $\sigma$ 1  $\beta$ -strand F, and hydrophobic portions of the D-E loop form a hydrophobic patch with JAM-A residues Leu72 and Tyr75. The observed interactions are in agreement with site-directed mutagenesis and the analysis of point mutants showing that JAM-A residues Arg59, Glu61, Lys63, Leu72, Tyr75, and Asn76 are important for T3D  $\sigma$ 1 binding (section 1.3.3) (Guglielmi *et al.*, 2007).

Instead of hydrogen bonds and salt bridges, the lower contact area of  $\sigma$ 1 features extensive hydrophobic interactions.  $\beta$ -spiral residue Tyr298, the  $\alpha$ -helix between  $\sigma$ 1 head and tail, the hydrophobic portion of Arg316, and Pro377 in the  $\sigma$ 1 D-E loop surround the B-C and F-G loops of JAM-A (figure 3.7D). Ser57 in the JAM-A B-C loop was previously shown to be involved in  $\sigma$ 1 binding (Forrest *et al.*, 2003).

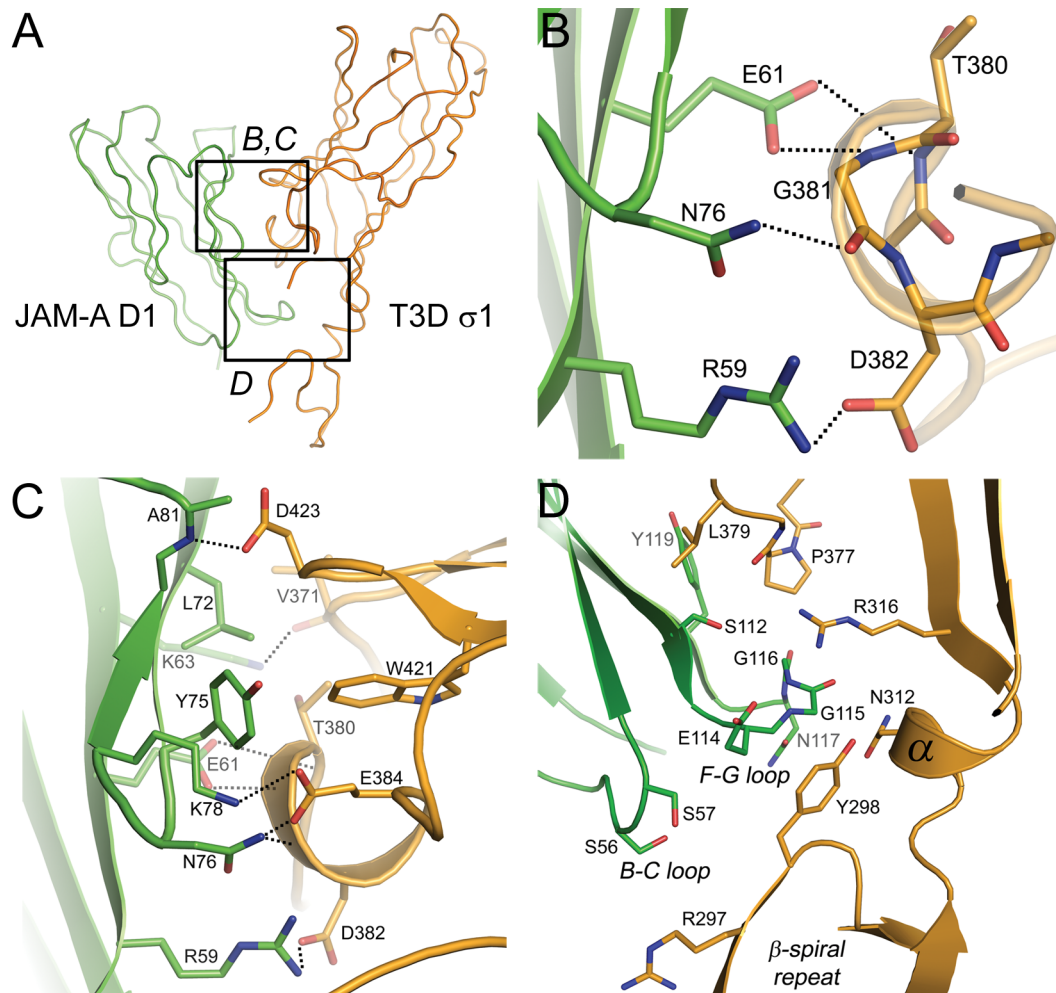


Figure 3.7: **Contacts in the  $\sigma$ 1-JAM-A interface.** (A) Overview of the contact area. The upper contact area shown in panels B and C, and the lower contact area shown in panel D are indicated.  $\sigma$ 1 is colored orange, JAM-A is colored green. (B-D) Views of the contact area. Carbon atoms are shown in orange ( $\sigma$ 1) or green (JAM-A), oxygen atoms in red, and nitrogen atoms in blue. Hydrogen bonds and salt bridges are represented as dotted lines. (B) Contacts between JAM-A and residues in the  $\sigma$ 1  $3_{10}$ -helix in the D-E loop. The helix is depicted transparently to display the contacts to main chain atoms. (C) Additional contacts between JAM-A and  $\sigma$ 1 around the region shown in B. (D) Interactions between the JAM-A B-C and F-G loops and  $\sigma$ 1. Figure modified from Kirchner *et al.* (2008).

3.2.2.4 Stability of the T3D  $\sigma$ 1-JAM-A complex

Most of the contacts between T3D  $\sigma$ 1 and JAM-A are polar, formed by hydrophilic and a surprisingly large number of charged residues.  $\sigma$ 1 residues Asp382, Glu384, and Asp432 contact JAM-A directly, and Arg297 and Arg316 also participate in JAM-A binding. Four charged residues are located in the contact area of JAM-A: Arg59, Glu61, Lys63, and Lys78. Therefore, strong electrostatic potentials are found on the interacting surfaces of the two proteins (figure 3.8 A). The upper contact area of  $\sigma$ 1 displays a strong electronegative potential, complementary to the JAM-A dimer interface to which it is binding. In contrast, the lower  $\sigma$ 1 contact area is electropositive, allowing binding to the electronegatively charged top of the JAM-A D1 domain.

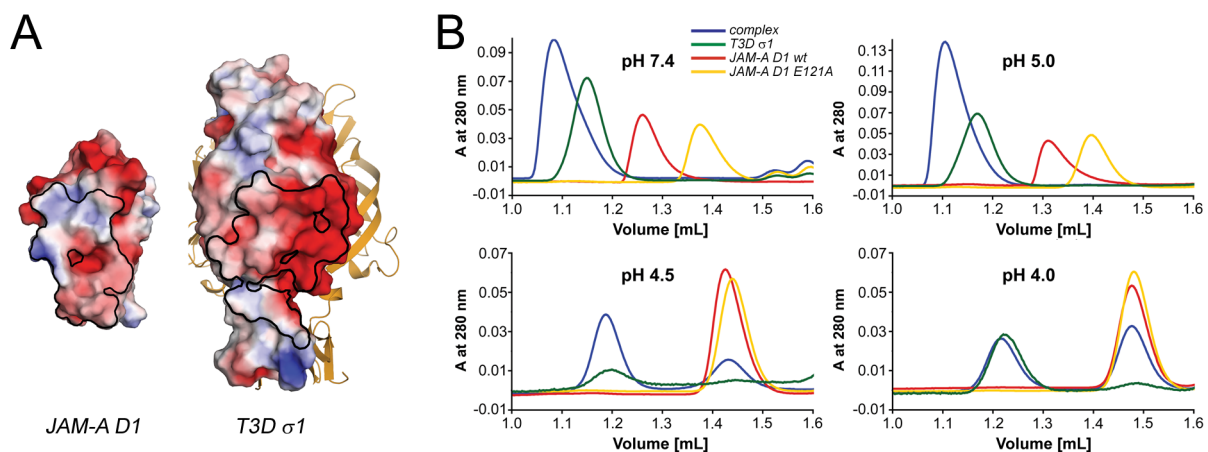


Figure 3.8: **Electrostatic potentials and stability of the complex at low pH.** (A) Electrostatic surface potentials of JAM-A D1 (left) and a  $\sigma$ 1 subunit (right) calculated with APBS tools (Lerner & Carlson, 2006). The scale ranges from -3 (red) to +3 (blue) in units of  $k_B T/e_c$ . The contact areas are outlined in black. (B) Size-exclusion chromatograms of the T3D  $\sigma$ 1-JAM-A complex at pH 7.4, 5.0, 4.5, and 4.0. At pH 4.5 and 4.0, the  $A_{280}$  of  $\sigma$ 1 was multiplied by a factor of 10 to compensate for the lower concentration due to precipitation. Figure modified from Kirchner *et al.* (2008).

Reovirus disassembly is triggered by the low pH environment of the endosome, and structural rearrangements of  $\sigma$ 1 are observed during this process (Chang & Zweerink, 1971; Silverstein *et al.*, 1972; Sturzenbecker *et al.*, 1987). It is therefore likely that the charges accumulated in the  $\sigma$ 1-JAM-A interface play a role in the conformational change of  $\sigma$ 1 during entry. To investigate the influence of charged residues in the T3D  $\sigma$ 1-JAM-A interaction, size-exclusion chromatography of the complex was performed using conditions of varied pH (figure 3.8 B; section 2.2.2.8). T3D  $\sigma$ 1, JAM-A D1, and the monomeric JAM-A D1 E121A mutant were used as controls to determine whether a shift in elution volume occurred due to dissociation of the complex into its components or due

to pH-dependent alteration of the elution behaviour of the proteins. Glu121 is located in the JAM-A homodimer interface, but does not contact  $\sigma$ 1 in the complex. Its mutation to alanine abolishes JAM-A dimerization, but not binding to  $\sigma$ 1 (Guglielmi *et al.*, 2007). At pH 7.4 and 5.0, the  $\sigma$ 1-JAM-A complex eluted earlier than the  $\sigma$ 1, JAM-A D1, and JAM-A D1 E121A samples, indicating a stable complex. The complex dissociated into its components at pH 4.0 and 4.5, eluting at the same volumes as  $\sigma$ 1 and JAM-A D1. JAM-A D1 also dissociated into monomers at the two low pH values, eluting at the same volume as the monomeric JAM-A D1 E121A mutant. Dissociation of the JAM-A dimer at low pH has been demonstrated in studies with the murine homolog of JAM-A (Bazzoni *et al.*, 2000). The dissociation of the  $\sigma$ 1-JAM-A complex at low pH values clearly demonstrates the importance of charged residues in the complex interface.

### 3.3. T1L $\sigma$ 1-JAM-A complex

The T1L  $\sigma$ 1 construct used to form the complex with JAM-A was designed to contain the head plus one  $\beta$ -spiral repeat (residues 308-470), analogous to the T3D  $\sigma$ 1 construct used to determine the structure of the T3D  $\sigma$ 1-JAM-A D1 complex. Purification of a tagged version of T1L  $\sigma$ 1 was carried out by Pierre Schelling and Cezar Böttinger, but always yielded protein that did not bind JAM-A, nor did it crystallize under the conditions tested. While it is obvious from the structure of the T3D  $\sigma$ 1-JAM-A complex why an uncleaved C-terminal hexahistidine tag, located very close to the binding interface, would abolish JAM-A binding, it is unclear why a cleaved N-terminal hexahistidine or GST tag would inhibit contact formation with JAM-A. Interestingly, the purified protein showed a different behaviour than T3D  $\sigma$ 1 in size-exclusion chromatography, eluting at a much smaller size, probably corresponding to a  $\sigma$ 1 dimer (Böttinger, 2006). It is possible that the affinity tag interferes with the correct folding and trimerization of T1L  $\sigma$ 1.

These results led to the purification of an untagged version of T1L  $\sigma$ 1 using JAM-A-affinity chromatography. Attempts were also made to purify untagged, uncomplexed T1L  $\sigma$ 1, using refolding from inclusion bodies or ammonium sulfate precipitation followed by anion-exchange chromatography, or anion-exchange followed by size-exclusion chromatography (results not shown). All three approaches yielded protein sufficiently pure to test JAM-A D1 and D1D2 binding using size-exclusion chromatography, but in no case did T1L  $\sigma$ 1 form a complex with JAM-A. It eluted from the column at the same low molecular weight observed for the T1L  $\sigma$ 1 proteins purified with an affinity tag (Böttinger, 2006). As it was not possible to elute T1L  $\sigma$ 1 from column-bound GST-JAM-A with a pH low enough to disrupt the T3D  $\sigma$ 1 complex, the structure of T1L  $\sigma$ 1 was determined in complex with JAM-A.

#### 3.3.1. Purification of the T1L $\sigma$ 1 complex

T1L  $\sigma$ 1 was purified using JAM-A-affinity chromatography and size-exclusion chromatography (section 2.2.2.7). A typical purification is shown in figure 3.9. GST-JAM-A was bound to the column, then cleared supernatant of T1L  $\sigma$ 1 was passed over the column, which allowed for the T1L  $\sigma$ 1-JAM-A complex to form. After cleavage of the GST-JAM-A fusion protein and elution of the complex (figure 3.9 A), fractions 1-5 were pooled.

Protein from several purifications was pooled and concentrated to 4.3 mg/mL. To separate from excess JAM-A, the protein solution was subjected to size-exclusion chro-

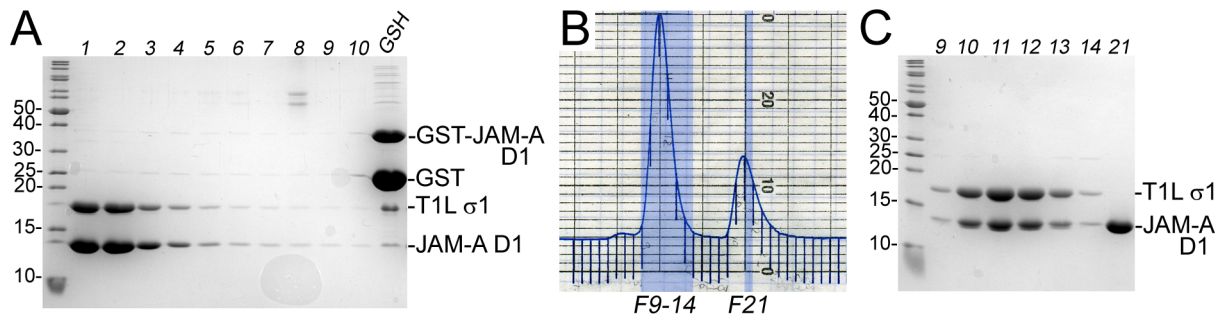


Figure 3.9: **Purification of the T1L  $\sigma$ 1-JAM-A complex.** (A) SDS-PAGE of the elution of the T1L  $\sigma$ 1-JAM-A complex (lanes 1-10). The lane labelled GSH shows a fraction of the column wash with GSH to remove bound GST and uncleaved GST-JAM-A D1 complexed with  $\sigma$ 1. (B) Elution profile of the size-exclusion chromatography used to separate the T1L  $\sigma$ 1-JAM-A complex from excess JAM-A D1. Samples of the fractions highlighted in blue (9-14 and 21) were loaded onto the SDS gel shown in C. (C) SDS-PAGE of fractions of the size-exclusion chromatography. (A, C) Positions of GST-JAM-A D1 (36 kDa), GST (25 kDa), T1L  $\sigma$ 1 (18 kDa) and JAM-A D1 (11 kDa) are indicated. Molecular weight standards are marked on the left in units of kDa.

matography (figure 3.9 B, C). The complex (87 kDa) elutes from the column first, followed by the smaller JAM-A D1 dimer (22 kDa). Fractions 10-14 were pooled.

In order to test if  $\sigma$ 1 was saturated with JAM-A, additional JAM-A D1 was added to the purified complex. This did not lead to a shift of the complex peak to higher molecular weight in analytical scale size-exclusion chromatography (data not shown). We therefore concluded that the purification described above leads to formation of a complex in which all JAM-A binding sites in  $\sigma$ 1 are occupied.

### 3.3.2. Structure determination of the T1L $\sigma$ 1-JAM-A complex

The complex was concentrated to 3.6 mg/mL and crystallized using the sitting drop method with a Tecan crystallization robot (section 2.2.3.1). The largest and best diffracting crystals were obtained at 20 °C in a Hampton Screen II condition containing 0.1 M MES pH 6.5, 12% PEG 20,000. Enlargement of crystals was achieved by varying pH and PEG concentration (figure 3.10).

Interestingly, the crystals could only be reproduced if a three-year old MES stock solution was used. Therefore, a 96 well crystallization plate was set up which contained newly prepared 0.1 M MES pH 6.5 in the wells, but three-year old 0.1 M MES buffer pH 6.4, 6.7, or 6.9 in the drops. Both well and drop solutions included PEG 20,000 in the range of 13-17.5%. The crystal from which the dataset was collected grew in 0.1 M MES pH 6.9,



Figure 3.10: **Crystals of the T1L  $\sigma$ 1-JAM-A complex.** Crystals grew as hexagonal rods, up to 800  $\mu\text{m}$  in length. Some of the crystals contained a central cavity.

17.1 % PEG 20,000 after two weeks, and was flash-frozen with 20 % MPD as cryoprotectant.

Data were collected at the PX III beamline of the SLS (Villigen, Switzerland). The structure was solved by molecular replacement using the T3D  $\sigma$ 1-JAM-A complex structure as the search model (section 2.2.3.4). The ASU contains one  $\sigma$ 1 molecule, complexed with three JAM-A D1 monomers, allowing for the use of threefold NCS restraints. Refinement to 3.2  $\text{\AA}$  resolution was carried out as described in section 2.2.3.5. Detailed data processing and refinement statistics can be found in the appendix (table 6.4 on page 85). The electron density of  $2F_{obs} - F_{calc}$  maps for the  $\sigma$ 1 trimer is well defined, and most of the side chains are visible in the electron density maps. In contrast to that, electron density for the JAM-A molecules is relatively poor, especially at the side where JAM-A does not contact  $\sigma$ 1. This observation is also reflected in the crystallographic temperature factors ( $B$ -factors). The overall  $B$ -factors for the JAM-A molecules are about 1.6 times higher than the ones for the  $\sigma$ 1 trimer, indicating a higher thermal mobility of the JAM-A D1 molecules. Moreover, the  $B$ -factors of the atoms in JAM-A increase the farther away the atoms are from  $\sigma$ 1 (figure 3.11 A). Crystal packing is mainly mediated by contacts between the  $\sigma$ 1 molecules. As the crystals grow as hexagonal rods that develop central cavities (figure 3.10), dissociation of JAM-A from the complex might occur, slowly dissolving the crystals and explaining the weaker electron density observed for JAM-A.

In contrast to the T3D  $\sigma$ 1-JAM-A complex, no high-resolution structure of T1L  $\sigma$ 1 is available that could generate a highly reliable model as a starting point for refinement. Therefore, analysis of the homomeric and heteromeric contacts can be regarded only as a preview at the current resolution, until higher-resolution data are available. Table 3.1 lists amino acids in T3D  $\sigma$ 1 located in the aspartic acid cluster and the JAM-A contact area, and the corresponding residues in T1L  $\sigma$ 1, based on sequence alignment with LALIGN (Huang & Miller, 1991).

Table 3.1: **Alignment of residues in T3D and T1L  $\sigma$ 1.** Residues highlighted in *italic* are conserved between strains T1L, T2J, and T3D.

	T3D $\sigma$ 1	T1L $\sigma$ 1	LOCATION
<i>Aspartic acid cluster</i>	Tyr313	Phe330	$\alpha$ -helix between head and tail
	Arg314	Gly331	
	<i>Asp345</i>	<i>Asp362</i>	$\beta$ -turn between strands B and C
	<i>Asp346</i>	<i>Asp363</i>	
Tyr347	Trp364	$\beta$ -strand C	
<i>JAM-A contact area</i>	Arg297	Arg312	$\beta$ -spiral
	Asn312	Arg329	$\alpha$ -helix between head and tail
	<i>Arg316</i>	<i>Arg333</i>	$\beta$ -strand A
	<i>Val371</i>	<i>Val388</i>	D-E loop
	Pro376	Ser393	
	Leu379	Gln396	
	<i>Thr380</i>	<i>Thr397</i>	$3_{10}$ -helix in D-E loop
	<i>Gly381</i>	<i>Gly398</i>	
	Asp382	Asp399	
	<i>Glu384</i>	<i>Glu401</i>	D-E loop
	<i>Trp421</i>	<i>Trp436</i>	$\beta$ -strand F
	Asp423	Asp438	F-G loop

### 3.3.3. Structure of the T1L $\sigma$ 1-JAM-A complex

#### 3.3.3.1 Structure of T1L $\sigma$ 1

The overall structure of the T1L  $\sigma$ 1-JAM-A complex is very similar to the T3D  $\sigma$ 1-JAM-A complex (figure 3.11B). Each subunit of the  $\sigma$ 1 trimer binds one JAM-A D1 domain. The overall fold of  $\sigma$ 1 is conserved between the T1L and T3D strains. SSM superposition (calculated in COOT) of one subunit of T1L  $\sigma$ 1 with one subunit of T3D  $\sigma$ 1 results in an r. m. s. d. of 1.6 Å for all 162 C $\alpha$  atoms (figure 3.11C). Differences occur mainly in the  $\beta$ -spiral repeat regions and in the D-E loop between the  $3_{10}$ -helix and  $\beta$ -strand E. Some  $\beta$ -strands are shifted slightly, leading to differences in the E-F and G-H loops on the top of the head domain.

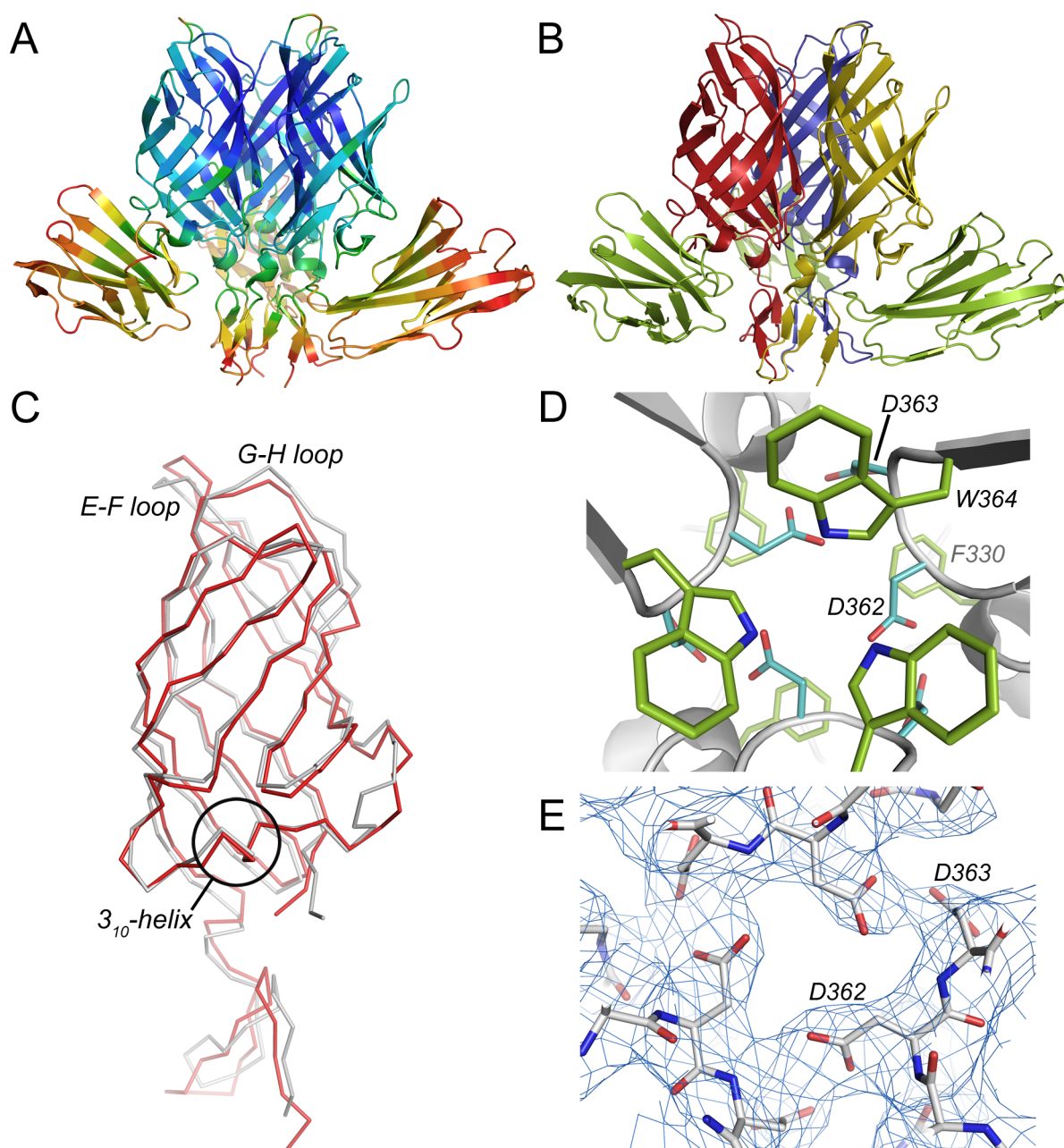


Figure 3.11: **Overall structure of the T1L  $\sigma$ 1-JAM-A complex.** (A)  $B$ -factor distribution in the T1L  $\sigma$ 1-JAM-A complex. The scale ranges from 36 Å<sup>2</sup> (blue) to 127 Å<sup>2</sup> (red). (B) Overall structure of the T1L  $\sigma$ 1-JAM-A complex.  $\sigma$ 1 subunits are shown in blue, yellow, and red; JAM-A D1 is shown in green. (C) Superposition of the  $\text{C}\alpha$ -tracings of one subunit of T1L  $\sigma$ 1 (red) and one subunit of T3D  $\sigma$ 1 (gray). (D) The T1L  $\sigma$ 1 aspartic acid cluster, viewed along the trimer axis from the top of the molecule. (E)  $2F_{\text{obs}} - F_{\text{calc}}$  electron density map at the region of the aspartic acid cluster of T1L  $\sigma$ 1, contoured at 1  $\sigma$ . (D, E) Oxygen atoms are shown in red, nitrogen atoms in blue. Hydrogen bonds are not depicted due to the limited resolution of the structure.

The composition of the aspartic acid cluster is very similar in T3D and T1L  $\sigma$ 1 (figure 3.11 D, E). Instead of the tyrosines present in T3D  $\sigma$ 1, T1L  $\sigma$ 1 uses three phenylalanines (Phe330) and three tryptophanes (Trp364) to shield the aspartic acid cluster from solvent. The conserved aspartic acid residues are oriented similarly in both serotypes, although T1L  $\sigma$ 1 lacks the arginine that is thought to stabilize Asp346 in T3D  $\sigma$ 1 (Arg314; table 3.1).

### 3.3.3.2 The T1L $\sigma$ 1-JAM-A interface

JAM-A binding by T1L  $\sigma$ 1 is nearly identical to its binding by T3D  $\sigma$ 1. JAM-A is bound at the region below the  $\beta$ -barrel, centered around the  $3_{10}$ -helix in the D-E loop, and also makes contacts with the  $\beta$ -spiral (figure 3.12 A). The combined contact area has a similar size in both complexes (1622  $\text{\AA}^2$  in the T3D and 1655  $\text{\AA}^2$  in the T1L  $\sigma$ 1 complex). However, the upper and the lower parts of the contact area are not as clearly delineated in the T1L  $\sigma$ 1-JAM-A complex as in the T3D  $\sigma$ 1-JAM-A complex. The interface in the T1L  $\sigma$ 1-JAM-A complex is more continuous, with a hydrogen bonding network ranging over the entire contact area.

Contacts at the highly conserved  $3_{10}$ -helix are nearly identical to the T3D  $\sigma$ 1-JAM-A complex (figure 3.12 B). However, an additional hydrogen bond exists between Gln396 and the main chain nitrogen atom of Arg59 in JAM-A. This interaction can not be formed by T3D  $\sigma$ 1, which has a leucine at this position (table 3.1). Interactions around the  $3_{10}$ -helix are also very similar in the T1L and T3D  $\sigma$ 1-JAM-A complexes (figure 3.12 C). The side chain of Glu401 is shifted upwards, contacting Tyr75 instead of Asn76. Another additional interaction is formed between T1L  $\sigma$ 1 residue Ser393 and JAM-A residue Tyr119.

The lower contact area exhibits good surface complementarity, as in the T3D  $\sigma$ 1-JAM-A complex. However, it contains more polar contacts in the T1L  $\sigma$ 1-complex (figure 3.12 D), where two arginine side chains contact the JAM-A F-G loop. Arg316 forms a salt bridge with JAM-A residue Glu114, and Arg329 contacts the main chain carbonyl of JAM-A residue Gly115 via a hydrogen bond.

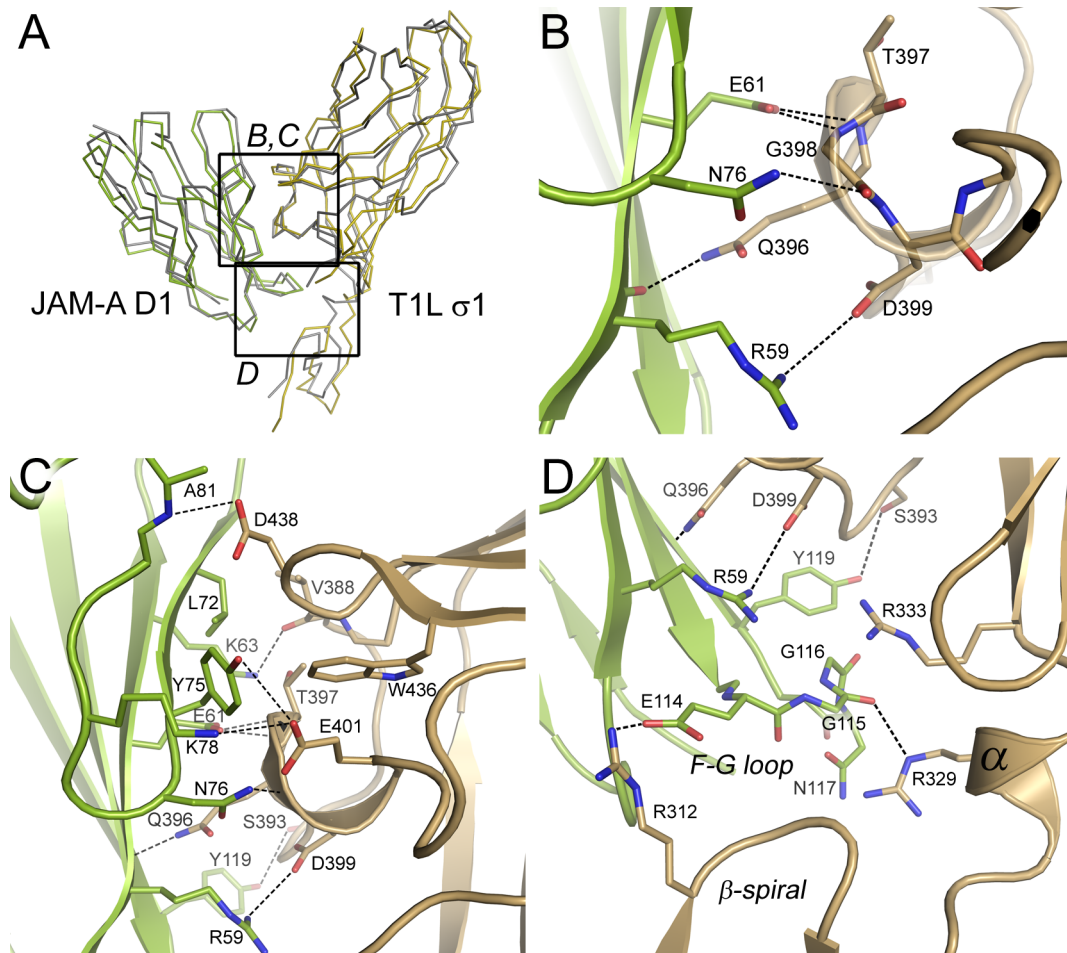


Figure 3.12: **Contacts in the T1L  $\sigma$ 1-JAM-A interface.** (A) C $\alpha$ -tracing of the contact area. The upper contact area shown in panels B and C, and the lower contact area shown in panel D are indicated.  $\sigma$ 1 is colored light brown, JAM-A is colored green. One subunit of the T3D  $\sigma$ 1 complex is superposed in gray (SSM superposition calculated in COOT). (B-D) Views of the contact area. Carbon atoms are shown in light brown ( $\sigma$ 1) or green (JAM-A), oxygen atoms in red, and nitrogen atoms in blue. Hydrogen bonds and salt bridges are represented with dotted lines. Not all contacts might be assigned correctly due to the limited resolution of the structure. (B) Contacts between JAM-A and residues in the  $\sigma$ 1  $3_{10}$ -helix in the D-E loop. The helix is depicted transparently to display the contacts to main chain atoms. (C) Additional contacts between JAM-A and  $\sigma$ 1 around the region shown in B. (D) Interactions between the JAM-A F-G loop and  $\sigma$ 1.

## 3.4. Stability of the JAM-A homodimer

### 3.4.1. Mixing of JAM-A D1 and D1D2

The T3D  $\sigma$ 1-JAM-A complex is produced readily in solution at 4 °C by mixing the two components. As  $\sigma$ 1 binds to the JAM-A homodimer interface, it either has to disrupt the JAM-A dimers or engage monomeric JAM-A present in solution. Although it has been shown that JAM-A dissociates under high salt or low pH conditions (Bazzoni *et al.*, 2000), no monomeric species has been detected at neutral pH with the low salt concentrations used for complex formation (data not shown). However, it is possible that monomeric JAM-A is present transiently under these conditions.  $\sigma$ 1 could trap monomeric JAM-A in a complex, since  $\sigma$ 1-JAM-A binding occurs with faster kinetics than JAM-A homophilic association in solid-phase binding assays (Forrest *et al.*, 2003). To test this hypothesis, dimeric JAM-A D1 and JAM-A D1D2 were incubated in an equimolar ratio, followed by size-exclusion chromatography. Since D1 and D1D2 dimers have molecular weights of 22 and 46 kDa, respectively, they can be distinguished by their elution volumes. If JAM-A transiently dissociates into monomers, one would expect the formation of a dimeric species with one monomer contributed by D1 and the other by D1D2. Such a species should produce a peak with an elution volume between the two observed peaks for the D1 and D1D2 dimers. No such species was observed after 60 min incubation at 21 °C, indicating that JAM-A does not dissociate into monomers under these conditions (figure 3.13). The same result was obtained for incubation at 4 °C for 5 or 60 min (data not shown). Although the two peaks are not fully separated, the differences compared to the unmixed proteins are presumably due to limits of column resolution. Thus, it can be concluded that, at least in solution,  $\sigma$ 1 possesses the ability to forcibly displace a JAM-A monomer to gain access to the JAM-A dimer interface.

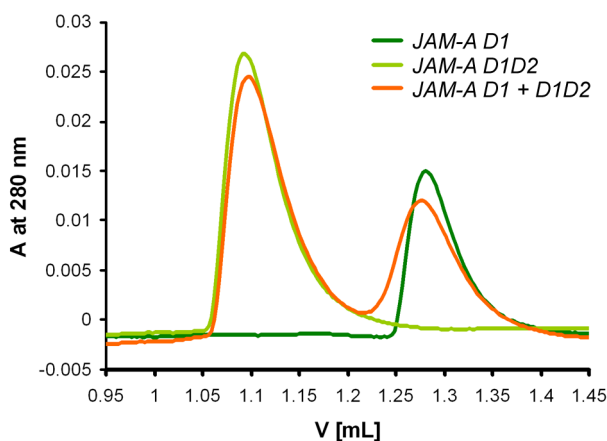


Figure 3.13: **Stability of the JAM-A dimer.** Size-exclusion chromatograms of JAM-A D1 (dark green), D1D2 (light green), and equimolar mixtures of both proteins (orange) after 60 min incubation at 21 °C.

### 3.4.2. Analytical ultracentrifugation

Disruption of JAM-A homodimers by  $\sigma 1$  could be facilitated by a significantly higher affinity between  $\sigma 1$  and JAM-A compared to the homophilic JAM-A interaction. The dissociation constant ( $K_D$ ) for the T3D  $\sigma 1$ -JAM-A complex, determined by surface plasmon resonance, lies in the low nanomolar range, between  $2.4 \times 10^{-9}$  M (Guglielmi *et al.*, 2007) and  $10 \times 10^{-9}$  M (Barton *et al.*, 2001b). In order to determine the  $K_D$  of the homomeric JAM-A interaction, analytical ultracentrifugation was performed by Holger Strauss (Nanolytics, Potsdam, Germany; section 2.2.4) at near-physiological conditions (Tris pH 7.5, 100 mM NaCl). SV experiments were performed at five concentrations of JAM-A D1 between 0.06 and 1.31 mg/mL. SV showed little concentration dependence of the sedimentation coefficient (figure 6.3 A on page 86 in the appendix). The main component sediments at 2.35 S, corresponding to molar masses between 19 and 22 kg/mol. This is close to the molar mass expected for dimeric JAM-A D1 (22 kg/mol). A second component, sedimenting at 3.8 S, could be detected. This species is most likely tetrameric JAM-A D1 (44 kg/mol). Tetramers of JAM-A have been observed in solution (Bazzoni *et al.*, 2000), but the analytical ultracentrifugation experiments did not reveal a concentration-dependent formation of tetramers. This suggests that the observed JAM-A tetramers are not physiologic.

Three different speeds between 17.5 and 35.0 krpm, and four different concentrations between 0.16 and 1.6 mg/mL were used for SE experiments. The best fit for the datasets obtained was for a monomer-dimer model with variable amounts of tetramer (figure 6.3 B on page 86 in the appendix). The fit showed an r. m. s. d. of  $1.99 \times 10^{-2}$  with 5109 degrees of freedom. The molar mass converged to a value of 10.94 kg/mol (10.90 to 11.16 kg/mol), very close to the expected molar mass of monomeric JAM-A D1 (11.5 kg/mol). The  $K_D$  obtained from this fit is  $1.1 \times 10^{-5}$  M (0.8 to  $1.4 \times 10^{-5}$  M). Thus, the  $K_D$  of the homomeric JAM-A interaction is about 1000-fold higher than that of the T3D  $\sigma 1$ -JAM-A complex, favoring complex formation with  $\sigma 1$  over the homodimeric interaction.

## 4. Discussion

### 4.1. The aspartic acid cluster

#### 4.1.1. Mutations in the aspartic acid sandwich

After the structure of T3D  $\sigma 1$  was solved at 2.6 Å resolution (Chappell *et al.*, 2002), a unusual cluster of conserved aspartic acid residues was found at the trimer interface. To further investigate the function of this unusual trimerization motif, a shorter construct of  $\sigma 1$  was crystallized by Pierre Schelling (Schelling *et al.*, 2007). Its structure was refined to 1.75 Å resolution and revealed details of the aspartic acid cluster. The six aspartic acids are located at the tip of a rigid  $\beta$ -hairpin and therefore possess limited mobility. Two water molecules are positioned on the trimer axis above and below the aspartic acid side chains. As the cluster is shielded from solvent with two layers of tyrosines, one layer on each side, it is unlikely that these water molecules can be exchanged. The location of the aspartic acids suggests that Asp345 is protonated to avoid accumulation of negative charges. This assumption was also confirmed by molecular dynamics studies (Cavalli *et al.*, 2004).

In order to test the hypothesis that Asp345 is protonated, Asp345 was mutated to asparagine. Asparagine can form the same hydrogen bond pattern as a protonated aspartate. The JAM-A binding properties of  $\sigma 1$  D345N were indistinguishable from wt protein in size-exclusion chromatography (section 3.1.2.2) and surface plasmon resonance assays, conducted by Kristen Guglielmi (Schelling *et al.*, 2007). Furthermore, its structure, refined to 1.85 Å, is highly similar to the wt structure (section 3.1.2.1). Even the two water molecules above and below the aspartic acid cluster are located at the same positions.

One of the tyrosine residues that shield the aspartic acid cluster from solvent was mutated to alanine (Schelling *et al.*, 2007). The properties of the mutant protein were analyzed by Bernhard Pätzold. The Y313A mutant was folded properly according to CD spectroscopy but eluted at the molecular weight of a monomer using size-exclusion

chromatography. It is therefore likely that mutation of Y313 into a less bulky and less hydrophobic residue renders the aspartic acid cluster accessible to solvent, leading to deprotonation of Asp345 and destabilization of the  $\sigma 1$  trimer (Schelling *et al.*, 2007). The analysis of the two mutants, D345N and Y313A, provides further evidence that Asp345 has to be protonated in the wt protein to allow formation of a stable trimer.

#### 4.1.2. Comparison of T1L and T3D $\sigma 1$

The structural organizations of the aspartic acid clusters of T1L and T3D  $\sigma 1$  are very similar. The aspartic acids are oriented in the same way in both serotypes and are shielded from solvent with bulky aromatic residues. T3D  $\sigma 1$  sandwiches the cluster between two layers of tyrosines (Tyr313 and Tyr347), whereas T1L  $\sigma 1$  has a phenylalanine and a tryptophane (Phe330 and Trp364) at the equivalent positions. The major difference between the serotypes is that T1L  $\sigma 1$  lacks the arginine that stabilizes Asp346 in T3D  $\sigma 1$  (Arg314), as the corresponding residue in T1L  $\sigma 1$  is a glycine (Gly331).

Does the missing arginine render the T1L  $\sigma 1$  trimer less stable compared to T3D  $\sigma 1$ ? The properties of the two proteins may provide an answer to this question. During attempts to purify T1L  $\sigma 1$  without JAM-A affinity chromatography, it was found that purified T1L  $\sigma 1$  did not bind JAM-A. Receptor-binding protein could not even be obtained when no ammonium sulfate precipitation, refolding, or freezing of the protein solution was used, and the purification was carried out in less than 24 h (data not shown). Furthermore, the purified protein eluted from size-exclusion columns at a lower molecular weight compared to T3D  $\sigma 1$ . Elution at lower molecular weight has been observed before for T1L  $\sigma 1$  purified with GST or hexahistidine tags (Böttinger, 2006). In all cases, the protein eluted at a molecular weight of about 35 kDa. This size corresponds to dimeric  $\sigma 1$ , but the elution behavior might also be caused by a partially misfolded protein. It is therefore possible that the aspartic acid cluster of T1L  $\sigma 1$  is not as stable or not as easily formed as the one in T3D  $\sigma 1$ . In the T1L  $\sigma 1$  construct comprising only the head domain and the most C-terminal  $\beta$ -spiral repeat, this might lead to changes in secondary and tertiary structure that abolish trimer formation and JAM-A binding.

#### 4.1.3. The aspartic acid cluster as a molecular switch

A cluster of aspartic acids has also been found in the G protein of the enveloped virus vesicular stomatitis virus (VSV) (Roche *et al.*, 2006). The G protein mediates membrane fusion of VSV, and the structures of both the prefusion form and the form adopted by the

protein at low pH were solved by X-ray crystallography (Roche *et al.*, 2006, 2007). The overall architecture of VSV G and reovirus  $\sigma 1$  is different (figure 4.1 A, C). However, the low pH conformer of VSV G also contains an aspartic acid cluster in which three aspartic acids are arranged in close proximity at the trimer interface (figure 4.1 B).

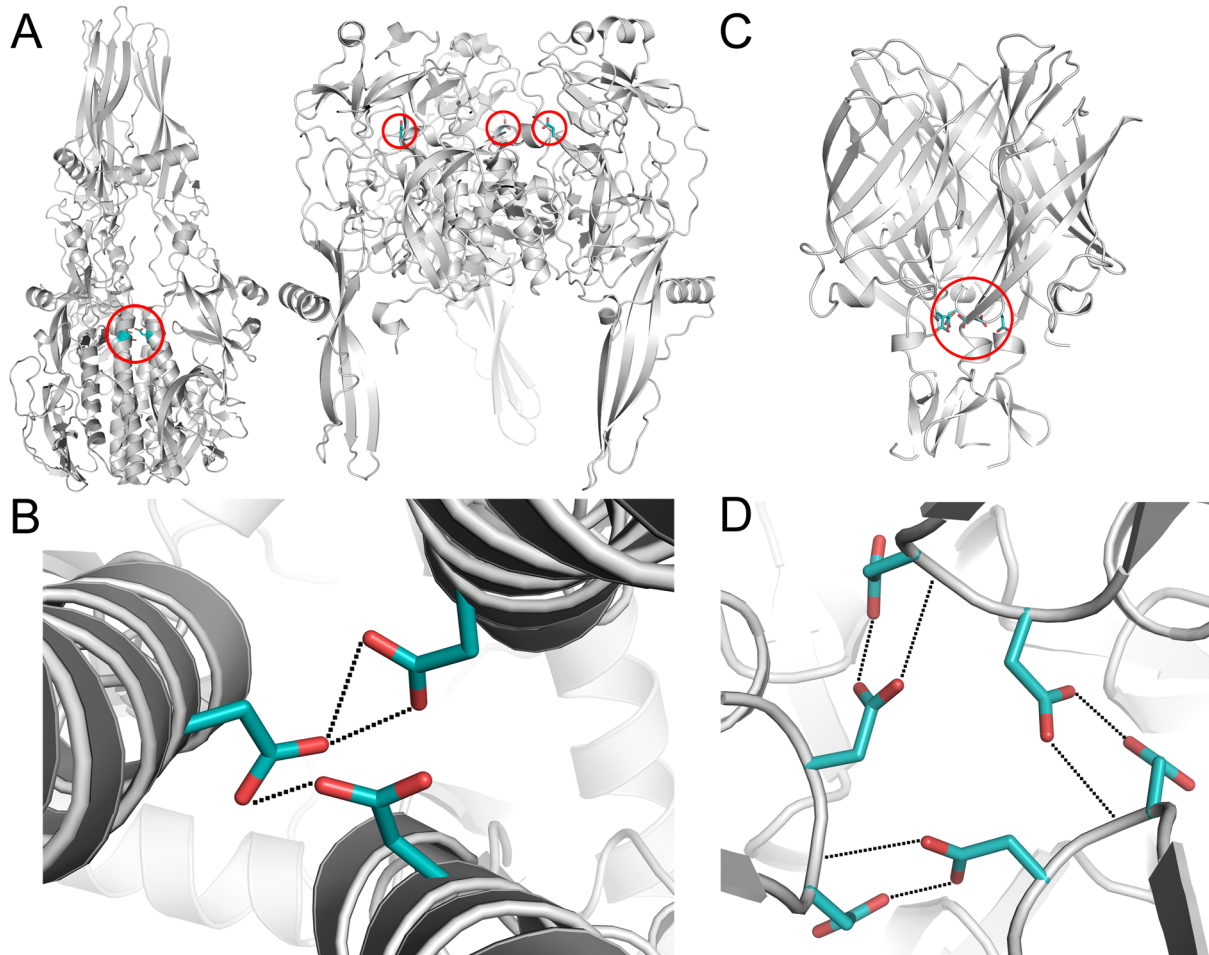


Figure 4.1: **The aspartic acid clusters in VSV G and reovirus  $\sigma 1$ .** (A) Ribbon drawings of the low pH (left) and prefusion forms (right) of VSV G (Roche *et al.*, 2006, 2007). The positions of the aspartic acids (Asp268) are indicated by red circles. (B) View of the aspartic acid cluster along the trimer axis of the low pH form of VSV G. (C) Ribbon drawing of T3D  $\sigma 1$  (Schelling *et al.*, 2007). The aspartic acid cluster (Asp345, Asp346) is indicated by a red circle. (D) View of the T3D  $\sigma 1$  aspartic acid cluster along the trimer axis. (A-D) Carbon atoms of the aspartic acid side chains are colored cyan, oxygen atoms are colored red. Hydrogen bonds are depicted as dotted lines. Figure modified from Schelling *et al.* (2007).

The arrangements of the aspartic acid clusters in VSV G and reovirus  $\sigma 1$  are surprisingly similar (figure 4.1 B, D). The aspartic acids of both trimers are located on relatively rigid backbone structures, an  $\alpha$ -helix in VSV G and a  $\beta$ -hairpin in reovirus  $\sigma 1$ . The plane defined by the aspartic acids is perpendicular to the trimer axes, and the aspartic

acids form several hydrogen bonds. Similar to reovirus  $\sigma 1$ , deprotonation of the aspartic acids in VSV G would destabilize the trimer. Moreover, both aspartic acid clusters contain trapped water molecules that form hydrogen bonds with the protonated carboxylate groups.

In the case of VSV G, the protein also exists in a form where the aspartic acids are located far away from each other in the trimer (figure 4.1 A) (Roche *et al.*, 2007). This form has been interpreted as the pre-fusion form. Low pH after endosomal uptake of VSV leads to protonation of the aspartic acids and thus permits a conformational change, bringing the aspartic acids in close proximity. The conformational change leads to fusion of VSV with the endosomal membrane, allowing the virus to escape into the cytoplasm. It is therefore likely that the reovirus  $\sigma 1$  aspartic acid cluster also serves as a molecular switch that disfavors trimerization when charged, but leads to trimerization in a low pH environment such as the endosome, where the aspartic acids are protonated. Both reovirus  $\sigma 1$  and the low pH form of VSV G were crystallized at close-to-neutral pH, but the crystallization conditions are far from physiologic in both cases. The crystallization conditions could have favored the protonation of the aspartic acids, e.g., by high salt concentrations. The fully trimerized reovirus  $\sigma 1$  is likely to be the energetically favored form of the protein (Schelling *et al.*, 2007). Therefore, it is also likely that the trimers form already during expression or purification of the T3D  $\sigma 1$  head domain, remaining stable even at neutral pH due to the effective shielding of the aspartic acid cluster.

In context of whole virions, the aspartic acid cluster in reovirus  $\sigma 1$  might mediate a structural transition between a protein that is partly detrimerized in the head region and a fully trimerized molecule, as seen in the crystal structure. The partly detrimerized molecule would be present on the virion at conditions of neutral pH, prior to viral entry. In this hypothetical scenario, the  $\sigma 1$  head domains are further apart from each other due to electrostatic repulsion in the region of the aspartic acid cluster, while the  $\sigma 1$  tail is trimerized, holding the subunits together. The long  $\sigma 1$  tail might be necessary for stabilization of the detrimerized head domains, a likely explanation for the problems occurring during purification of the  $\sigma 1$  constructs. For example, cleavage of the T3D GST- $\sigma 1$  fusion protein often led to precipitation of large amounts of  $\sigma 1$  (Schelling *et al.*, 2007). The highly soluble GST tag may have the same effect as the  $\sigma 1$  tail, stabilizing monomeric  $\sigma 1$  head domains. If the aspartic acids are not protonated during cleavage, the  $\sigma 1$  molecules can not trimerize, leading to precipitation of the protein.

Another possibility for a structural rearrangement is a dimer-trimer transition of full-length  $\sigma 1$  during viral entry. Rotavirus, another member of the *Reoviridae* family, exhibits such a conformational change. The rotavirus attachment proteins, VP4, protrude from the

virion as spikes with approximate two-fold symmetry in cryoelectron microscopy image reconstructions (Shaw *et al.*, 1993; Yeager *et al.*, 1994). The base of the molecule, however, has approximate three-fold symmetry (Yeager *et al.*, 1994). A triggering event, probably low pH, leads to a rearrangement, in which the two subunits fold back on themselves, forming a trimer with a third subunit (Dormitzer *et al.*, 2004). The conformation of VP4 observed in the averaged cryoelectron microscopy images may include not only the rigid dimer in the protruding spike, but also a third subunit, which is not visible in the averaged images due to flexibility. Similarly to  $\sigma 1$ , the base of the trimeric form of VP4 is formed by an  $\alpha$ -helical coiled coil close to the virion surface. Furthermore, the core of rotavirus VP4 forms an eight-stranded  $\beta$ -sandwich, whose closest structural homolog is reovirus T3D  $\sigma 1$  (Yoder & Dormitzer, 2006). Although the homology between reovirus  $\sigma 1$  and rotavirus VP4 does not extend beyond these two domains, the transition from a dimer to a trimer during viral entry of rotavirus may also be a mechanism used in reovirus entry.

After uptake of the reovirus virions into the endosome, the pH is low enough to favor protonation of the aspartic acids. The head domain or the full-length protein can now trimerize, adopting the energetically more favored form (Schelling *et al.*, 2007). Such a conformational change could facilitate the structural rearrangements and proteolytic disassembly of reovirus virions occurring in the endosome (section 1.2.2).

## 4.2. The reovirus $\sigma 1$ -JAM-A complex

### 4.2.1. Disruption of JAM-A homodimers

JAM-A forms dimers in solution (Bazzoni *et al.*, 2000) and most likely also at the cell surface. However, the structures of T1L and T3D  $\sigma 1$  in complex with the JAM-A D1 domain reveal that the JAM-A dimers have to be disrupted in order to form the complex. Comparison of the thermodynamic properties of the T3D  $\sigma 1$ -JAM-A complex and the JAM-A homodimer interaction revealed a possible strategy employed by reovirus in order to engage the JAM-A dimer interface: Analytical ultracentrifugation showed that formation of the T3D  $\sigma 1$ -JAM-A complex is clearly preferred over the formation of JAM-A homodimers. The  $K_D$  of the interaction between T3D  $\sigma 1$  and JAM-A is about 1000-fold lower (Barton *et al.*, 2001b; Guglielmi *et al.*, 2007) than the  $K_D$  for the JAM-A homodimer interaction (section 3.4.2). The large differences in affinity are surprising, given that both interactions bury a contact area similar in size and share many of the same residues (figure 4.2 A, B). Moreover,  $\sigma 1$  mimics JAM-A homodimer interactions. For example,

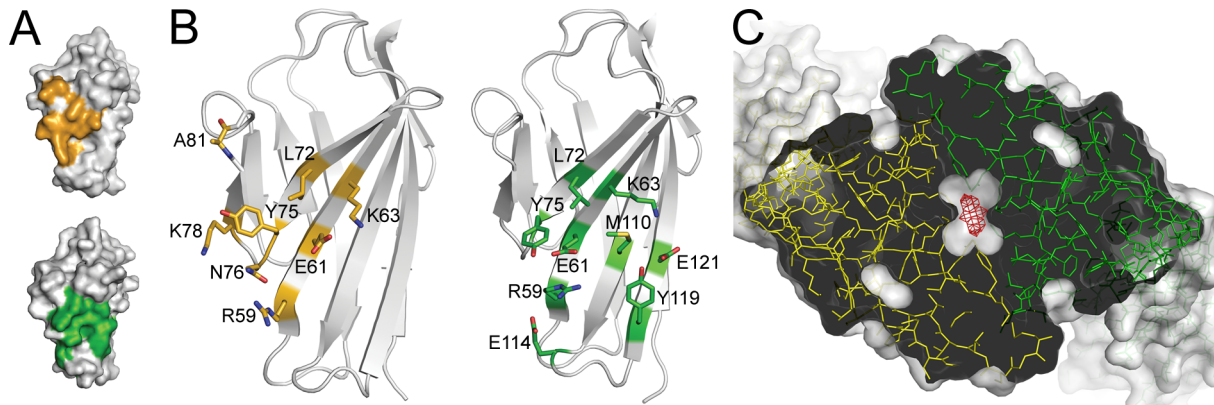


Figure 4.2: **Interactions in the JAM-A dimer and in the T3D  $\sigma 1$ -JAM-A complex.** (A) Surface representations of JAM-A D1. Key contact residues (residues forming hydrogen bonds, salt bridges, or close hydrophobic contacts) are highlighted in orange for the T3D  $\sigma 1$ -JAM-A complex (top), and in green for the JAM-A dimer (Prota *et al.*, 2003) (bottom). (B) Ribbon drawings of JAM-A D1. The residues highlighted in A are shown as stick representations. Carbon atoms are shown in orange for the T3D  $\sigma 1$ -JAM-A complex (left), and in green for the JAM-A dimer (right). Oxygen atoms are colored red, nitrogen atoms blue, and sulfur atoms yellow. (C) Cavity at the JAM-A dimer interface. The JAM-A homodimer (Prota *et al.*, 2003) is viewed along the dimer axis. The two subunits are depicted in stick representation (green and yellow). The protein surface is shown as a semitransparent white rendering. The JAM-A D1 domain was cross-sectioned to reveal the cavity. The cavity is shown as a red mesh and was calculated using VOIDOO (Kleywegt & Jones, 1994). Figure modified from Kirchner *et al.* (2008).

JAM-A residue Arg59 forms a salt bridge with Asp382 in the complex with T3D  $\sigma 1$ , and a salt bridge with Glu61 in the JAM-A homodimer. Also, Leu72 and Tyr75 are engaged in hydrophobic interactions in both the  $\sigma 1$ -JAM-A complex and the JAM-A dimer.

One possible explanation for the significantly lower affinity in the JAM-A homodimer is the fact that a cavity of about  $7 \text{ \AA}^3$  in size is located directly in the contact area formed between two JAM-A D1 domains (figure 4.2 C). Murine JAM-A, to which  $\sigma 1$  can bind as well (Barton *et al.*, 2001b), exhibits a similar cavity at its homodimeric interface (Kostrewa *et al.*, 2001). No such cavity is found in the  $\sigma 1$ -JAM-A complex, where the contact areas exhibit nearly perfect surface complementarity. Two water molecules are visible in the cavity of the JAM-A interface, and two more are located adjacent to this surface (Prota *et al.*, 2003). Water molecules in cavities can significantly destabilize hydrogen bonds and salt bridges by lowering the dielectric constant of the medium. Therefore, the presence of water molecules in the cavity could weaken the homomeric JAM-A interaction. The JAM-A dimer interface is of a dynamic nature, facilitating transitions between monomeric and dimeric forms (Prota *et al.*, 2003). This behavior might play a role in the regulation of tight junction permeability.

Reovirus is not the only pathogen that takes advantage of these special features of protein interactions in regions of cell-cell contact. Many other viruses such as HIV, measles virus, and poliovirus, use adhesion molecules as receptors (discussed in Wang (2002)). In this way, the viruses may take advantage of the relatively weak binding affinity involved in cell adhesions, evolving a stronger affinity, which allows for successful competition with physiological receptors.

#### 4.2.2. Cell attachment by reovirus T3D $\sigma 1$

Combining the structures of the T3D  $\sigma 1$ -JAM-A complex, the JAM-A extracellular domains (Prota *et al.*, 2003), and the C-terminal part of T3D  $\sigma 1$  (Chappell *et al.*, 2002) allows a visualization of how  $\sigma 1$  interacts with JAM-A at the cell surface (figure 4.3).

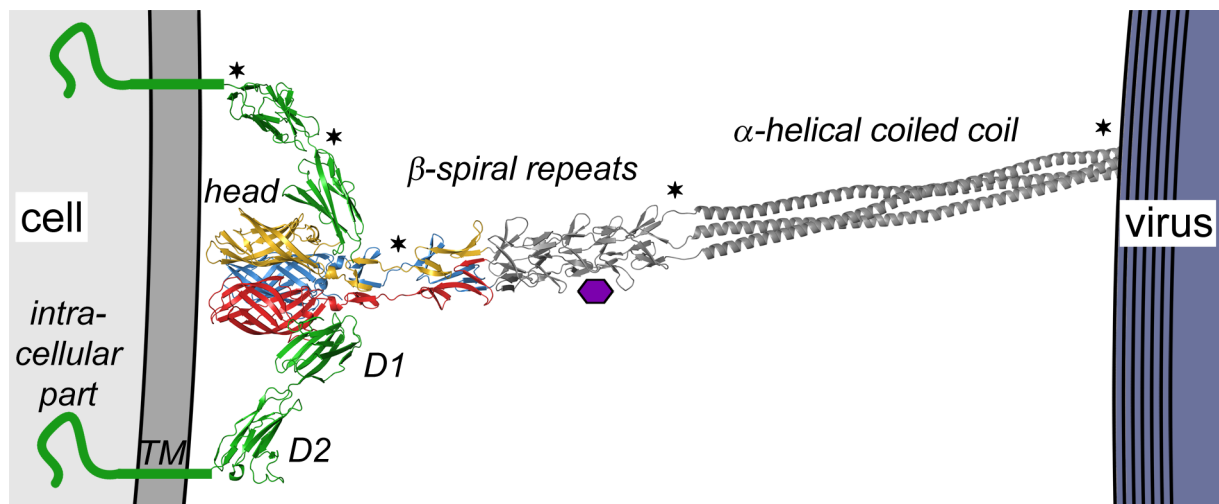


Figure 4.3: **Full-length model of the T3D  $\sigma 1$ -JAM-A complex.** Ribbon drawing of a full-length model of T3D  $\sigma 1$ , extending from the schematic representation of a virion. The known structure of the C-terminus (Chappell *et al.*, 2002) is shown in tricolor, the predicted structure of the N-terminus in gray. The extracellular domains of JAM-A (Prota *et al.*, 2003) are shown as a green ribbon trace, completed by schematic representations of the transmembrane (TM) and intracellular domains. For clarity, only two JAM-A molecules are shown. The predicted sialic acid binding site is represented by a purple hexagon. Regions of flexibility in both proteins are indicated by asterisks. The coordinate files for the models of the  $\sigma 1$   $\beta$ -spiral and coiled coil regions were generated by Dirk Reiter and Thilo Stehle, respectively. Figure modified from Kirchner *et al.* (2008).

The full-length model of  $\sigma 1$  and the structure of the JAM-A D1D2 domains (Prota *et al.*, 2003), were superimposed onto the structure of the T3D  $\sigma 1$ -JAM-A complex by SSM superposition in COOT (Emsley & Cowtan, 2004). The model illustrates that JAM-A must reach beyond the approaching  $\sigma 1$  head to access the binding site. The predicted sialic

acid binding site of T3D  $\sigma$ 1 is located near the midpoint of the elongated  $\sigma$ 1 molecule. It is likely that the known regions of flexibility in both the receptor and the attachment protein (Fraser *et al.*, 1990; Furlong *et al.*, 1988; Prota *et al.*, 2003) facilitate reovirus attachment. If both subunits of a JAM-A dimer are located on the same cell,  $\sigma$ 1 could disrupt the dimer into monomers and thus engage more than one JAM-A molecule simultaneously. The clamp formed by several molecules of JAM-A would then tightly adhere the virus to the cell surface.

### 4.2.3. Mutations in the $\sigma$ 1-JAM-A interface

The  $3_{10}$ -helix of  $\sigma$ 1 forms the center of the contact area with JAM-A. Therefore, several of the amino acids located in and around this region in reovirus T3D  $\sigma$ 1 were mutated to alanine in order to identify the contributions of individual residues to the complex interaction (Kirchner *et al.*, 2008). These experiments were conducted by Kristen Guglielmi (Vanderbilt University). Using the plasmid-based reverse genetics system available for reovirus (Kobayashi *et al.*, 2007), T3D virions with mutations in the gene encoding  $\sigma$ 1 were isolated. They were tested for infectivity in cell culture using indirect immunofluorescence, and for binding to GST-JAM-A using surface plasmon resonance. Of all mutations tested, N369A, T380A, G381A, and D423A exhibited the largest decrease in infectivity or binding (Kirchner *et al.*, 2008). Thr380, Gly381, and Asp423 are located directly at the complex interface (figure 3.7 in section 3.2.2.3), and Asn369 is located at the beginning of the D-E loop. The decrease in infectivity and binding can be explained by the structure of the T3D  $\sigma$ 1-JAM-A complex. Mutation of the conserved Gly381 to any other residue would lead to steric clashes of the side chains with JAM-A residues in the vicinity of  $\sigma$ 1 residue 381. The sidechains of Thr380, which is also conserved between the serotypes, and Asp384 likely shield hydrophobic interactions in the interface from solvent. Thr380 also makes contacts with other residues in  $\sigma$ 1. It is therefore likely that truncation of the threonine side chain affects the structural integrity of the  $3_{10}$ -helix. Asn369 does not contact JAM-A directly, but is located in the D-E loop and thus in proximity to the binding interface. It probably stabilizes the  $3_{10}$ -helix by contacting the main chain nitrogen of Val371. Thus, the reduced binding observed for the N369A mutant might also be attributable to changes in local structure.

Before the structure of the  $\sigma$ 1-JAM-A complex was solved, several residues in the dimer interface of JAM-A were mutated to alanine (Guglielmi *et al.*, 2007). Infectivity assays with T1L, T2J, and T3SA- (a type 3 reovirus that does not bind sialic acid) virions and surface plasmon resonance with the purified T3D  $\sigma$ 1 head domain were conducted

by Kristen Guglielmi (Vanderbilt University) to determine the residues in JAM-A important for binding of  $\sigma 1$ . Residues Glu61, Lys63, and Leu72 were required for efficient engagement of JAM-A by reovirus T3D, and Arg59, Tyr75, and Asn76 were identified as additionally important contacts (see also figure 1.5 in section 1.3.3) (Guglielmi *et al.*, 2007). These residues form key contacts in the T3D  $\sigma 1$ -JAM-A complex, mediating hydrogen bonds, salt bridges or close hydrophobic interactions. For engagement of reovirus T1L and T2J, only infectivity assays could be conducted, as purified T1L or T2J  $\sigma 1$  protein was not available. Binding of both T1L and T2J reovirions was not as affected by mutations in the JAM-A interface as observed for T3SA- virions (Guglielmi *et al.*, 2007). T1L virions showed reduced infectivity for the R59A/E61A double mutant, and only a slight decrease in infectivity for K63A and the E61A/K63A double mutant. It is certainly possible that T1L virions utilize another receptor, e. g., a carbohydrate, thus diminishing the effect of the mutations in JAM-A. The results might also be explained with the structure of the T1L  $\sigma 1$ -JAM-A complex. Compared to the T3D  $\sigma 1$ -JAM-A complex, the T1L complex comprises two additional hydrogen bonds and one additional salt bridge (section 3.3.3.2). One of those hydrogen bonds is located at the  $3_{10}$ -helix, with Gln396 contacting the main chain nitrogen of JAM-A residue Arg59. Due to an additional main chain contact in the center of the interface, the interaction between T1L  $\sigma 1$  and JAM-A might not be as dependent on a single mutation in this area as it is the case for T3D  $\sigma 1$ .

#### 4.2.4. Related virus-receptor complexes

##### 4.2.4.1 Comparison to the adenovirus fiber-CAR complex

The structural analysis of reovirus  $\sigma 1$  and JAM-A revealed striking similarities to another virus-receptor interaction. The adenovirus (Ad) attachment protein, fiber, and the coxsackievirus and adenovirus receptor (CAR) closely resemble reovirus  $\sigma 1$  and JAM-A, respectively, pointing to an evolutionary relationship in the attachment strategies used by these non-enveloped viruses (Stehle & Dermody, 2003, 2004). The overall architecture of adenovirus fiber is very similar to reovirus  $\sigma 1$ . Fiber is also an elongated trimer with a globular head and a fibrous tail, with the head domain forming  $\beta$ -barrels composed of Greek-key motifs, and the tail forming  $\beta$ -spiral repeats (van Raaij *et al.*, 1999). Moreover, fiber is also anchored into a pentameric protein, the penton base, at the virion surface. In adenovirus fiber, however, the individual  $\beta$ -strands of the head domain are connected by much longer loops than in the reovirus  $\sigma 1$  head. The viral receptors, JAM-A and CAR, are both components of tight junctions with two extracellular Ig-like domains. Fur-

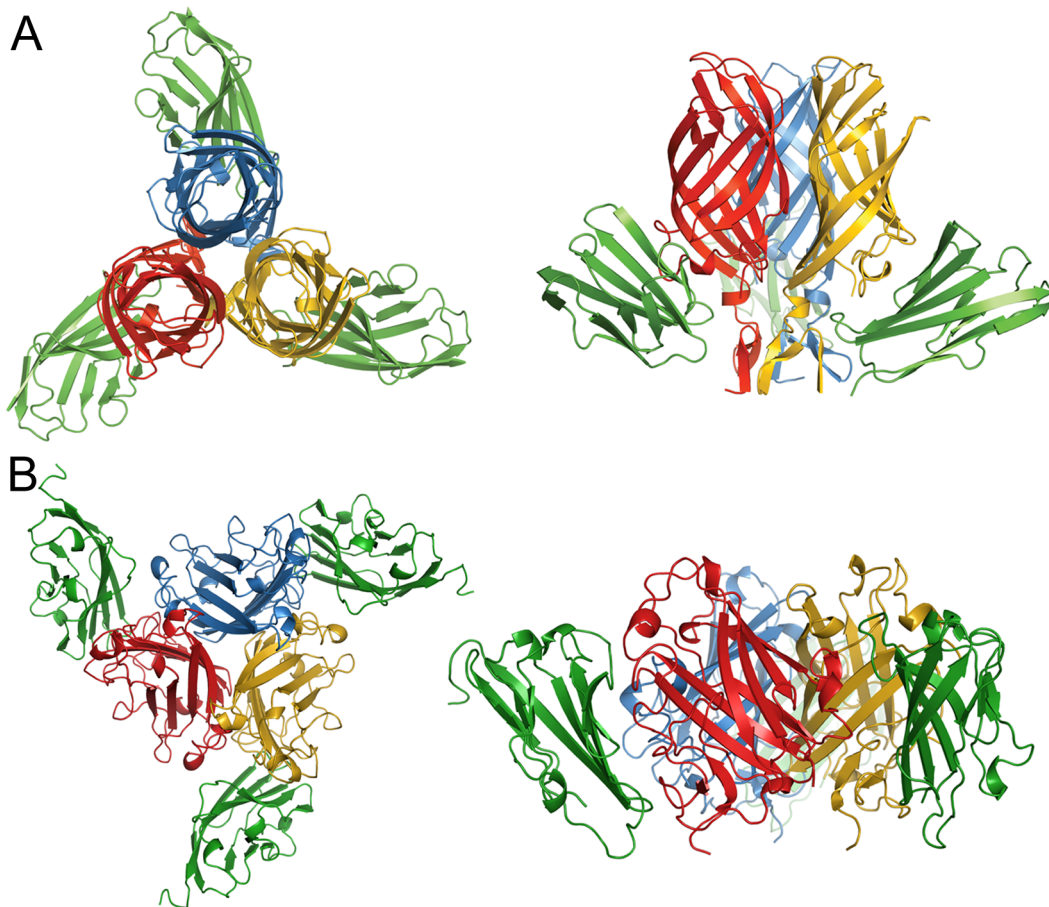


Figure 4.4: **Comparison of the reovirus  $\sigma 1$ -JAM-A and the adenovirus fiber-CAR complex.** The T3D  $\sigma 1$ -JAM-A complex (A) and the Ad12 fiber-CAR complex (Bewley *et al.*, 1999) (B) viewed along the trimer axis (left) and from the side (right). The trimeric attachment proteins  $\sigma 1$  and fiber are shown in red, blue, and yellow; the receptors JAM-A and CAR are shown in green.

thermore, both proteins dimerize using the GFCC<sup>1</sup>-sheets of their membrane-distal D1 domains (Prota *et al.*, 2003; van Raaij *et al.*, 2000).

The structure of the reovirus  $\sigma 1$ -JAM-A complex provides additional support for the theory of common ancestry between adenovirus and reovirus. Both attachment proteins form trimers that engage three molecules of the monomeric D1 domains of their receptors (figure 4.4) (Bewley *et al.*, 1999). Like JAM-A, CAR uses its dimer interface and top to contact the viral attachment protein. In both cases, the contact residues are located on and adjacent to  $\beta$ -strands C, C', C'', F, and G. The dissociation constants are also similar in both interactions, favoring formation of the virus-receptor complex over receptor dimerization. As in the case of the reovirus  $\sigma 1$ -JAM-A interaction, the  $K_D$  for the adenovirus fiber-CAR complex is in the nanomolar range ( $0.5$  to  $1.5 \times 10^{-8}$  M for Ad5)

(Kirby *et al.*, 2000), and thus 1000-fold lower than the  $K_D$  for the homodimeric CAR interaction ( $1.6 \times 10^{-5}$  M) (van Raaij *et al.*, 2000).

However, there are differences in the virus-receptor complexes in the location of the binding sites on the viral attachment proteins. The binding site for CAR on adenovirus fiber is located entirely on the head domain and does not include regions of the tail (figure 4.4). Many of the contact residues are provided by the long loops between the  $\beta$ -strands in the fiber head domain. In contrast to the  $\sigma 1$ -JAM-A complex, in which one JAM-A D1 domain exclusively contacts one  $\sigma 1$  subunit, CAR also forms some contacts with a second subunit of the fiber trimer. The two virus-receptor complexes are therefore similar in the contact areas formed by the receptor molecules and concerning the thermodynamic forces that lead to complex formation, but the viral attachment proteins engage the receptors using different binding sites.

#### 4.2.4.2 JAM-A and CAR as receptors for other viruses

JAM-A and CAR are also targeted by viruses other than reovirus and adenovirus, respectively. Feline calicivirus binds the feline homolog of JAM-A, fJAM-1 (Makino *et al.*, 2006), while CAR is used as a receptor by coxsackievirus (Bergelson *et al.*, 1997). Feline calicivirus and coxsackievirus are both spherical non-enveloped viruses. In contrast to reovirus and adenovirus, they seem to require both extracellular domains of their receptors, D1 and D2, for efficient receptor engagement (He *et al.*, 2001; Ossiboff & Parker, 2007). For both interactions, cryoelectron microscopy structures are available. The structure of feline calicivirus in complex with fJAM-1 shows both domains of fJAM-1 bound to the virus, with the majority of contacts located on the D1 domain (Bhella *et al.*, 2008). Only the D1 domain of CAR binds to coxsackievirus in the complex structure, but the formation of the complex requires both domains of CAR, D1 and D2 (He *et al.*, 2001). CAR D2 might be necessary for the separation of the D1 domains by coxsackievirus.

#### 4.2.5. Ig superfamily members as viral receptors

Reovirus receptor JAM-A comprises two extracellular Ig-like domains (Prota *et al.*, 2003). The Ig fold is named after the characteristic fold of immunoglobulins, consisting of two  $\beta$ -sheets formed by antiparallel  $\beta$ -strands (Bork *et al.*, 1994; Harpaz & Chothia, 1994). The four  $\beta$ -strands B, C, E, and F form the core of the fold, completed by three to five additional strands, A, C', C'', D, and G. Two main subtypes of the Ig fold can be distinguished, named C-set and V-set after the fold of the constant and variable domains

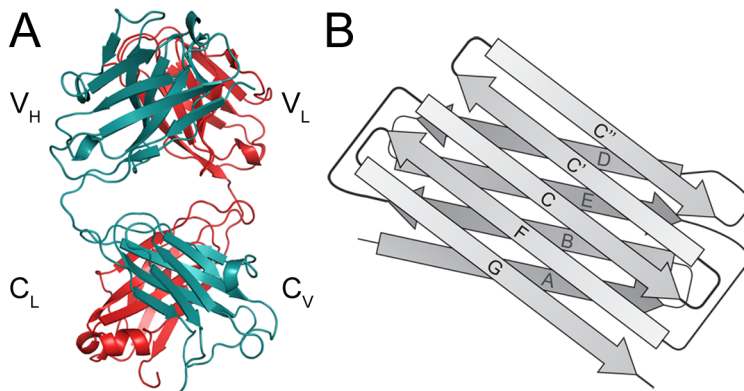


Figure 4.5: **The Ig fold.** (A) Ribbon tracing of a Fab fragment of Mab231 (Harris *et al.*, 1997). Variable (V) and constant (C) domains of heavy (H) and light (L) chains are indicated. (B) Schematic representation of the V-set Ig domain fold.

occurring in immunoglobulins (figure 4.5). The I-set is an intermediate between the V- and C-set domains.

The membrane-distal D1 domain of JAM-A belongs to the V-set (Prota *et al.*, 2003). Many other examples are known where a viral attachment protein uses a member of the Ig superfamily as a receptor (discussed in Dermody *et al.* (2009)). For example, adenovirus engages CAR (Bergelson *et al.*, 1997; Tomko *et al.*, 1997), HIV binds to CD4 (Dalglish *et al.*, 1984; Maddon *et al.*, 1986), and rhinovirus to ICAM-1 (Greve *et al.*, 1989; Staunton *et al.*, 1989; Tomassini *et al.*, 1989). All these viruses engage the GFCC' sheet of the most membrane-distal domain, D1, of their respective receptors, and most of the D1 domains belong to the V-set of Ig-like domains. The D1 domain of ICAM-1 belongs to the structurally very similar I-set. Therefore, engagement of receptors of the Ig superfamily seems to be a beneficial strategy used by viruses, because the virus can easily compete with an existing receptor interface.

## 5. Outlook

The studies performed in this thesis provide information about the forces holding the reovirus  $\sigma 1$  trimer together and serve as a basis for hypotheses about conformational changes occurring during viral entry. This work also defines the receptor-binding mechanism of reovirus at an atomic level and reveals common strategies used by viruses to engage their cell-surface receptors. However, many details about the attachment and entry process of reovirus remain unclear.

Does reovirus  $\sigma 1$  detramerize partly or along its full length before the aspartic acids are protonated? Is a lack of stabilization of the aspartic acid cluster by a positively charged side chain in T1L  $\sigma 1$  responsible for the problems occurring during purification of the  $\sigma 1$  protein of this serotype? A high resolution structure of T1L  $\sigma 1$  will provide clarity about the precise interactions occurring in this protein. The analysis of T1L  $\sigma 1$  mutants, e.g., a mutation of Gly331 to arginine, will yield information about the importance of stabilization by charge compensation in the aspartic acid cluster. In addition, CD spectroscopy and dynamic light scattering experiments might help in understanding conformational changes occurring in wt and mutant T3D and T1L  $\sigma 1$ .

How is the tropism of the reovirus serotypes determined? Are the forces occurring in the T1L and T3D  $\sigma 1$  complexes similar? The crystal structures of T1L and T3D  $\sigma 1$  in complex with JAM-A are very similar and do not explain the distinct tropism of the different reovirus serotypes. It is therefore likely that the tropism is determined by carbohydrate binding or by engagement of yet unidentified reovirus receptors. Determination of the interactions between the  $\sigma 1$  proteins and their respective carbohydrate receptors at an atomic level will show if carbohydrate binding is responsible for the tropism of the reovirus serotypes. In order to understand the T1L  $\sigma 1$ -JAM-A interaction more clearly, a higher resolution structure of the T1L  $\sigma 1$ -JAM-A complex is necessary. Therefore, optimization of the crystallization conditions of this complex needs to be performed. Furthermore, binding studies with uncomplexed T1L  $\sigma 1$  will give insights into the different forces occurring in the T1L and T3D  $\sigma 1$ -JAM-A complexes. However, purification of T1L  $\sigma 1$  is not easily achieved, as the protein seems to undergo conformational changes

that abolish JAM-A binding. It might be possible to separate the T1L  $\sigma$ 1-JAM-A complex after purification. Low pH leads to dissociation of the T3D  $\sigma$ 1-JAM-A complex. Therefore, it seems feasible to purify T1L  $\sigma$ 1 as a complex with JAM-A and separate the components after purification in order to obtain uncomplexed T1L  $\sigma$ 1. Employing the reovirus reverse genetics system, using chimeric T1L-T3D  $\sigma$ 1 proteins or T1L  $\sigma$ 1 point mutations, will also help in defining the differences between the complexes of the reovirus serotypes. All these experiments will add substantially to the understanding of reovirus receptor engagement and entry.

## 6. Appendix

### 6.1. Protein sequences and structures

Table 6.1: **Sequence and PDB codes.**

<i>Protein</i>	<i>Protein sequence</i> <sup>a</sup>	<i>PDB ID</i> <sup>b</sup>	<i>structural reference</i>
Ad12 fiber-CAR complex	P36711, P78310	1KAC	Bewley <i>et al.</i> (1999)
mFab Mab231	P01865	1IGT	Harris <i>et al.</i> (1997)
hJAM-A	Q9Y624	1NBQ	Prota <i>et al.</i> (2003)
Reovirus T1L $\sigma$ 1	P04506	n/a	n/a
Reovirus T3D $\sigma$ 1	P03528	1KKE 2OJ5	Chappell <i>et al.</i> (2002) Schelling <i>et al.</i> (2007)
Reovirus T3D $\sigma$ 1 D345N	P03528 (D345N)	2OJ6	Schelling <i>et al.</i> (2007)
Reovirus T1L $\sigma$ 1- JAM-A complex	P04506, Q9Y624	n/a	n/a
Reovirus T3D $\sigma$ 1- JAM-A complex	P03528, Q9Y624	3EOY	Kirchner <i>et al.</i> (2008)
VSV G	Q89000	2J6J, 2CMZ	Roche <i>et al.</i> (2006, 2007)

<sup>a</sup> UniProtKB/Swiss-Prot accession code (<http://www.expasy.org>)

<sup>b</sup> Protein data bank (<http://www.pdb.org>)

## 6.2. Crystallographic statistics and structure quality

6.2.1. T3D  $\sigma$ 1 D345NTable 6.2: Crystallographic statistics for T3D  $\sigma$ 1 D345N.

<i>Data collection</i>	
Space group	P2 <sub>1</sub>
Unit cell dimensions [Å]	a = 84.0, b = 51.6, c = 108.9
Unit cell angles [°]	$\alpha = \gamma = 90.0$ , $\beta = 95.6$
Resolution range [Å]	30.00 - 1.85 (1.92 - 1.85) <sup>a</sup>
Completeness [%]	98.7 (97.9)
Total reflections	347,405
Redundancy	4.4 (4.0)
$R_{merge}$ [%]	9.6 (41.6)
$I/\sigma I$	6.5 (1.4)
$B$ -factor from Wilson plot [Å <sup>2</sup> ]	17.1
<i>Refinement</i>	
$R_{work}$ [%]	17.5 (23.0)
$R_{free}$ [%] <sup>b</sup>	22.4 (27.3)
Overall $B$ -factor [Å <sup>2</sup> ]	17.2
R. m. s. d. bond lengths [Å]	0.012
R. m. s. d. bond angles [°]	1.202
Number of water molecules	953
<i>Ramachandran plot:</i> <sup>c</sup>	
Most favorable regions [%]	87.9
Additional allowed regions [%]	10.5
Generously allowed regions [%]	1.5
Disallowed regions [%]	0.0

<sup>a</sup> Values in parentheses refer to the outermost resolution shell.

<sup>b</sup> Free set (Brünger, 1992) contains 10 % of the data.

<sup>c</sup> Calculated with PROCHECK (CCP4, 1994).

6.2.2. T3D  $\sigma$ 1-JAM-A complexTable 6.3: Crystallographic statistics for the T3D  $\sigma$ 1-JAM-A complex.

<i>Data collection</i> <sup>a</sup>	
Space group	P2 <sub>1</sub> 2 <sub>1</sub> 2
Unit cell dimensions [Å]	a = 105.9, b = 124.3, c = 130.6
Unit cell angles [°]	$\alpha = \beta = \gamma = 90.0$
Resolution range [Å]	30.00 - 3.40 (3.52 - 3.40) <sup>b</sup>
Completeness [%]	90.2 (69.7)
Redundancy	3.6 (1.9)
$R_{merge}$ [%]	16.3 (21.2)
$I/\sigma I$	6.9 (2.7)
$B$ -factor from Wilson plot [Å <sup>2</sup> ]	64.5
<i>Refinement</i>	
$R_{work}$ [%]	21.0 (28.4)
$R_{free}$ [%] <sup>c</sup>	25.2 (32.8)
Number of reflections	21,954
Number of atoms	12,227
$B$ -factor, overall [Å <sup>2</sup> ]	62.1
$B$ -factor, $\sigma$ 1 [Å <sup>2</sup> ]	56.1
$B$ -factor, JAM-A D1 [Å <sup>2</sup> ]	71.8
R. m. s. d. bond lengths [Å]	0.011
R. m. s. d. bond angles [°]	1.544
<i>Ramachandran plot</i> : <sup>d</sup>	
Favored region (%)	91.2
Allowed region (%)	8.8
Outlier region (%)	0.1

<sup>a</sup> Three crystals were used to assemble the dataset.

<sup>b</sup> Values in parentheses refer to the outermost resolution shell.

<sup>c</sup> Free set (Brünger, 1992) contains 10 % of the data.

<sup>d</sup> Calculated with RAMPAGE (CCP4, 1994).

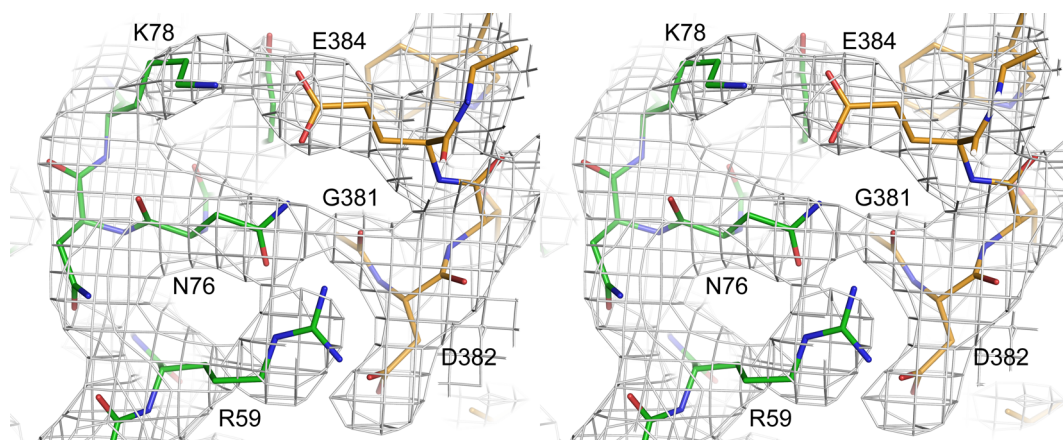


Figure 6.1: **Composite annealed omit map of a T3D  $\sigma$ 1-JAM-A contact area.** Stereo representation of a  $2F_{obs} - F_{calc}$  composite annealed omit map (calculated with CNS (Brünger *et al.*, 1998)) contoured at  $1\sigma$ . For calculation of an omit map, small regions of the molecule are omitted sequentially, and electron density maps are calculated. Simulated annealing and coordinate refinement are performed prior to map calculation to reduce the model bias. The map depicted above shows key residues at interface of the complex. Carbon atoms of JAM-A and  $\sigma$ 1 are shown in green and orange, respectively. Oxygen atoms are shown in red and nitrogen atoms in blue. Figure modified from Kirchner *et al.* (2008).

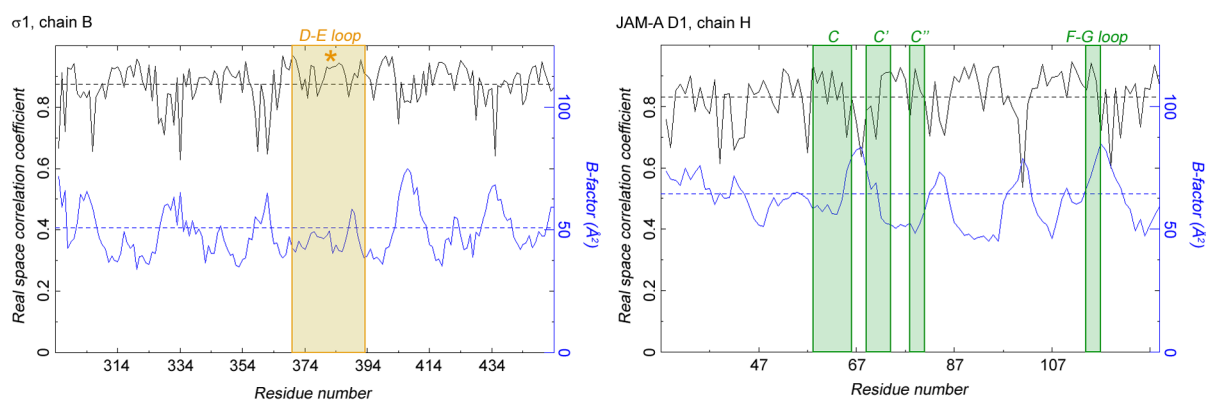


Figure 6.2: **Real space correlation plots for the T3D  $\sigma$ 1-JAM-A complex.** Real space correlation plots (Brändén & Jones, 1990) (black) and B-factor plots (blue) for a  $\sigma$ 1 (left) and a JAM-A chain (right). Selected regions participating in complex contacts are shaded. The position of the  $3_{10}$  helix is indicated by an asterisk. The plots were calculated at the TB consortium bias removal server (<http://tuna.tamu.edu>). Figure modified from Kirchner *et al.* (2008).

6.2.3. T1L  $\sigma$ 1-JAM-A complexTable 6.4: Crystallographic statistics for the T1L  $\sigma$ 1-JAM-A complex.

<i>Data collection</i>	
Space group	P3 <sub>1</sub> 21
Unit cell dimensions [Å]	a = b = 156.8, c = 96.5
Unit cell angles [°]	$\alpha = \beta = 90.0$ , $\gamma = 120.0$
Resolution range [Å]	30.00 - 3.20 (3.28 - 3.20) <sup>a</sup>
Completeness [%]	99.1 (99.5)
Unique reflections	22,673
Redundancy	4.8 (3.8)
$R_{meas}$ [%] <sup>b</sup>	8.6 (43.8)
$R_{mrgd-F}$ [%] <sup>b</sup>	11.1 (50.6)
$I/\sigma I$	14.8 (3.3)
$B$ -factor from Wilson plot [Å <sup>2</sup> ]	43.5
<i>Refinement</i>	
$R_{work}$ [%]	25.4 (34.2)
$R_{free}$ [%] <sup>c</sup>	29.1 (39.6)
Number of atoms	6276
$B$ -factor, overall [Å <sup>2</sup> ]	77.5
$B$ -factor, $\sigma$ 1 [Å <sup>2</sup> ]	62.4
$B$ -factor, JAM-A D1 [Å <sup>2</sup> ]	101.9
R. m. s. d. bond lengths [Å]	0.012
R. m. s. d. bond angles [°]	1.684
<i>Ramachandran plot</i> . <sup>d</sup>	
Most favorable regions [%]	77.9
Additional allowed regions [%]	19.4
Generously allowed regions [%]	1.0
Disallowed regions [%]	1.6

<sup>a</sup> Values in parentheses refer to the outermost resolution shell.

<sup>b</sup> As defined by Diederichs & Karplus (1997).

<sup>c</sup> Free set (Brünger, 1992) contains 10 % of the data.

<sup>d</sup> Calculated with PROCHECK (CCP4, 1994).

## 6.3. Analytical ultracentrifugation

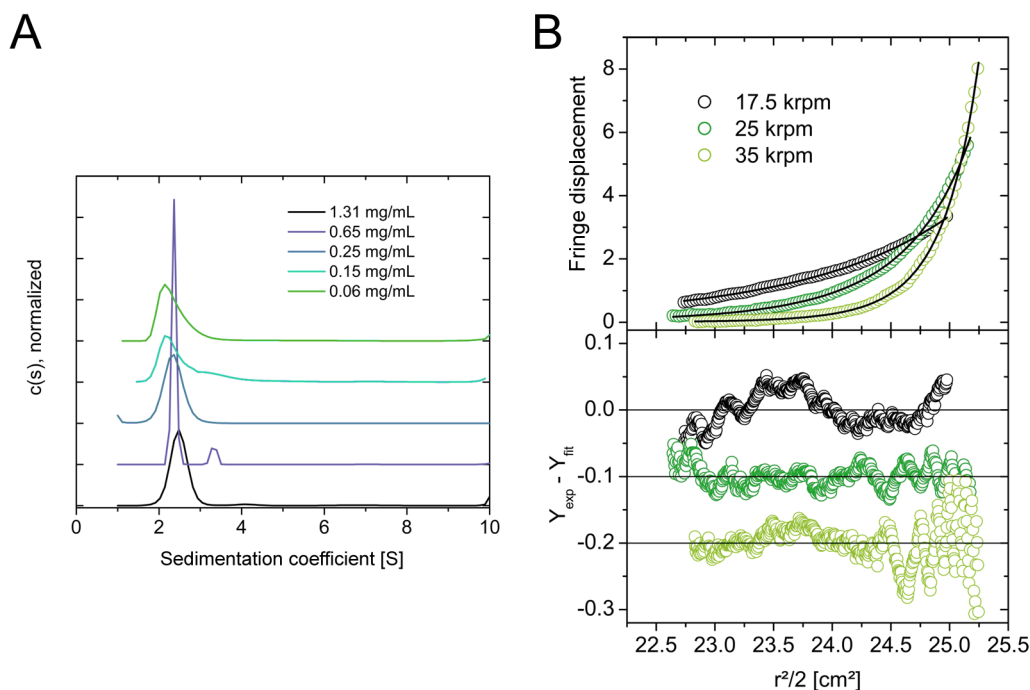


Figure 6.3: **Analytical ultracentrifugation of JAM-A D1.** (A) SV experiments. Sedimentation coefficient ( $c(S)$ ) distributions, with  $c(s)$  as the concentration of species with sedimentation coefficients between  $s$  and  $s + ds$  for five concentrations of JAM-A D1. Only little change is observed in the sedimentation coefficient of the main component around 2.35 S. The small additional peak seen in variable amounts around 3.8 S likely corresponds to JAM-A tetramers. The curves have been normalized to a total area of unity and offset for clarity. The exact shape of the  $c(S)$ -traces depends on the signal-to-noise ratio and the detailed structure of the systematic noise from the interference data. (B) SE results. Top: Raw experimental data (colored dots) for three different velocities at 0.8 mg/mL, together with the theoretical curves for a monomer-dimer equilibrium (black lines) from which the equilibrium coefficient was derived. For clarity, only every 5th data point is displayed for only one of the four starting concentrations. Bottom: Local deviations between theoretical and experimental curves. All data points are shown. Residuals were offset by a factor of 0.1 for clarity. Figure modified from Kirchner *et al.* (2008).

## 7. References

- Adams, P. D., Grosse-Kunstleve, R. W., Hung, L. W., Ioerger, T. R., McCoy, A. J., Moriarty, N. W., Read, R. J., Sacchettini, J. C., Sauter, N. K., & Terwilliger, T. C. (2002). PHENIX: building new software for automated crystallographic structure determination. *Acta Crystallogr D Biol Crystallogr*, **58** (11), 1948–1954.
- Attoui, H., Biagini, P., Stirling, J., Mertens, P. P., Cantaloube, J. F., Meyer, A., de Micco, P., & de Lamballerie, X. (2001). Sequence characterization of Ndelle virus genome segments 1, 5, 7, 8, and 10: evidence for reassignment to the genus Orthoreovirus, family Reoviridae. *Biochem Biophys Res Commun*, **287** (2), 583–588.
- Barton, E. S., Connolly, J. L., Forrest, J. C., Chappell, J. D., & Dermody, T. S. (2001a). Utilization of sialic acid as a coreceptor enhances reovirus attachment by multistep adhesion strengthening. *J Biol Chem*, **276** (3), 2200–2211.
- Barton, E. S., Forrest, J. C., Connolly, J. L., Chappell, J. D., Liu, Y., Schnell, F. J., Nusrat, A., Parkos, C. A., & Dermody, T. S. (2001b). Junction adhesion molecule is a receptor for reovirus. *Cell*, **104** (3), 441–451.
- Bass, D. M., Bodkin, D., Dambrauskas, R., Trier, J. S., Fields, B. N., & Wolf, J. L. (1990). Intraluminal proteolytic activation plays an important role in replication of type 1 reovirus in the intestines of neonatal mice. *J Virol*, **64** (4), 1830–1833.
- Bazzoni, G., Martinez-Estrada, O. M., Mueller, F., Nelboeck, P., Schmid, G., Bartfai, T., Dejana, E., & Brockhaus, M. (2000). Homophilic interaction of junctional adhesion molecule. *J Biol Chem*, **275** (40), 30970–30976.
- Bergelson, J. M., Cunningham, J. A., Droguett, G., Kurt-Jones, E. A., Krithivas, A., Hong, J. S., Horwitz, M. S., Crowell, R. L., & Finberg, R. W. (1997). Isolation of a common receptor for Coxsackie B viruses and adenoviruses 2 and 5. *Science*, **275** (5304), 1320–1323.
- Bewley, M. C., Springer, K., Zhang, Y. B., Freimuth, P., & Flanagan, J. M. (1999). Structural analysis of the mechanism of adenovirus binding to its human cellular receptor, CAR. *Science*, **286** (5444), 1579–1583.
- Bhella, D., Gatherer, D., Chaudhry, Y., Pink, R., & Goodfellow, I. G. (2008). Structural insights into calicivirus attachment and uncoating. *J Virol*, **82** (16), 8051–8058.

## 7. References

---

- Bodkin, D. K., Nibert, M. L., & Fields, B. N. (1989). Proteolytic digestion of reovirus in the intestinal lumens of neonatal mice. *J Virol*, **63** (11), 4676–4681.
- Bork, P., Holm, L., & Sander, C. (1994). The immunoglobulin fold. Structural classification, sequence patterns and common core. *J Mol Biol*, **242** (4), 309–320.
- Borsa, J., Morash, B. D., Sargent, M. D., Copps, T. P., Lievaart, P. A., & Szekely, J. G. (1979). Two modes of entry of reovirus particles into L cells. *J Gen Virol*, **45** (1), 161–170.
- Borsa, J., Sargent, M. D., Lievaart, P. A., & Copps, T. P. (1981). Reovirus: evidence for a second step in the intracellular uncoating and transcriptase activation process. *Virology*, **111** (1), 191–200.
- Böttinger, C. (2006). Strukturelle und funktionelle Charakterisierung des reoviralen Typ1-Zelladsorptionsproteins Sigma 1. Master's thesis Universität Tübingen.
- Bradford, M. M. (1976). A rapid and sensitive method for the quantitation of microgram quantities of protein utilizing the principle of protein-dye binding. *Anal Biochem*, **72**, 248–254.
- Brändén, C.-I. & Jones, T. A. (1990). Between objectivity and subjectivity. *Nature*, **343**, 687 – 689.
- Breun, L. A., Broering, T. J., McCutcheon, A. M., Harrison, S. J., Luongo, C. L., & Nibert, M. L. (2001). Mammalian reovirus L2 gene and lambda2 core spike protein sequences and whole-genome comparisons of reoviruses type 1 Lang, type 2 Jones, and type 3 Dearing. *Virology*, **287** (2), 333–348.
- Brünger, A. T. (1992). Free R value: a novel statistical quantity for assessing the accuracy of crystal structures. *Nature*, **355** (6359), 472–475.
- Brünger, A. T., Adams, P. D., Clore, G. M., DeLano, W. L., Gros, P., Grosse-Kunstleve, R. W., Jiang, J. S., Kuszewski, J., Nilges, M., Pannu, N. S., Read, R. J., Rice, L. M., Simonson, T., & Warren, G. L. (1998). Crystallography & NMR system: A new software suite for macromolecular structure determination. *Acta Crystallogr D Biol Crystallogr*, **54** (5), 905–921.
- Brünger, A. T. & Rice, L. M. (1997). Crystallographic refinement by simulated annealing: methods and applications. *Methods Enzymol*, **277**, 243–269.
- Campbell, J. A., Schelling, P., Wetzell, J. D., Johnson, E. M., Forrest, J. C., Wilson, G. A. R., Aurrand-Lions, M., Imhof, B. A., Stehle, T., & Dermody, T. S. (2005). Junctional adhesion molecule a serves as a receptor for prototype and field-isolate strains of mammalian reovirus. *J Virol*, **79** (13), 7967–7978.
- Caspar, D. L. & Klug, A. (1962). Physical principles in the construction of regular viruses. *Cold Spring Harb Symp Quant Biol*, **27**, 1–24.

## 7. References

---

- Cavalli, A., Prota, A. E., Stehle, T., Dermody, T. S., Recanatini, M., Folkers, G., & Scapozza, L. (2004). A molecular dynamics study of reovirus attachment protein sigma1 reveals conformational changes in sigma1 structure. *Biophys J*, **86** (6), 3423–3431.
- Chandran, K., Farsetta, D. L., & Nibert, M. L. (2002). Strategy for nonenveloped virus entry: a hydrophobic conformer of the reovirus membrane penetration protein micro 1 mediates membrane disruption. *J Virol*, **76** (19), 9920–9933.
- Chang, C. T. & Zweerink, H. J. (1971). Fate of parental reovirus in infected cell. *Virology*, **46** (3), 544–555.
- Chappell, J. D., Duong, J. L., Wright, B. W., & Dermody, T. S. (2000). Identification of carbohydrate-binding domains in the attachment proteins of type 1 and type 3 reoviruses. *J Virol*, **74** (18), 8472–8479.
- Chappell, J. D., Gunn, V. L., Wetzel, J. D., Baer, G. S., & Dermody, T. S. (1997). Mutations in type 3 reovirus that determine binding to sialic acid are contained in the fibrous tail domain of viral attachment protein sigma1. *J Virol*, **71** (3), 1834–1841.
- Chappell, J. D., Prota, A. E., Dermody, T. S., & Stehle, T. (2002). Crystal structure of reovirus attachment protein sigma1 reveals evolutionary relationship to adenovirus fiber. *EMBO J*, **21** (1-2), 1–11.
- Coffey, M. C., Strong, J. E., Forsyth, P. A., & Lee, P. W. (1998). Reovirus therapy of tumors with activated Ras pathway. *Science*, **282** (5392), 1332–1334.
- Collaborative Computational Project number 4 (CCP4) (1994). The CCP4 suite: programs for protein crystallography. *Acta Crystallogr D Biol Crystallogr*, **50** (5), 760–763.
- Connolly, J. L., Rodgers, S. E., Clarke, P., Ballard, D. W., Kerr, L. D., Tyler, K. L., & Dermody, T. S. (2000). Reovirus-induced apoptosis requires activation of transcription factor NF-kappaB. *J Virol*, **74** (7), 2981–2989.
- Coombs, K. M. (1998). Stoichiometry of reovirus structural proteins in virus, ISVP, and core particles. *Virology*, **243** (1), 218–228.
- Dagleish, A. G., Beverley, P. C., Clapham, P. R., Crawford, D. H., Greaves, M. F., & Weiss, R. A. (1984). The CD4 (T4) antigen is an essential component of the receptor for the AIDS retrovirus. *Nature*, **312** (5996), 763–767.
- Danthi, P., Coffey, C. M., Parker, J. S. L., Abel, T. W., & Dermody, T. S. (2008). Independent regulation of reovirus membrane penetration and apoptosis by the mu1 phi domain. *PLoS Pathog*, **4** (12), e1000248.
- Del Maschio, A., De Luigi, A., Martin-Padura, I., Brockhaus, M., Bartfai, T., Fruscella, P., Adorini, L., Martino, G., Furlan, R., De Simoni, M. G., & Dejana, E. (1999). Leukocyte recruitment in the cerebrospinal fluid of mice with experimental meningitis is inhibited by an antibody to junctional adhesion molecule (JAM). *J Exp Med*, **190** (9), 1351–1356.

## 7. References

---

- DeLano, W. L. (2002). The PyMOL Molecular Graphics System. [www.pymol.org](http://www.pymol.org). DeLano Scientific, San Carlos, USA.
- Dermody, T. S., Kirchner, E., Guglielmi, K. M., & Stehle, T. (2009). Immunoglobulin superfamily pathogen receptors and the evolution of adaptive immunity. *PLoS Pathog*, **in press**.
- Dermody, T. S., Schiff, L. A., Nibert, M. L., Coombs, K. M., & Fields, B. N. (1991). The S2 gene nucleotide sequences of prototype strains of the three reovirus serotypes: characterization of reovirus core protein sigma 2. *J Virol*, **65** (11), 5721–5731.
- Diederichs, K. & Karplus, P. A. (1997). Improved R-factors for diffraction data analysis in macromolecular crystallography. *Nat Struct Biol*, **4** (4), 269–275.
- Dormitzer, P. R., Nason, E. B., Prasad, B. V. V., & Harrison, S. C. (2004). Structural rearrangements in the membrane penetration protein of a non-enveloped virus. *Nature*, **430** (7003), 1053–1058.
- Dryden, K. A., Farsetta, D. L., Wang, G., Keegan, J. M., Fields, B. N., Baker, T. S., & Nibert, M. L. (1998). Internal structures containing transcriptase-related proteins in top component particles of mammalian orthoreovirus. *Virology*, **245** (1), 33–46.
- Dryden, K. A., Wang, G., Yeager, M., Nibert, M. L., Coombs, K. M., Furlong, D. B., Fields, B. N., & Baker, T. S. (1993). Early steps in reovirus infection are associated with dramatic changes in supramolecular structure and protein conformation: analysis of virions and subviral particles by cryoelectron microscopy and image reconstruction. *J Cell Biol*, **122** (5), 1023–1041.
- Duncan, M. R., Stanish, S. M., & Cox, D. C. (1978). Differential sensitivity of normal and transformed human cells to reovirus infection. *J Virol*, **28** (2), 444–449.
- Ebnet, K., Aurrand-Lions, M., Kuhn, A., Kiefer, F., Butz, S., Zander, K., zu Brickwedde, M.-K. M., Suzuki, A., Imhof, B. A., & Vestweber, D. (2003). The junctional adhesion molecule (JAM) family members JAM-2 and JAM-3 associate with the cell polarity protein PAR-3: a possible role for JAMs in endothelial cell polarity. *J Cell Sci*, **116** (Pt 19), 3879–3891.
- Edelstein, M. L., Abedi, M. R., & Wixon, J. (2007). Gene therapy clinical trials worldwide to 2007 - an update. *J Gene Med*, **9** (10), 833–842.
- Ehrlich, M., Boll, W., Oijen, A. V., Hariharan, R., Chandran, K., Nibert, M. L., & Kirchhausen, T. (2004). Endocytosis by random initiation and stabilization of clathrin-coated pits. *Cell*, **118** (5), 591–605.
- Emsley, P. & Cowtan, K. (2004). Coot: model-building tools for molecular graphics. *Acta Crystallogr D Biol Crystallogr*, **60** (12-1), 2126–2132.
- Engh, R. A. & Huber, R. (1991). Accurate bond and angle parameters for X-ray protein structure refinement. *Acta Crystallogr A Found Crystallogr*, **A47**, 392–400.

- Fields, B. N., Nibert, M. L., & Schiff, L. A. (1996). *Virology*, volume volume 2. Lippincott-Raven, Philadelphia, New York, third edition edition.
- Forrest, J. C., Campbell, J. A., Schelling, P., Stehle, T., & Dermody, T. S. (2003). Structure-function analysis of reovirus binding to junctional adhesion molecule 1. Implications for the mechanism of reovirus attachment. *J Biol Chem*, **278** (48), 48434–48444.
- Fraser, R. D., Furlong, D. B., Trus, B. L., Nibert, M. L., Fields, B. N., & Steven, A. C. (1990). Molecular structure of the cell-attachment protein of reovirus: correlation of computer-processed electron micrographs with sequence-based predictions. *J Virol*, **64** (6), 2990–3000.
- Furlong, D. B., Nibert, M. L., & Fields, B. N. (1988). Sigma 1 protein of mammalian reoviruses extends from the surfaces of viral particles. *J Virol*, **62** (1), 246–256.
- Gamblin, S. J., Rodgers, D. W., & Stehle, T. (1996). Improving electron density maps calculated from weak or anisotropic data. In: *Proceedings of the CCP4 Study Weekend* pp. 160–163. Daresbury Laboratory Daresbury, UK.
- Gentsch, J. R. & Pacitti, A. F. (1987). Differential interaction of reovirus type 3 with sialylated receptor components on animal cells. *Virology*, **161** (1), 245–248.
- Greve, J. M., Davis, G., Meyer, A. M., Forte, C. P., Yost, S. C., Marlor, C. W., Kamarck, M. E., & McClelland, A. (1989). The major human rhinovirus receptor is ICAM-1. *Cell*, **56** (5), 839–847.
- Guardado Calvo, P., Fox, G. C., Hermo Parrado, X. L., Llamas-Saiz, A. L., Costas, C., Martínez-Costas, J., Benavente, J., & van Raaij, M. J. (2005). Structure of the carboxy-terminal receptor-binding domain of avian reovirus fibre sigmaC. *J Mol Biol*, **354** (1), 137–149.
- Guglielmi, K. M., Kirchner, E., Holm, G. H., Stehle, T., & Dermody, T. S. (2007). Reovirus binding determinants in junctional adhesion molecule-A. *J Biol Chem*, **282** (24), 17930–17940.
- Harpaz, Y. & Chothia, C. (1994). Many of the immunoglobulin superfamily domains in cell adhesion molecules and surface receptors belong to a new structural set which is close to that containing variable domains. *J Mol Biol*, **238** (4), 528–539.
- Harris, L. J., Larson, S. B., Hasel, K. W., & McPherson, A. (1997). Refined structure of an intact IgG2a monoclonal antibody. *Biochemistry*, **36** (7), 1581–1597.
- He, Y., Chipman, P. R., Howitt, J., Bator, C. M., Whitt, M. A., Baker, T. S., Kuhn, R. J., Anderson, C. W., Freimuth, P., & Rossmann, M. G. (2001). Interaction of coxsackievirus B3 with the full length coxsackievirus-adenovirus receptor. *Nat Struct Biol*, **8** (10), 874–878.

## 7. References

---

- Hirasawa, K., Nishikawa, S. G., Norman, K. L., Alain, T., Kossakowska, A., & Lee, P. W. K. (2002). Oncolytic reovirus against ovarian and colon cancer. *Cancer Res*, **62** (6), 1696–1701.
- Holm, G. H., Zurney, J., Tumilasci, V., Leveille, S., Danthi, P., Hiscott, J., Sherry, B., & Dermody, T. S. (2007). Retinoic acid-inducible gene-I and interferon-beta promoter stimulator-1 augment proapoptotic responses following mammalian reovirus infection via interferon regulatory factor-3. *J Biol Chem*, **282** (30), 21953–21961.
- Hooper, J. W. & Fields, B. N. (1996). Role of the mu 1 protein in reovirus stability and capacity to cause chromium release from host cells. *J Virol*, **70** (1), 459–467.
- Huang, X. & Miller, W. (1991). A time-efficient, linear-space local similarity algorithm. *Adv Appl Math*, **12**, 337–357.
- Ivanovic, T., Agosto, M. A., Zhang, L., Chandran, K., Harrison, S. C., & Nibert, M. L. (2008). Peptides released from reovirus outer capsid form membrane pores that recruit virus particles. *EMBO J*, **27** (8), 1289–1298.
- Kabsch, W. (1993). Automatic processing of rotation diffraction data from crystals of initially unknown symmetry and cell constants. *J Appl Crystallogr*, **26** (6), 795–800.
- Kirby, I., Davison, E., Beavil, A. J., Soh, C. P., Wickham, T. J., Roelvink, P. W., Kovesdi, I., Sutton, B. J., & Santis, G. (2000). Identification of contact residues and definition of the CAR-binding site of adenovirus type 5 fiber protein. *J Virol*, **74** (6), 2804–2813.
- Kirchner, E., Guglielmi, K. M., Strauss, H. M., Dermody, T. S., & Stehle, T. (2008). Structure of reovirus sigma1 in complex with its receptor junctional adhesion molecule-A. *PLoS Pathog*, **4** (12), e1000235.
- Kleywegt, G. J. & Jones, T. A. (1994). Detection, delineation, measurement and display of cavities in macromolecular structures. *Acta Crystallogr D Biol Crystallogr*, **50** (2), 178–185.
- Kobayashi, T., Antar, A. A. R., Boehme, K. W., Danthi, P., Eby, E. A., Guglielmi, K. M., Holm, G. H., Johnson, E. M., Maginnis, M. S., Naik, S., Skelton, W. B., Wetzel, J. D., Wilson, G. J., Chappell, J. D., & Dermody, T. S. (2007). A plasmid-based reverse genetics system for animal double-stranded RNA viruses. *Cell Host Microbe*, **1** (2), 147–157.
- Kostrewa, D., Brockhaus, M., D’Arcy, A., Dale, G. E., Nelboeck, P., Schmid, G., Mueller, F., Bazzoni, G., Dejana, E., Bartfai, T., Winkler, F. K., & Hennig, M. (2001). X-ray structure of junctional adhesion molecule: structural basis for homophilic adhesion via a novel dimerization motif. *EMBO J*, **20** (16), 4391–4398.
- Krissinel, E. & Henrick, K. (2004). Secondary-structure matching (SSM), a new tool for fast protein structure alignment in three dimensions. *Acta Crystallogr D Biol Crystallogr*, **60** (12-1), 2256–2268.

- Laemmli, U. K. (1970). Cleavage of structural proteins during the assembly of the head of bacteriophage T4. *Nature*, **227** (5259), 680–685.
- Layne, E. (1957). Spectrophotometric and turbidimetric methods for measuring proteins. *Meth Enzymol*, **3**, 447–454.
- Lebowitz, J., Lewis, M. S., & Schuck, P. (2002). Modern analytical ultracentrifugation in protein science: a tutorial review. *Protein Sci*, **11** (9), 2067–2079.
- Lerner, M. G. & Carlson, H. A. (2006). *APBS plugin for PyMOL*. University of Michigan Ann Arbor.
- Liemann, S., Chandran, K., Baker, T. S., Nibert, M. L., & Harrison, S. C. (2002). Structure of the reovirus membrane-penetration protein, Mu1, in a complex with its protector protein, Sigma3. *Cell*, **108** (2), 283–295.
- Liu, Y., Nusrat, A., Schnell, F. J., Reaves, T. A., Walsh, S., Pochet, M., & Parkos, C. A. (2000). Human junction adhesion molecule regulates tight junction resealing in epithelia. *J Cell Sci*, **113** (13), 2363–2374.
- Lucia-Jandris, P., Hooper, J. W., & Fields, B. N. (1993). Reovirus M2 gene is associated with chromium release from mouse L cells. *J Virol*, **67** (9), 5339–5345.
- Maddon, P. J., Dagleish, A. G., McDougal, J. S., Clapham, P. R., Weiss, R. A., & Axel, R. (1986). The T4 gene encodes the AIDS virus receptor and is expressed in the immune system and the brain. *Cell*, **47** (3), 333–348.
- Maginnis, M. S., Forrest, J. C., Kopecky-Bromberg, S. A., Dickeson, S. K., Santoro, S. A., Zutter, M. M., Nemerow, G. R., Bergelson, J. M., & Dermody, T. S. (2006). Beta1 integrin mediates internalization of mammalian reovirus. *J Virol*, **80** (6), 2760–2770.
- Maginnis, M. S., Mainou, B. A., Derdowski, A., Johnson, E. M., Zent, R., & Dermody, T. S. (2008). NPXY motifs in the beta1 integrin cytoplasmic tail are required for functional reovirus entry. *J Virol*, **82** (7), 3181–3191.
- Makino, A., Shimojima, M., Miyazawa, T., Kato, K., Tohya, Y., & Akashi, H. (2006). Junctional adhesion molecule 1 is a functional receptor for feline calicivirus. *J Virol*, **80** (9), 4482–4490.
- Mann, M. A., Knipe, D. M., Fischbach, G. D., & Fields, B. N. (2002). Type 3 reovirus neuroinvasion after intramuscular inoculation: direct invasion of nerve terminals and age-dependent pathogenesis. *Virology*, **303** (2), 222–231.
- Martín-Padura, I., Lostaglio, S., Schneemann, M., Williams, L., Romano, M., Fruscella, P., Panzeri, C., Stoppacciaro, A., Rucó, L., Villa, A., Simmons, D., & Dejana, E. (1998). Junctional adhesion molecule, a novel member of the immunoglobulin superfamily that distributes at intercellular junctions and modulates monocyte transmigration. *J Cell Biol*, **142** (1), 117–127.

## 7. References

---

- Matthews, B. W. (1968). Solvent content of protein crystals. *J Mol Biol*, **33** (2), 491–497.
- McCoy, A. J., Grosse-Kunstleve, R. W., Adams, P. D., Winn, M. D., Storoni, L. C., & Read, R. J. (2007). *Phaser* crystallographic software. *J Appl Crystallogr*, **40** (4), 658–674.
- McCoy, A. J., Grosse-Kunstleve, R. W., Storoni, L. C., & Read, R. J. (2005). Likelihood-enhanced fast translation functions. *Acta Crystallogr D Biol Crystallogr*, **61** (4), 458–464.
- Mercier, G. T., Campbell, J. A., Chappell, J. D., Stehle, T., Dermody, T. S., & Barry, M. A. (2004). A chimeric adenovirus vector encoding reovirus attachment protein sigma1 targets cells expressing junctional adhesion molecule 1. *Proc Natl Acad Sci U S A*, **101** (16), 6188–6193.
- Merckel, M. C., Huiskonen, J. T., Bamford, D. H., Goldman, A., & Tuma, R. (2005). The structure of the bacteriophage PRD1 spike sheds light on the evolution of viral capsid architecture. *Mol Cell*, **18** (2), 161–170.
- Metcalf, P. (1982). The symmetry of the reovirus outer shell. *J Ultrastruct Res*, **78** (3), 292–301.
- Modrow, S., Falke, D., & Truyen, U. (2003). *Molekulare Virologie*. Spektrum Akademischer Verlag Heidelberg, Berlin, 2nd edition.
- Morrison, L. A., Sidman, R. L., & Fields, B. N. (1991). Direct spread of reovirus from the intestinal lumen to the central nervous system through vagal autonomic nerve fibers. *Proc Natl Acad Sci U S A*, **88** (9), 3852–3856.
- Murshudov, G. N., Vagin, A. A., & Dodson, E. J. (1997). Refinement of macromolecular structures by the maximum-likelihood method. *Acta Crystallogr D Biol Crystallogr*, **53** (3), 240–255.
- Nason, E. L., Wetzel, J. D., Mukherjee, S. K., Barton, E. S., Prasad, B. V., & Dermody, T. S. (2001). A monoclonal antibody specific for reovirus outer-capsid protein sigma3 inhibits sigma1-mediated hemagglutination by steric hindrance. *J Virol*, **75** (14), 6625–6634.
- Navaza, J. (1994). AMoRe: an automated package for molecular replacement. *Acta Crystallogr A Found Crystallogr*, **50** (2), 157–163.
- Nesterenko, M. V., Tilley, M., & Upton, S. J. (1994). A simple modification of Blum's silver stain method allows for 30 minute detection of proteins in polyacrylamide gels. *J Biochem Biophys Methods*, **28** (3), 239–242.
- Nibert, M. L., Chappell, J. D., & Dermody, T. S. (1995). Infectious subvirion particles of reovirus type 3 Dearing exhibit a loss in infectivity and contain a cleaved sigma 1 protein. *J Virol*, **69** (8), 5057–5067.

## 7. References

---

- Nibert, M. L., Dermody, T. S., & Fields, B. N. (1990). Structure of the reovirus cell-attachment protein: a model for the domain organization of sigma 1. *J Virol*, **64** (6), 2976–2989.
- Norman, K. L. & Lee, P. W. (2000). Reovirus as a novel oncolytic agent. *J Clin Invest*, **105** (8), 1035–1038.
- Odegard, A. L., Chandran, K., Zhang, X., Parker, J. S. L., Baker, T. S., & Nibert, M. L. (2004). Putative autocleavage of outer capsid protein micro1, allowing release of myristoylated peptide micro1N during particle uncoating, is critical for cell entry by reovirus. *J Virol*, **78** (16), 8732–8745.
- Ossiboff, R. J. & Parker, J. S. L. (2007). Identification of regions and residues in feline junctional adhesion molecule required for feline calicivirus binding and infection. *J Virol*, **81** (24), 13608–13621.
- Ostermann, G., Weber, K. S. C., Zerneck, A., Schröder, A., & Weber, C. (2002). JAM-1 is a ligand of the beta(2) integrin LFA-1 involved in transendothelial migration of leukocytes. *Nat Immunol*, **3** (2), 151–158.
- Paul, R. W., Choi, A. H., & Lee, P. W. (1989). The alpha-anomeric form of sialic acid is the minimal receptor determinant recognized by reovirus. *Virology*, **172** (1), 382–385.
- Prota, A. E., Campbell, J. A., Schelling, P., Forrest, J. C., Watson, M. J., Peters, T. R., Aurrand-Lions, M., Imhof, B. A., Dermody, T. S., & Stehle, T. (2003). Crystal structure of human junctional adhesion molecule 1: implications for reovirus binding. *Proc Natl Acad Sci U S A*, **100** (9), 5366–5371.
- Reinisch, K. M., Nibert, M. L., & Harrison, S. C. (2000). Structure of the reovirus core at 3.6 Å resolution. *Nature*, **404** (6781), 960–967.
- Roche, S., Bressanelli, S., Rey, F. A., & Gaudin, Y. (2006). Crystal structure of the low-pH form of the vesicular stomatitis virus glycoprotein G. *Science*, **313** (5784), 187–191.
- Roche, S., Rey, F. A., Gaudin, Y., & Bressanelli, S. (2007). Structure of the prefusion form of the vesicular stomatitis virus glycoprotein G. *Science*, **315** (5813), 843–848.
- Rodgers, D. W. (1994). Cryocrystallography. *Structure*, **2** (12), 1135–1140.
- Sabin, A. B. (1959). Reoviruses. A new group of respiratory and enteric viruses formerly classified as ECHO type 10 is described. *Science*, **130**, 1387–1389.
- Schelling, P., Guglielmi, K. M., Kirchner, E., Paetzold, B., Dermody, T. S., & Stehle, T. (2007). The reovirus sigma1 aspartic acid sandwich: a trimerization motif poised for conformational change. *J Biol Chem*, **282** (15), 11582–11589.
- Schuck, P. (2000). Size-distribution analysis of macromolecules by sedimentation velocity ultracentrifugation and lamm equation modeling. *Biophys J*, **78** (3), 1606–1619.

## 7. References

---

- Seliger, L. S., Giantini, M., & Shatkin, A. J. (1992). Translational effects and sequence comparisons of the three serotypes of the reovirus S4 gene. *Virology*, **187** (1), 202–210.
- Seliger, L. S., Zheng, K., & Shatkin, A. J. (1987). Complete nucleotide sequence of reovirus L2 gene and deduced amino acid sequence of viral mRNA guanylyltransferase. *J Biol Chem*, **262** (34), 16289–16293.
- Shatkin, A. J., Sipe, J. D., & Loh, P. (1968). Separation of ten reovirus genome segments by polyacrylamide gel electrophoresis. *J Virol*, **2** (10), 986–991.
- Shaw, A. L., Rothnagel, R., Chen, D., Ramig, R. F., Chiu, W., & Prasad, B. V. (1993). Three-dimensional visualization of the rotavirus hemagglutinin structure. *Cell*, **74** (4), 693–701.
- Silverstein, S. C., Astell, C., Levin, D. H., Schonberg, M., & Acs, G. (1972). The mechanisms of reovirus uncoating and gene activation in vivo. *Virology*, **47** (3), 797–806.
- Staunton, D. E., Merluzzi, V. J., Rothlein, R., Barton, R., Marlin, S. D., & Springer, T. A. (1989). A cell adhesion molecule, ICAM-1, is the major surface receptor for rhinoviruses. *Cell*, **56** (5), 849–853.
- Stehle, T. & Dermody, T. S. (2003). Structural evidence for common functions and ancestry of the reovirus and adenovirus attachment proteins. *Rev Med Virol*, **13** (2), 123–132.
- Stehle, T. & Dermody, T. S. (2004). Structural similarities in the cellular receptors used by adenovirus and reovirus. *Viral Immunol*, **17** (2), 129–143.
- Stoeckel, J. & Hay, J. G. (2006). Drug evaluation: Reolysin - wild-type reovirus as a cancer therapeutic. *Curr Opin Mol Ther*, **8** (3), 249–260.
- Sturzenbecker, L. J., Nibert, M., Furlong, D., & Fields, B. N. (1987). Intracellular digestion of reovirus particles requires a low pH and is an essential step in the viral infectious cycle. *J Virol*, **61** (8), 2351–2361.
- Tardieu, M., Powers, M. L., & Weiner, H. L. (1983). Age dependent susceptibility to Reovirus type 3 encephalitis: role of viral and host factors. *Ann Neurol*, **13** (6), 602–607.
- Tomassini, J. E., Graham, D., DeWitt, C. M., Lineberger, D. W., Rodkey, J. A., & Colonno, R. J. (1989). cDNA cloning reveals that the major group rhinovirus receptor on HeLa cells is intercellular adhesion molecule 1. *Proc Natl Acad Sci U S A*, **86** (13), 4907–4911.
- Tomko, R. P., Xu, R., & Philipson, L. (1997). HCAR and MCAR: the human and mouse cellular receptors for subgroup C adenoviruses and group B coxsackieviruses. *Proc Natl Acad Sci U S A*, **94** (7), 3352–3356.

- Tsukita, S., Furuse, M., & Itoh, M. (2001). Multifunctional strands in tight junctions. *Nat Rev Mol Cell Biol*, **2** (4), 285–293.
- Tyler, K. L., Barton, E. S., Ibach, M. L., Robinson, C., Campbell, J. A., O'Donnell, S. M., Valyi-Nagy, T., Clarke, P., Wetzel, J. D., & Dermody, T. S. (2004). Isolation and molecular characterization of a novel type 3 reovirus from a child with meningitis. *J Infect Dis*, **189** (9), 1664–1675.
- Tyler, K. L., McPhee, D. A., & Fields, B. N. (1986). Distinct pathways of viral spread in the host determined by reovirus S1 gene segment. *Science*, **233** (4765), 770–774.
- van Raaij, M. J., Chouin, E., van der Zandt, H., Bergelson, J. M., & Cusack, S. (2000). Dimeric structure of the coxsackievirus and adenovirus receptor D1 domain at 1.7 Å resolution. *Structure*, **8** (11), 1147–1155.
- van Raaij, M. J., Mitraki, A., Lavigne, G., & Cusack, S. (1999). A triple beta-spiral in the adenovirus fibre shaft reveals a new structural motif for a fibrous protein. *Nature*, **401** (6756), 935–938.
- Wang, J. (2002). Protein recognition by cell surface receptors: physiological receptors versus virus interactions. *Trends Biochem Sci*, **27** (3), 122–126.
- Weiner, H. L., Drayna, D., Averill, D. R., & Fields, B. N. (1977). Molecular basis of reovirus virulence: role of the S1 gene. *Proc Natl Acad Sci U S A*, **74** (12), 5744–5748.
- Weiner, H. L., Powers, M. L., & Fields, B. N. (1980). Absolute linkage of virulence and central nervous system cell tropism of reoviruses to viral hemagglutinin. *J Infect Dis*, **141** (5), 609–616.
- Wiener, J. R. & Joklik, W. K. (1989). The sequences of the reovirus serotype 1, 2, and 3 L1 genome segments and analysis of the mode of divergence of the reovirus serotypes. *Virology*, **169** (1), 194–203.
- Williams, L. A., Martin-Padura, I., Dejana, E., Hogg, N., & Simmons, D. L. (1999). Identification and characterisation of human Junctional Adhesion Molecule (JAM). *Mol Immunol*, **36** (17), 1175–1188.
- Wilson, A. J. C. (1949). X-ray diffraction by random layers: ideal line profiles and determination of structure amplitudes from observed line profiles. *Acta Crystallogr*, **2** (4), 245–251.
- Woodfin, A., Reichel, C. A., Khandoga, A., Corada, M., Voisin, M.-B., Scheiermann, C., Haskard, D. O., Dejana, E., Krombach, F., & Nourshargh, S. (2007). JAM-A mediates neutrophil transmigration in a stimulus-specific manner in vivo: evidence for sequential roles for JAM-A and PECAM-1 in neutrophil transmigration. *Blood*, **110** (6), 1848–1856.

## 7. References

---

- Yeager, M., Berriman, J. A., Baker, T. S., & Bellamy, A. R. (1994). Three-dimensional structure of the rotavirus haemagglutinin VP4 by cryo-electron microscopy and difference map analysis. *EMBO J*, **13** (5), 1011–1018.
- Yoder, J. D. & Dormitzer, P. R. (2006). Alternative intermolecular contacts underlie the rotavirus VP5\* two- to three-fold rearrangement. *EMBO J*, **25** (7), 1559–1568.

# Publications

Publications marked with an asterisk contain results presented in this thesis.

- \* Schelling, P., Guglielmi, K. M., **Kirchner, E.**, Paetzold, B., Dermody, T. S., & Stehle, T. (2007). The reovirus sigma1 aspartic acid sandwich: a trimerization motif poised for conformational change. *J Biol Chem*, **282** (15), 11582-11589.

*This article discusses the  $\sigma 1$  aspartic acid cluster on the basis of the high-resolution structures of the wt and D345N T3D  $\sigma 1$  head domains. Furthermore, the functional properties of wt T3D  $\sigma 1$  and the aspartic acid cluster mutants D345N and Y313A were analyzed.*

- Guglielmi, K. M., **Kirchner, E.**, Holm, G. H., Stehle, T., & Dermody, T. S. (2007). Reovirus binding determinants in junctional adhesion molecule-A. *J Biol Chem*, **282** (24), 17930-17940.

*To determine residues in JAM-A necessary for binding to reovirus T1L, T2J, and T3D, residues in the JAM-A dimer interface were mutated to alanine. The mutants were analyzed using infectivity assays and surface plasmon resonance. Their multimeric state and complex formation with  $\sigma 1$  were investigated using size-exclusion chromatography. The results are not presented in this thesis, but some are discussed in chapter 4.*

- Mi, J., **Kirchner, E.**, & Cristobal, S. (2007). Quantitative proteomic comparison of mouse peroxisomes from liver and kidney. *Proteomics*, **7** (11), 1916-1928.

*An article totally unrelated to the work presented in this thesis.*

- Vedula, S. R. K., Lim, T. S., **Kirchner, E.**, Guglielmi, K. M., Dermody, T. S., Stehle, T., Hunziker, W., & Lim, C. T. (2008). A comparative molecular force spectroscopy study of homophilic JAM-A interactions and JAM-A interactions with reovirus attachment protein sigma1. *J Mol Recognit*, **21** (4), 210-216.

*In this article, single molecular force spectroscopy was used to compare the kinetics of the homomeric JAM-A and the JAM-A- $\sigma 1$  interactions. In accordance with the physiological functions of the respective interactions, the bond half-life of the homomeric JAM-A interaction was found to be significantly shorter than the one of the JAM-A- $\sigma 1$  interaction.*

- \* **Kirchner, E.**, Guglielmi, K. M., Strauss, H. M., Dermody, T. S., & Stehle, T. (2008). Structure of reovirus sigma1 in complex with its receptor junctional adhesion molecule-A. *PLoS Pathog*, **4** (12), e1000235.

*The structure of the T3D  $\sigma 1$ -JAM-A complex is presented in this article. Furthermore, amino acids in  $\sigma 1$  located in and adjacent to the JAM-A contact area were mutated to alanine. The mutant reovirus virions were tested for infectivity in cell culture, and their binding to GST-JAM-A was investigated using surface plasmon resonance. The dissociation constant of JAM-A homodimers was determined using analytical ultracentrifugation.*

## Thanks to...

- Thilo Stehle for the opportunity of doing my PhD in your lab. Terry was right: You're the best possible supervisor! Thank you for always being there to answer questions and handle problems. I could never have done this without your infinite optimism about  $\sigma 1$ , the evil-protein-from-hell.
- Terry Dermody, my second supervisor from far, far away, for all the good suggestions and ideas. No matter how frustrating the lab work was, you always made me smile during our video conferences!
- The whole Stehle lab for a great working atmosphere.
- Dirk and Kristen for sharing in the evil of  $\sigma 1$  research. And good luck now to Kerstin!
- Ulla and Sonja for spontaneous "let's go and get some chocolate"-breaks and, together with the rest of the gamers, the fight against the basilisk king, a.k.a. de-escalation training.
- David for being the living proof that it is possible to survive doing a PhD without going totally insane. And for a great New Year's Eve.
- Sebastian for the invaluable lesson that friendship can be found in the person in whom you expected it the least.
- All my other friends from outside the lab for talking about things not related to science. And a lot more.
- Danke natürlich auch an meine Eltern und ihre Partner für all ihre Unterstützung in so langer Zeit.
- And of course thanks to Oskar and Candy for shedding some whiskers that I could use for streak seeding!

## Academic teachers at the University of Tübingen

Prof. Dr. C.-F. Bardele	zoology
Dr. E. O. Bayer	organic biochemistry
Prof. Dr. H. Bisswanger	enzyme kinetics
Prof. Dr. P. Bohley	biochemistry of cell organelles
Prof. Dr. G. Dodt	cell culture
Prof. Dr. R. Dringen	protein purification
Prof. Dr. M. Duszenko	biochemistry of parasites
Prof. Dr. G. Gauglitz	physical chemistry
Prof. Dr. G. Häfelinger	organic chemistry
Prof. Dr. B. Hamprecht	biochemistry
Prof. Dr. W. Jäger	law for chemists
Prof. Dr. E. Lindner	anorganic chemistry
Prof. Dr. H.-J. Machulla	cell culture, radioisotopes
Prof. Dr. F. Madeo	yeast genetics
Prof. Dr. M. E. Maier	organic chemistry
Dr. Mayer	botany
Prof. Dr. P. Münzel	pharmacology-toxicology
Prof. Dr. H. Ninnemann	plant biochemistry
Prof. Dr. H. Oberhammer	physical chemistry
PD Dr. H. Pommer	mathematics
Prof. Dr. H. Probst	biochemistry
Prof. Dr. K. Reutter	anatomy
Dr. W. Sarrazin	radioisotopes
Prof. Dr. H. Schott	organic chemistry
Prof. Dr. M. Schwarz	pharmacology-toxicology
Prof. Dr. T. Stehle	structural biology
Dr. G. Steinbrück	zoology
Prof. Dr. Dr. h. c. J. Strähle	anorganic chemistry
PD Dr. S. Verleysdonk	protein purification
Prof. Dr. Dr. h. c. mult. W. Voelter	physical biochemistry
Prof. Dr. G. J. Wagner	physics
Prof. Dr. J. Werringloer	pharmacology-toxicology
Prof. Dr. U. Weser	anorganic biochemistry
Prof. Dr. W. Wohlleben	microbiology
Prof. Dr. K.-P. Zeller	spectroscopy of organic compounds
Prof. Dr. T. Ziegler	organic chemistry

# Curriculum vitae

---

## PERSONAL DETAILS

---

Name: **Eva Kirchner**<sup>a</sup>  
Date of birth: 16.10.1980  
Place of birth: Villingen-Schwenningen, Germany  
Address: Käsenbachstr. 18, 72076 Tübingen, Germany  
E-mail: eva.kirchner@uni-tuebingen.de  
Nationality: german

---

## EDUCATION

---

09/1987 – 08/1988 Elementary school: Grund- und Hauptschule Pfaffenweiler, Villingen-Schwenningen, Germany  
09/1988 – 08/1991 Elementary school: Freie Waldorfschule Uhlandshöhe, Stuttgart, Germany  
09/1991 – 07/2000 **Abitur**  
Geschwister-Scholl-Gymnasium, Stuttgart, Germany  
10/2000 – 02/2006 Studies at the University of Tübingen, Germany  
03/2004 – 08/2004 Studies at the University of Uppsala, Sweden  
07/2005 – 02/2006 **Diploma thesis in biochemistry**  
University of Tübingen, Germany  
Interfaculty Institute of Biochemistry  
Supervisor: Prof. Dr. T. Stehle  
“Structural and functional studies on the attachment protein  $\sigma 1$  of reovirus type 2 Jones and type 3 Dearing”  
04/2006 – 06/2009 **PhD in biochemistry**  
University of Tübingen, Germany  
Interfaculty Institute of Biochemistry  
Supervisor: Prof. Dr. T. Stehle  
“Structural and functional studies of the reovirus attachment protein  $\sigma 1$  and its interaction with the receptor JAM-A”

---

<sup>a</sup> Actually, it's Eva Maria Catharina Julia Felicitas Barbara Luise Elisabeth Kirchner, but this name does never fit in any input field.

---